# Complex Pattern Formation in Carbon Thin Films and Multi-Layer Graphene through Low Temperature Etching by Catalytic Combustion

by

Lutfiye Bulut

B.Sc., Middle East Technical University, 2003

M.Sc., Brown University, 2006

A DISSERTATION SUBMITTED IN PARTIAL FULFILLMENT OF THE REQUIREMENTS FOR THE DEGREE OF DOCTOR OF PHILOSOPHY IN THE DIVISION OF ENGINEERING AT BROWN UNIVERISTY

PROVIDENCE, RHODE ISLAND

MAY, 2010

This dissertation by Lutfiye Bulut is accepted in its present form by the Division of Engineering as satisfying the dissertation requirement for the degree of Doctor of Philosophy.

Date _____ _____

Professor Robert H. Hurt, Advisor

Recommended to the Graduate Council

Date _____ _____

Professor Eric Suuberg, Reader

Date _____ _____

Professor Shouheng Sun, Reader

Approved by the Graduate Council

Date _____ _____

Professor Sheila Bonde,
Dean of the Graduate School

# Vita

Lutfiye Bulut was born on 23rd March, 1980 in Ankara, Turkey. She graduated from Mechanical Engineering Department at Middle East Technical University and got her Bachelor of Engineering degree in June, 2003. She started her graduate studies in Division of Engineering at Brown University in January, 2004 and got her Master of Science degree in 2006. During her doctoral studies at Brown, she mainly focused on catalytic micro- and nanopatterning of graphene and carbon materials.

# Acknowledgements

First and foremost, I would like to express my sincere gratitude to my advisor, Professor Robert H. Hurt for his guidance, his enthusiasm and continuous encouragement. Without his scientific knowledge and his inspiration none of this work would have been possible. I would like to thank Professor Eric Suuberg and Professor Shouheng Sun very much for serving in my thesis committee.

I would like to acknowledge the members of Prof. Hurt's group: Dr. Indrek Kulaots for his help with thermogravimetric analysis and technical assistance with the experimental setups; Aihui Yan and Xinyuan Liu for answering all my chemistry related questions and for providing numerous ideas and useful discussions; Dr. Love Sarin, for always listening to me and passing his positive attitude and for sharing the difficult times during the writing period of the thesis; Dr. Lin Guo and Lorin Jakubek, for the relaxing times we spent together. I also want to thank Dr. Kenching Jian and Youming Gao who helped me in my first years in Prof. Hurt's group. I appreciate Essie Yamoah and Charlie Yongpravat for their contribution during their summer studies. Jingyu, Fei, Will, Natalie, Brian, Shin, Saira are also sincerely acknowledged. I will always remember our lab with lots of good memories.

I would like to thank my best friend Didem who is close to me like a sister, for always being there, for her understanding and motivation. Many thanks to my friends Goker Tuncol, Huseyin Erdim, Ozgur Bozkurt, Fatih Yigitol and Idil Ugur for all the support and wonderful times we spent together. I also wish to thank my extended family very much for providing a loving family environment in New Jersey. I send my dear thanks to my sisters Deniz Heper and Funda Ciper for the emotional support and caring they provided.

I owe my deep loving thanks to my husband, Murat Altay, who always stands by me with his support and love. Without his encouragement, motivation, and entertainment this thesis would not have been a reality.

Most importantly, I would like to send my greatest thanks to my mother Gulderen Bulut, and to my father Ali Bulut for always letting me feel that I am surrounded with their endless support and unconditional love where ever I am. It is to them that I dedicate this work.

Abstract of “Complex Pattern Formation in Carbon Thin Films and Multi-Layer Graphene through Low Temperature Etching by Catalytic Combustion” by Lutfiye Bulut, Ph.D., Brown University, May 2010

This dissertation describes the development of a novel technique for complex pattern formation and shape control in carbon and graphite films which has significant importance on the properties of carbon based materials for variety of applications. Carbons are quite resistant to solvents, acids, and bases and thus cannot easily be patterned by conventional techniques. The main difficulty in current patterning technology is inability to produce large amounts of identical carbon nanostructures and precision is not possible with combination of existing lithographic and chemical methods.

This thesis demonstrates the use of catalytic combustion as a new and flexible approach to selectively etch carbon materials and focuses on controlling the etching direction by using magnetically steered catalyst particles. Catalytic combustion provides a way of using oxygen as a dry etchant by acting selectively on catalyst particles positioned by controlled metal deposition. Liquid phase catalyst deposition and carbon thin films as a model material and reaction system were used for the demonstration of this new concept. A polydimethylsiloxane stamping technique was used to transfer metal chloride solutions onto carbon thin films in the form of ordered droplet microarrays that dry to produce catalytic micropatches. The results showed that under the correct drying and reaction conditions, it is possible to convert these microdroplet arrays into well-defined micropatterned carbon films by controlled catalytic combustion. Catalyst selection,

drying behavior, etchant selectivity ratio and effect of carbon substrate on the fidelity of combustion pattern were discussed.

In addition, behavior of magnetic catalyst particles on the surface of natural graphite during carbon oxidation reaction has been investigated and it has been proved that an external magnetic field could influence the mode of catalytic attack significantly. Ability to create complex, preset patterns in multi-layer graphene by catalytic channeling in the presence of external magnetic fields has been demonstrated. Graphene films were obtained from natural single graphite crystals by mechanical exfoliation. A custom resistive heat treatment device was developed to allow close proximity access for high temperature resistant powerful magnets. The mode of etching along the basal plane of graphene layers was explicitly controlled by active steering of magnetic particles and this technique has been successfully applied to create directional etched channels and predetermined complex patterns in graphene.

# Table of Contents

VITA……...iv

ACKNOWLEDGEMENTS……v

ABSTRACT……..……vii

TABLE OF CONTENTS……ix

LIST OF FIGURES……..…xiv

LIST OF TABLES……xix

Chapter 1 ..... 1

*Introduction*..... 1

1.1 Carbon Materials and Nanotechnology..... 1

1.2 Objectives..... 8

1.3 Thesis Outline ..... 9

References ..... 10

Chapter 2 ..... 14

*Relevant Background* ..... 14

2.1 Carbon Thin Films ..... 14

2.1.1 Liquid Crystalline Derived Carbon Films ..... 15

2.1.2 Physical Vapor Deposition Films ..... 17

2.2 Single Crystal Natural Graphite ..... 18

2.2.1 Graphene ..... 19

2.2.2 Graphene Nanoribbons ..... 26

2.3 Patterning Techniques for Carbon Thin Films and Graphene ..... 28

2.3.1 Lithography ..... 29

2.3.1.1 Selective Growth or Deposition on Pre-patterned Surfaces ..... 29

2.3.1.2 Transfer Printing ..... 33

2.3.2 Electrocatalysis ..... 35

2.4 Motivation ..... 36

References ..... 38

Chapter 3 ..... 48

*Catalytic Combustion of Carbon* ..... 48

3.1 Catalytic Gasification of Carbon ..... 48

3.1.1 Alkali Metals ..... 49

3.1.2 Alkaline Earth Metals ..... 50

3.1.3 Transition Metals ..... 51

3.2 Catalyst Behavior on Graphite ..... 53

3.2.1 Modes of Catalytic Attack ..... 54

3.2.1.1 Catalytic Pitting ..... 55

3.2.1.2 Catalytic Channeling ..... 56

3.2.1.3 Edge Recession ..... 60

References ..... 63

Chapter 4 ..... 66

*Experimental Techniques* ..... 66

4.1 Thermogravimetric Analyzer ..... 66

4.2 Resistive Heat Treatment Device ..... 69

4.3 Optical Microscopy ..... 71

4.4 Scanning Electron Microscopy ..... 73

References ..... 76

Chapter 5 ..... 77

*Catalytic Combustion as a Synthesis Tool for Micropatterned Carbon Materials* ..... 77

5.1 Introduction ..... 77

5.2 Experimental ..... 82

5.3 Results ..... 86

5.3.1 Catalyst Screening ..... 86

5.3.2 Effect of Carbon Substrate ..... 90

5.3.3 Effect of Salt Concentration ..... 92

5.3.4 Kinetics and Selectivity ..... 94

5.3.5 Micropatterning ..... 97

5.4 Discussion ..... 98

5.5 Conclusions ..... 104

References ..... 105

Chapter 6 ..... 110

*A Magneto-Catalytic Writing Technique for Etching Complex Channel Patterns In Multi-Layer Graphene* ..... 110

6.1 Introduction ..... 110

6.1.1 Catalyst Selection ..... 114

6.2 Experimental Details ..... 115

6.3 Results ..... 118

6.3.1 Pitting ..... 118

6.3.2 Channeling and Complex Pattern Formation ..... 121

6.4 Characterization ..... 124

6.4.1 Thermagravimetric Analysis ..... 124

6.4.2 XRD analysis ..... 126

6.5 Conclusions ..... 129

References ..... 131

Chapter 7 ..... 137

*Conclusions and Recommendations* ..... 137

7.1 Conclusions ..... 137

7.2 Recommendations for future work ..... 141

References ..... 142

# List of Figures

Figure 1.1. Schematic structure of carbon nanofibers and nanotubes. (a) Graphene layer, (b) stacked cone (herringbone) nanofiber, and (c) nanotube. [10]……..……3

Figure 1.2. (a) 1.4-nm-diameter SWNTs in a bundle [11], (b) a MWNT containing a concentric array of nine SWNTs [12]……..……4

Figure 1.3. (a) Herringbone and (b) bamboo-type carbon nanofibers [10]. ..... 4

Figure 1.4. NanoBud: Fullerene is attached to the surface of SWNT [8]. .....5

Figure 2.1. Digital photographs of spin coated carbon thin films. ……16

Figure 2.2. PVD carbon films with different thicknesses……..18

Figure 2.3. Schematic view of graphitic forms. [38]…….....19

Figure 2.4. Graphene graphite relation……...……..….21

Figure 2.5. Large graphene crystal prepared on an oxidized Si wafer by the scotch tape technique……..…..22

Figure 2.6. (a) Scanning-electron micrograph of a large graphene crystal showing armchair and zigzag edges [38] (b) Suspension of graphene microcrystals obtained by ultrasound cleavage of graphite in chloroform and printed graphene film on a substrate……..…23

Figure 2.7. (a) SEM picture of GNR devices fabricated on a 200 nm $SiO_2$ substrate…...27

Figure 2.8. Chemically derived graphene nanoribbons down to sub-10-nm width…..…...28

Figure 2.9. (a) Schematic of procedure used to pattern carbon black thin films (b) Optical micrographs of patterned carbon films. The scale bars are 20, 10, and 25m moving from left to right……..……30

Figure 2.10. Top: Schematic illustration of the procedure for generating three-dimensional (3D) aligned CNTs. Bottom: SEM images of 3D aligned CNT arrays grow selectively on silver-patterned substrate……...…….31

Figure 2.11. (a) Aligned carbon nanotube pattern fabricated by photolithography based on pyrolysis of FePc. (b) of acetylene……...……32

Figure 2.12. Direct growth of graphene patterns from pre-patterned Ni structures. (a) Optical image of a pre-patterned Ni film on $SiO_2$/ Si. (b) CVD graphene is grown on the surface of the Ni pattern……..……...32

Figure 2.13. Schematic of transfer printing of graphene onto a substrate (top) and resulting graphene pattern on $SiO_2$…….…...34

Figure 2.14. Raised feature of height 8nm (left) and trench of half width 35 nm (right) on a-C film by tip induced local modification in vacuum and in oxygen……..….36

Figure 3.1. Schematic representation of graphite structure showing basal plane, edge plane and steps……...…55

Figure 3.2. Scanning electron microscope image of a pit produced by platinum particles.....56

Figure 3.3 Catalytic channeling by KOH at 500$^{o}$C [34]……58

Figure 3.4 Catalytic channeling of Pt particles during graphite oxidation at 750$^{o}$C…….59

Figure 3.5. Channeling of Ni particles in $H_2$ at 800$^{o}$C [29]…….....59

Figure 3.6. Relation between wetting tendency of a catalyst and the mode of catalytic attack [36]…….61

Figure 3.7. Catalyzed edge recession by calcium in steam at 715$^{o}$C [35]…….....61

Figure 4.1. Thermogravimetric analyzer systems with (a) vertical balance and furnace (b) horizontal balance and furnace……..68

Figure 4.2. Digital micrograph of the hot stage oxidizing microscope…….70

Figure 4.3. Example of a liquid crystal texture with different molecular orientations obtained by polarized optical microscopy [4]…….....72

Figure 4.4. An optical microscope image of a cleaved graphite sample containing regions of many different thicknesses. Color shifts indicate a thinner graphene layer in region I compared to region II [6]……...……....73

Figure 4.5. The schematic view of scanning process and image formation of the SEM...74

Figure 5.1. Optical microscope images of PDMS stamp with feature size 200 μm (left), PDMS stamping technique (right)…….85

Figure 5.2. Optical microscope images of metal salt deposits on carbon thin films following microdroplet deposition and drying……...……...88

Figure 5.3. Optical microscope images of gradual appearance of sodium chloride catalysis which at first forms an active but optically invisible thin film……..….90

Figure 5.4. Combustion pattern of Na salt on PVD carbon films…….....91

Figure 5.5. Drying (left) and combustion patterns (right) of Cr salt on as-produced (a) and ozonated (b) spin-coated carbon films……...92

Figure 5.6. Effect of salt concentration on the generation of features by selective combustion…….93

Figure 5.7. Comparison of catalytic and noncatalytic rates on carbon nanoparticles [50,51] prepared from the same precursor and carbonization conditions as the liquid-crystal-derived films…….....96

Figure 5.8. Selection of micropatterning behaviors. (a) Optical micrograph of NaCl micropattern showing excess salt crystals but no visible salt film, (b) same array with salt film visible by SEM, (c) NaCl-catalyzed single-circle feature at high magnification postcombustion (10 min), (d) example of circle features at different stages of combustion in a single sample due to spatial gradients where arrows indicate probable sites of horizontal catalyst migration (10 min), (e) $CrCl_3$ array after drying, and (f) $CrCl_3$ array after partial combustion (3 min)….....98

Figure 5.9. Schematic diagram of the salt film droplet on carbon film……...100

Figure 5.10. Salt film surface density predicted by Eq. (3) as a function of feature size and water contact angle……102

Figure 5.11. Salt film surface density predicted by Eq. (3) as a function of feature radius, *R*, and initial salt concentration, [*C*]……103

Figure 6.1. Optical microscope images of natural graphite surface before (a) and after mechanical exfoliation (b)……...105

Figure 6.2. Hot stage oxidizing microscope modified for close-proximity ferromagnetic actuation….....117

Figure 6.3. SEM images of (a) cobalt particles on natural graphite surface after air oxidation at 560$^{o}$C. (b) Vertical pitting (only in presence of the permanent magnet mounted in fixed position below the substrate)…….....120

Figure 6.4. Demonstration of controlled reactive etching of freshly cleaved natural graphite by magnetic steering. Reaction conditions are 550-580 $^{o}$C in air and $Sm_2Co_{17}$ permanent magnet……..……..123

Figure 6.5. Oxidation behavior of cobalt, graphite and cobalt/graphite mixture by non-isothermal TGA in air at heating rate of 10 $^{o}$C/min…….....…...125

Figure 6.6. XRD spectra of cobalt particles after: (A): air oxidation for 10 min at 400 $^{o}$C (representing early-stage reaction); (B) air oxidation for 30 min at 550 $^{o}$C (representing late-stage reaction); (C) air oxidation for 30 min at 550$^{o}$C in contact with exfoliated graphite with $Sm_2Co_{17}$ permanent magnet below substrate to improve catalyst/carbon contact (to characterize the effect of carbon on Co phase behavior)……..…….128

# List of Tables

Table 2.1. Comparison of electron mobility of materials at room temperature…….24

Table2.2. Room temperature thermal conductivity of graphene and other carbon materials…….....25

Table 3.1. Effect of alkali and alkaline earth oxides on the oxidation……...51

Table 3.2. Effect of catalysts on the ignition temperature of graphite in $O_2$…….52

Table 5.1. Selectivity ratios measured for carbon thin fims doped with saturated solutions of various catalytic salts……..…95

# Chapter 1

# *Introduction*

## 1.1 Carbon Materials and Nanotechnology

Carbon is one of the few elements known since ancient times in the form of charcoal which is usually produced from burned wood. Carbon is widely distributed in nature and carbon compounds form the basis of all known life on Earth. There are several structurally different forms of carbon of which the naturally occurring ones are graphite and diamond. The physical properties of carbon vary widely with the allotropic form. For example, diamond is highly transparent, while graphite is opaque and black. Diamond is among the hardest materials known, while graphite can be one of the softest. Diamond has a very low electrical conductivity, while graphite is a very good conductor. All other carbon products including coke, carbon black or soot, activated carbon, carbon/graphite films, carbon composites and many more are produced from carbonaceous precursors. Until the late twentieth century, carbon compounds have been utilized extensively as combustion materials for the production of synthetic gas, fuel gases and activated carbons

and also for the production of cokes for metallurgical operations. However, discovery of fullerenes in 1985, a family of nanostructred carbon allotropes [1] , made a significant impact in many different scientific areas and led to the synthesis of new forms of carbon including spherical buckyballs [2], carbon fibers [3], carbon nanotubes [4, 5, 6, 7] , carbon nanobuds [8] , glassy carbon and graphene sheets [9] (see Figures 1.1-1.4). These new carbon materials are leading candidates for use in many future technologies, including hydrogen storage, fuel cells, advanced batteries, and high-strength composites. The design, synthesis and modification of these novel carbon-based materials have become the primary research interest in engineering nanotechnology and materials science due to unlimited possibilities of applications.

All these carbon forms are based on the graphite lattice. Graphite consists of stacked up graphene layers, each layer has $sp^2$-bonded carbon atoms densely packed in a honeycomb structure. The $sp^2$-bonded nature of the carbon atoms allows for structural possibilities. Graphene layers are highly anisotropic having different properties when measured in different directions. Therefore, orientational patterns create many structural forms of carbon and are key to the most of the bulk material properties. Introduction of structural defects within the graphene layer causes a distortion of the planar structure. As in the case of fullerenes, insertion of pentagonal rings causes the graphene sheet fold around onto itself to form a cage. Similarly, single wall nanotubes (SWNT) are considered as a graphene sheet that is rolled up into nanoscale tube form. There may be additional graphene tubes around the core of a SWNT to form multi wall nanotubes (MWNTs).

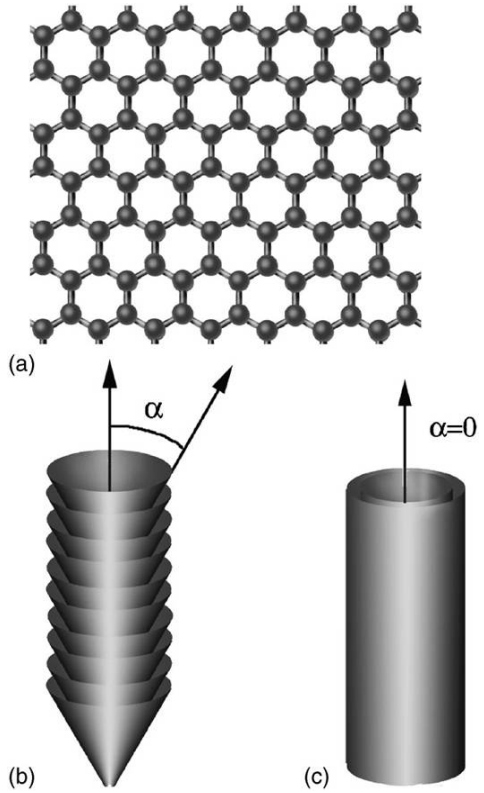


**Figure 1.1.** Schematic structure of carbon nanofibers and nanotubes. (a) Graphene layer, (b) stacked cone (herringbone) nanofiber, and (c) nanotube. [10]

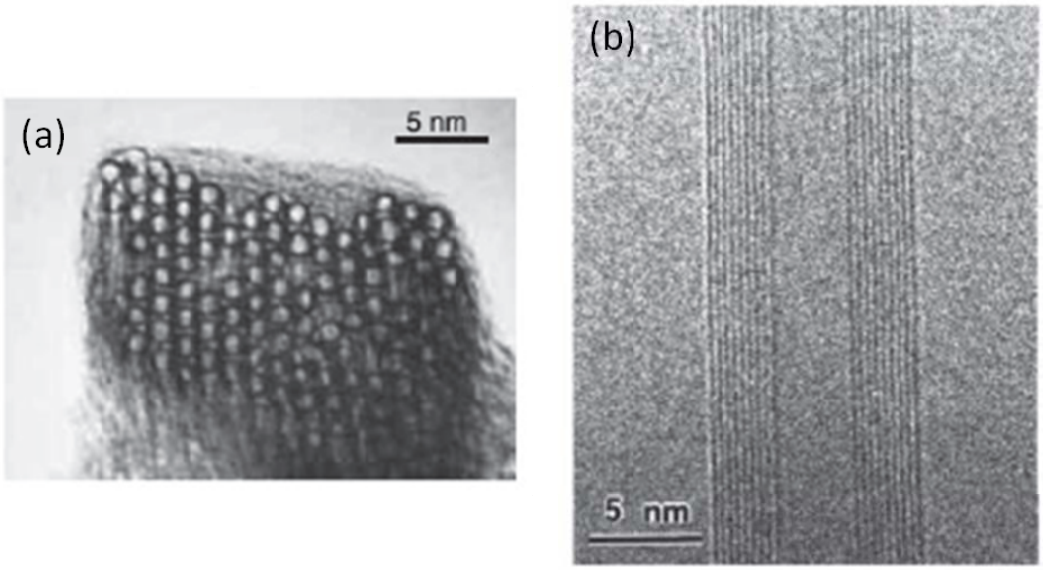


**Figure 1.2.** (a) 1.4-nm-diameter SWNTs in a bundle [11], (b) a MWNT containing a concentric array of nine SWNTs [12].

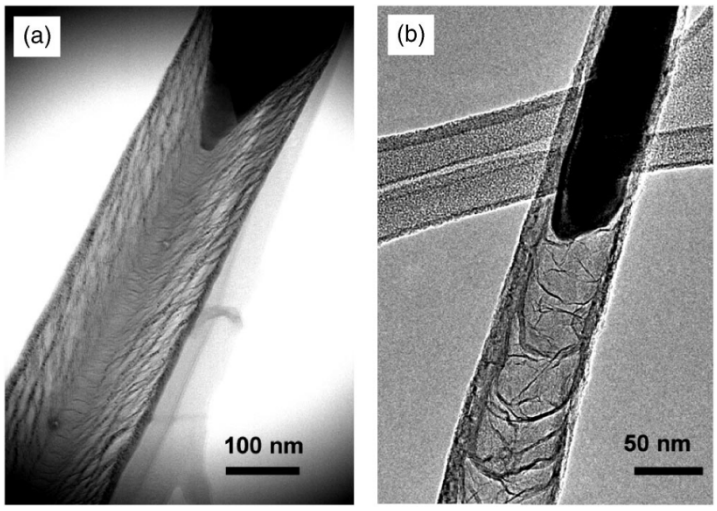


**Figure 1.3.** (a) Herringbone and (b) bamboo-type carbon nanofibers [10].

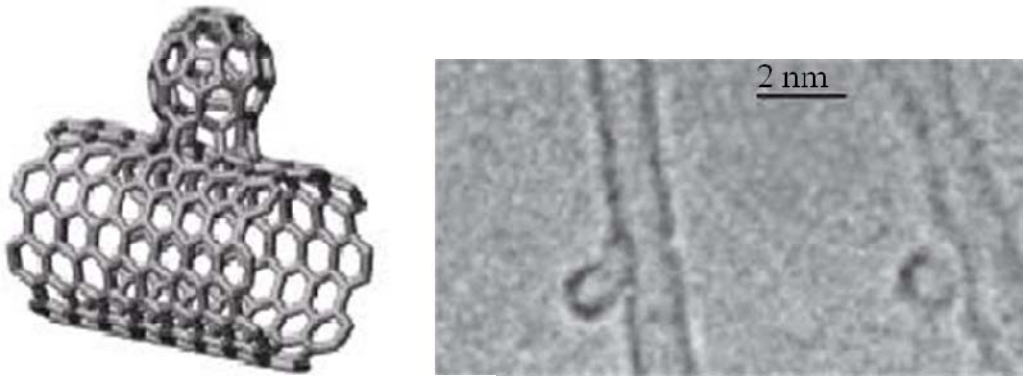


**Figure 1.4.** NanoBud: Fullerene is attached to the surface of SWNT [8].

Depending on the different arrangements of atoms in the material, these new carbon forms show unique and fascinating properties. The most widely used methods to produce carbon nanomaterials especially nanotubes are electric arc discharge [5, 13] laser ablation [11] and chemical vapor deposition (CVD) of hydrocarbons onto catalysis [14,15]. In the arc discharge process, two graphite electrodes are separated by a short distance inside a chamber filled with an inert gas [16, 17, 18]. When current is passed through the electrodes, carbon is vaporized from the graphite anode and deposited onto the negative electrode in the form of small carbon clusters. These clusters rearrange themselves into tubular structures forming multi-walled carbon nanotubes (MWCNT) [19] and single-walled carbon nanotubes (SWCNT) in the presence of metallic nanoparticles [20, 21, 22]. In the laser ablation or evaporation process, a pulsed laser vaporizes a graphite target in a high-temperature reactor while an inert gas is fed into the chamber. Carbon atoms from the high-temperature zone are transferred by the carrier gas to a cold copper collector on which they condense into nanotubes [18]. Along with SWCNTs and MWCNTs,

fullerenes, amorphous carbon, and other carbon products are produced when using the laser ablation technique [23,24, 25]. In a chemical vapor deposition method, after the hydrocarbon decomposes into hydrogen and carbon atoms at high temperatures, carbon atoms diffuse into the metal surface and precipitate out in the form of nanotubes [26, 27]. One of the advantages of the CVD method is that the growth of carbon nanotubes can be controlled by changing the type, size and shape of the catalyst and also adjusting the temperature and type of the hydrocarbon.

In recent years catalytic approach has been used to deposit CNTs on pre-designed lithographic structures [28], producing vertically aligned and ordered arrays of CNTs. Pre-patterning of catalysts by photo-and/or soft lithographic techniques enables controlled synthesis of carbon-based structures through selective growth of CNTs on substrates. Uniformly sized and spaced arrays of aligned CNTs are highly desirable for many applications including microelectronics, electrochemical probes, composite materials, chemical filters and microfluidic devices [10, 29, 30].

Over the last decade, one of the particular interests in carbon nanotechnology is carbon thin films due to their unique optical, mechanical and chemical properties [31, 32, 33, 34]. A variety of graphene layer arrangements in carbon films gives rise to new directional properties and functions. It is not surprising that a number of studies have focused on controling graphene layer orientations in carbon materials for possible applications in molecular electronics, photoconductors, molecular wires and liquid crystal displays [35, 36, 37, 38]. Carbon thin films with controlled electronic and optical properties can lead to a variety of other applications in interdisciplinary fields, which cover chemistry, physics, biology, medicine, materials science and engineering. Isolated

graphene layers as 2D carbon materials [9] have also triggered an intense research activity for the last years. Studies mainly focus on how to understand its properties, and try to find ways to produce it in larger quantities for extensive research and eventually for commercial applications. The design, synthesis and modification of graphene and carbon thin films would create novel carbon materials with variety of unique and potentially very useful characteristics.

Therefore shape control in carbon nanotubes, carbon thin films, graphene layers and other advanced carbon materials in a large-scale is one of the fundamental challenges for the development, construction and application of functional devices in today's nanotechnology.

## 1.2 Objectives

In this thesis low-temperature catalytic oxidation will be presented as a novel technique for shape control and complex pattern formation on carbon materials. Our main interest is to control the geometry and surface structure of carbon thin films and graphene layers in order to obtain pre-determined and specific properties which would be significantly essential for the fabrication of functional carbon-based devices in next generation nanoelectronics and many future technologies.

The work in this thesis was performed with the following objectives:

(1) to demonstrate the concept of catalytic combustion as a synthesis tool for shape/structure control in advanced carbon materials using carbon thin films as a model material and liquid-phase catalyst deposition and dioxygen reaction as a model reaction system.

(2) to explore the possibility of creating arbitrarily complex patterns in multi-layer graphene or graphite films through magnetic steering of single catalyst particles through low temperature oxidation,

(3) to discuss the potential of controlled oxidative etching to extract nanoscale graphitic structures (for example, cut-to-size carbon films, or nanoscale graphene sheets) from larger domains of these materials which would create extemely promising materials for all sorts of applications.

## 1.3 Thesis Outline

General introduction to carbon materials and goals of the thesis are presented in Chapter 1. Chapter 2 provides detailed background for carbon thin films, graphite films, graphene as materials tested in this study. Conventional patterning techniques and challanges for carbon materials are also discussed briefly in Chapter 2. In Chapter 3, catalytic oxidation of carbon as a synthesis or patterning tool and catalyst behaviour on graphite surfaces will be explored. Selection of the catalyst, substrate, reactant and reaction temperature and their dependence on the mode of the catalytic attack will be discussed in detail. Experimental and characterization techniques are described in Chapter 4. Chapter 5 demonstrates the synthesis of patterned carbon thin films through controlled catalytic combustion at 400 $^{o}$C by using microdroplet patterning or polydimethylsiloxane stamping technique to transfer metal salt solutions onto carbon surfaces. Results of testing different metal catalysts, the effect of carbon substrate and salt concentration, kinetics and selectivity of catalysts are discussed in this chapter. In chapter 6, a novel technique is developed for single particle etching of graphite films and multi-layer graphene in complex preset patterns. Ability to produce and control uniform and distinct reaction modes by using external magnetic fields to steer single catalyst particles will be illustrated in detail. Conclusions and the possible directions for future developments will be discussed in Chapter 7.

## References


**[1]** Kroto H.W., Health J. R., O'Brian S. C., Curl R. F., Smalley R. E., *Nature*, (1985) 318, 162

**[2]** Kroto, H. W., Fischer, J. E.&Cox, D. E., eds. (1993) in "*The Fullerenes"* Pergamon, Oxford.

**[3]** Rodriguez N. M., Chambers A., Baker R. T. K., *Langmuir*, (1995) 11, 3862-3866

**[4]** Iijima S., *Nature*, 1991, 354 (6348), 56-58

**[5]** Ebbesen, T. W.; Ajayan, P. M. *Nature* (1992), 358*,* 220-222

**[6]** Chopra, N. G., Luyken, R. J., Cherrey, K., Crespi, V. H., Cohen, M. L., Louie, S. G. and Zettl, A. *Science* (1995)*,* 269**,** 966–967.

**[7]** Tenne, R., Margulis, L., Genut, M. & Hodes, G. *Nature,* (1992)*,* 360**,** 444–446.

**[8]** Nasibulin, Albert G.; et al. "A novel hybrid carbon material". *Nature Nanotechnology*, (2007).2 (3): 156–161.

**[9]** Novoselov, K. S., Geim, A. K., Morozov, S. V., Jiang, D., Zhang, Y., Dubonos, S. V., Grigorieva, I. V. & Firsov, A. A. *Science* (2004), 306**,** 666–669.

**[10]** Melechko, A. V., V. I. Merkulov, T. E. McKnight, M. A. Guillorn, K. L. Klein, D. H. Lowndes, and M. L. Simpson, *J. Appl. Phys*., (2005), 97,041301

**[11]** Thess A., Lee R., Nikolaev P., Dai H., Petit P., Robert J., Xu C, Lee Y. H., Kim S. G, Rinzler A. G., Colbert D. T., Scuseria G. E., Tomanek D., Fischer J. E., Smalley R. E., *Science* (1996)*,* 273, 483.

**[12]** Baughman R. H., Zakhidov A. A., de Heer W. A. , *Science* (2002), 297: 787-792.

**[13]** Journet C, Maser WK, Bernier P, et al., *Nature* (1997) 338, 6644, 756-758

**[14]** Terrones M, Grobert N, Olivares J, et al., *Nature* (1997) 338, 6637, 1997, 52-55

**[15]** Biris, A. R., A. S. Biris, D. Lupu, S. Trigwell, E. Dervishi, Z. Rahman, & P. Marginean. *Chem. Phys. Lett.* (2006) 429: 204–208.

**[16]** Joensson, M., Nerushev, O. A.,Campbell, E. E. B., *Appl. Phys. A*, (2007) 88, 2, 261-267

**[17]** Gamaly E.G., Ebbesen T.W., *Phys. Rev. B,* (1995) 52,3, 2083-2089

**[18]** Poole, C. P., and Owens, F. J. in "*Introduction to Nanotechnology*"; Wiley-Interscience: Weinheim, Germany, 2003.

**[19]** Ajayan PM, Redlich P, Ruhle M, *J. Mater. Search*, (1997) 12, 1, 244-152

**[20]** Zhang Y, Iijima S, Shi Z, Gu Z, *Phil. Mag. Letters*.(1999) 79, 7,473-479

**[21]** Stephan O, Ajayan P.M., Colliex C, Redlich P, Lambert J.M., Bernier P, Lefin P., *Science* (1994) 266, (5191), 1683-1685

**[22]** Dresselhaus, M. S.; Dresselhaus, G.; Eklund, P. C. in "*Science of Fullerenes and Carbon Nanotubes"*; Academic Press, 1996.

**[23]** Guo, T.; Nikolaev, P.; Rinzler, A. G.; Tomanek, D.; Colbert, D. T.; Smalley, R. E., *J. Phys. Chem.* (1995), *99*, 10694-10697.

**[24]** Jorio A.,Saito R., Hafner J.H., Lieber C.M., Hunter M., McClure T., Dresselhaus G. and Dresselhaus M.S.*,Phys. Rev. Lett.* (2001), 86

**[25]** Saito, R.; Fujita, M.; Dresselhaus, G.; Dresselhaus, M. S., *Appl. Phys. Lett.* (1992), *60*, 2204-2206.

**[26]** Ren, W. C.; Li, F.; Cheng, H. M., *J. Phys. Chem. B* (2006), *110*, 16941-16946.

**[27]** Kong, J.; Soh, H. T.; Cassell, A. M.; Quate, C. F.; Dai, H. J., *Nature* (1998), *395*, 878-881.

**[28]** Dresselhaus M.S., Dresselhaus G. and Avouris P., In "*Carbon Nanotubes: Synthesis, Structure, Properties and Applications*" Springer Series in Topics in Applied Physics vol. 80**,** Springer, Berlin (2001).

**[29]** Fan S. S., Chapline M. G., Franklin N. R., Tombler T. W., Cassell A. M., Dai H. J.,*Science*, (1999) 283 (5401) , 512-514

**[30]** Jensen, K., Weldon, J., Garcia, H.), Zettl, A., *Nano Letters*, (2007) 7 (11), 3508-3511

**[31]** Kiema G.K., Brett M.J., *J. Electrochem. Soc.* (2003) 150 (7) E342–E347.

**[32]** Narayan R.J., *Int. Mater. Rev*. (2006) 51 (2) 127–143.

**[33]** Vanhulsel A., Velasco F., Jacobs R., Eersels L., Havermans D., Roberts E.W., Sherrington I., Anderson M.J., Gaillard L., *Tribol. Int.* (2007) 40 (7) 1186–1194.

**[34]** Harris S.J., Weiner A.M., Tung S.C., Simko S.J.,. Militello M.C, *Surf. Coat. Technol*. (1993) 62 (1–3) 550–557.

**[35]** Samori P., Rabe J. P., *J. Phys. Cond. Matter*., (2002), 14, 9955-9973

**[36]** Keil M., Samori P., des Sandtos D. A., Kugler T., Stafstrom S., Brand J. D., Mullen K., Bredas J. L., Rabe J. P., Salaneck W. R., *J. Phys. Chem. B*., (2000), 104, 3967

**[37]** Kawata K., *Chemical Record*, (2002), 2, 59-80

**[38]** Adam D., Schuhmacher P., Simmerer J., Haussling L., Siemensmeyer K., Etzbach K. H., Ringsdorf H., Haarer D., *Nature*, (1994), 371, 141-143

# Chapter 2

# *Relevant Background*

## 2.1 Carbon Thin Films

Carbon films have outstanding properties such as chemical inertness, high hardness, high electrical resistivity, high thermal conductivity, high dielectric strength and infrared transparency. These films find application as thin film electrodes [1-3], lithographic masks [4-6], optical components, gas separation, ultrafiltration membranes [7-10] or material coatings designed for biocompatibility [11,12], lubrication [13,14], abrasion resistance [14,16], corrosion resistance or thermal and electrical conductivity [17,18]. Existing synthesis routes for carbon films include physical vapor deposition (PVD), pulsed laser deposition [19, 20, 21] ion beam deposition [22,23], sputtering [24,25], chemical vapor deposition (CVD) [26, 27] and microwave plasma CVD and pyrolytic deposition [28-30]. The properties of carbon films strongly depend on the precursor

material and method of deposition. Depending on the conditions, varying proportions of $sp^3$ and $sp^2$ bonded carbon films can be obtained in which composition ranges from $sp^2$-rich (almost 100% $sp^2$), glassy or sputtered carbon, to $sp^3$-rich (up to 80% $sp^3$), tetrahedral a-C (ta-C) or amorphic diamond (a-D) [7]. a-C materials are astonishingly different, as they can be either dark and soft (evaporated carbon), or almost as hard as diamond and quite transparent (ta-C). Of particular interest is to have patterned carbon thin films on substrates which would give rise to new directional properties and functions.

### 2.1.1 Liquid Crystalline Derived Carbon Films

Carbon films with different crystal structures, such as carbon films with graphene layers lying perpendicular to the substrate surface are not readily obtainable by conventional high-temperature synthesis routes. Jian et al. showed a new technique for molecular control in carbon films using liquid crystalline surface anchoring and flow [31]. Liquid crystal (LC) is a state of matter that is intermediate between an isotropic liquid and a crystalline solid. In general, liquid crystals are thermotropic (those that form as temperature increases) or lyotropic (those that form as their concentration in solution increases), and can be calamitic (rod-like) or discotic (disk-like).

Carbon thin films can be prepared from alternative liquid crystalline precursors composed of sulfonated polyaromatic dyes. These disk-like planar molecules undergo massive π-stacking in aqueous solution to form rod-like aggregates. At high concentrations or on surfaces, these rods or molecular columns align by repulsive

interactions (lyotropic behavior), giving rise to a transverse alignment of the stacked polyaromatic disks. The water-soluble lyotropic dye, indanthrone disulfonate, is one of the precursors in which polyaromatic faces remain hydrophilic, and this leads to extensive π-stacking in aqueous solution [32, 33, 34]. In other words, indanthrone disulfonate exhibits liquid crystallinity while in low viscosity solution and therefore, can be processed in water at room temperature allowing it to be spin coated or bar-coated into uniform fully dense carbon films. These films exhibit surfaces rich in graphene edge-sites and are either anisotropic unidirectional (by bar coating) or multi-domain with long-range isotropy (by spin coating). Such thin films can be obtained by spin coating or meyer bar coating of indanthrone disulfonate on quartz substrates followed by drying and direct carbonization at 700 $^{o}$C. Detailed information can be found in [31]. Carbon films produced by spin coating are fully dense, 100% anisotropic, thin (200-300nm) and partially transparent. (see Figure 2.1)

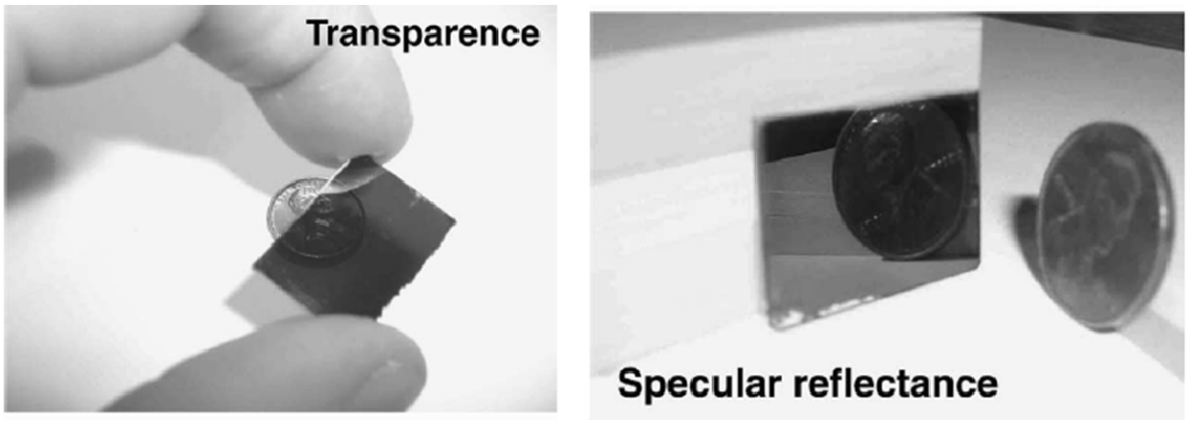


**Figure 2.1.** Digital photographs of spin coated carbon thin films.

### 2.1.2 Physical Vapor Deposition Films

Physical vapor deposition (PVD) is one of the common techniques to make carbon thin films on substrates. PVD is a process in which thin film of material is deposited on a substrate in a high vacuum environment. First, carbon thread is converted into vapor phase by applying heat, causing it to undergo evaporation. Then, the vapor undergoes condensation on the substrate to form the thin film of carbon. Heating of the carbon thread usually involves resistive heating, where a wire of low vapor pressure metal such as tungsten is used to support strips of the material to be evaporated [35]. The wire is then resistively heated, so that the carbon thread melts first and then evaporates. This is done in a high-vacuum environment, so that the vaporized atoms or molecules will be transported to the substrate with minimal collision interference from other gas atoms or molecules. One of the advantages of using PVD is that film thickness can easily be controlled by fixing the operating parameters and adjusting the deposition time. Also, because this technique requires high vacuum conditions, purity of the resulting carbon thin films is also very high.

Figure 2.2 shows PVD films made by vaporizing doubly-configured carbon thread (Technotrade International, Inc.; BU007131-T) onto quartz substrate for 6 s below 1 Pa in a Bal-Tec CED 030 carbon evaporator. [36, 37]

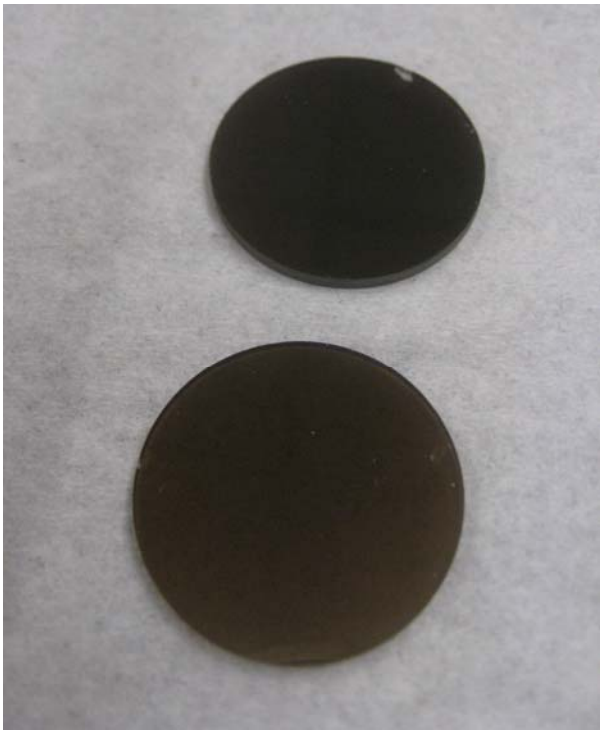

**Figure 2.2.** PVD carbon films with different thicknesses.

## 2.2 Single Crystal Natural Graphite

Nearly perfect crystals of graphite can be found in nature or obtained synthetically by high-temperature treatment of pyrolytic graphite. Synthetic graphites are referred as highly oriented pyrolytic graphite (HOPG) and they consist of high degree of preferred crystallographic orientation. Natural crystals of graphite (NG) occur in a number of locations, such as Madagaskar, Russia and the Ticonderoga area in NY. Among these selected crystals from Ticonderoga, NY occur as large flakes of single crystals of high crystallographic perfection. Both HOPG and NG have been extensively used in research for measurements of physical properties, studies of reactivity changes or catalytic

oxidation reactions. Recently, most of the experimental and theoretical studies carried out on these single crystals have focused on characteristic cleaving properties so that 2D graphene layers can be isolated from 3D graphite crystals.

### 2.2.1 Graphene

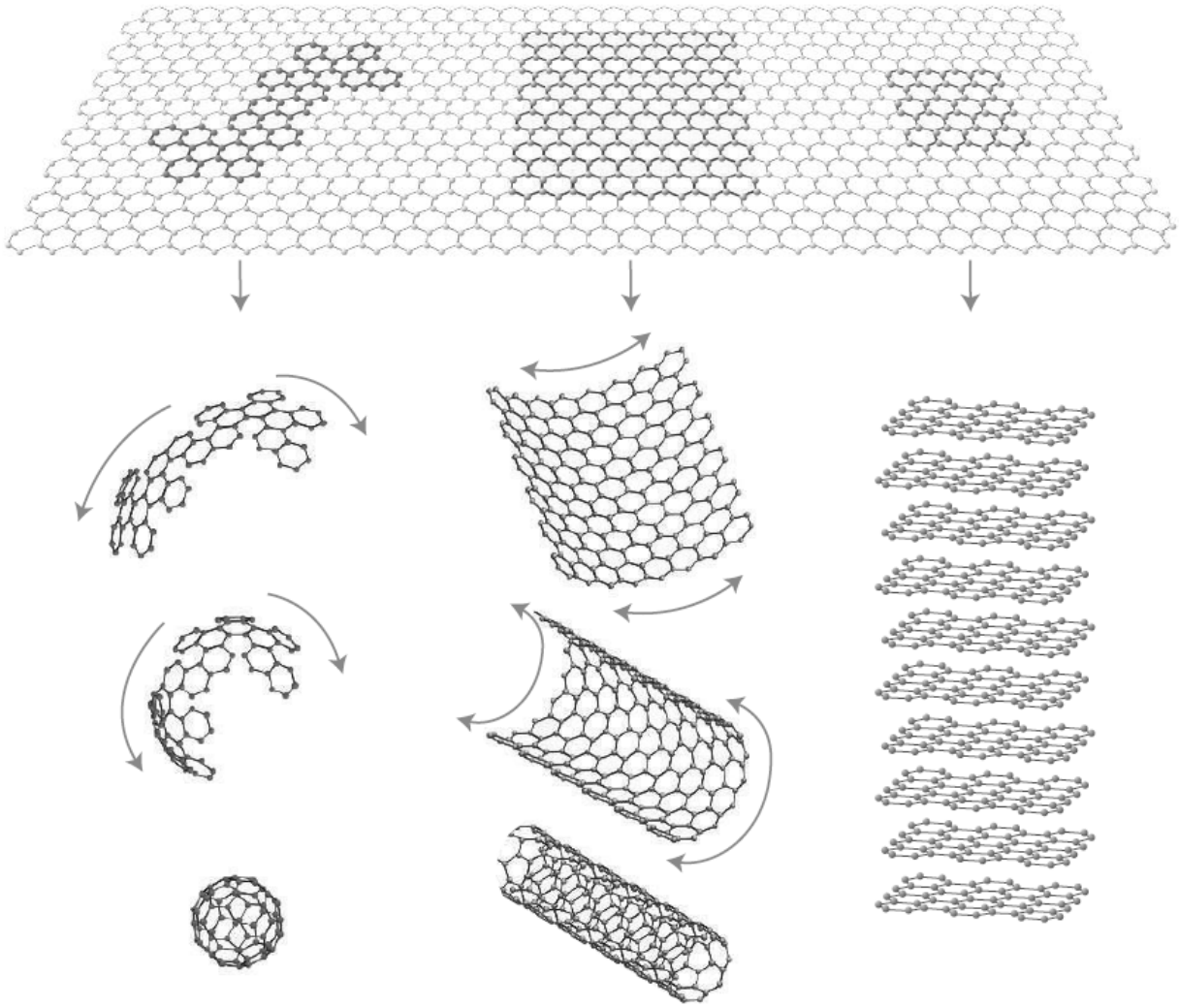

**Figure 2.3.** Schematic view of graphitic forms. [38]

Graphene is a two-dimensional material in which $sp^2$-bonded carbon atoms are arranged in a honeycomb lattice that is just one layer of atoms thick (see figure 2.3). Surprising mechanical, structural, and electronic properties of one-atom-thin graphene sheets quickly grabbed widespread attention in the scientific world. Most of the research focuses on exploring methods for synthesizing graphene in commercial quantities, chemically modifying the material and having predetermined specific properties for potential commercial applications. The graphene structure has been known since long before its first discovery in 2004 [39] as a free standing two dimensional crystals. Basically, graphite has been used as pencil lead for centuries and every time one scrapes a line on a paper, the resulting mark contains flakes of graphene. Similarly, for years, scientists have discussed and described the properties of many carbon-based materials in terms of sheets of graphene. Graphite, for example, is described as a three-dimensional crystal built from graphene layers (Figure 2.4). And fullerenes, including carbon nanotubes and buckyballs, which have been known since the 1980s, are thought of as wrapped or rolled-up forms of graphene sheets. On the other hand, although known as an integral part of 3D materials, graphene was assumed not to exist in the free state and was believed to be unstable with respect to formation of curved structures such as soot, fullerenes and nanotubes.

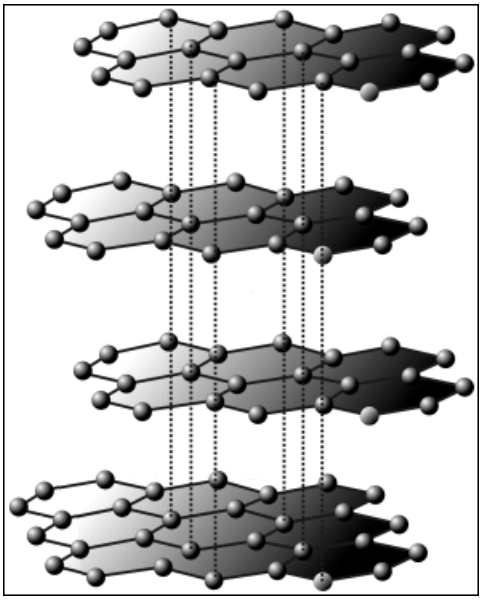

**Figure2.4.** Graphene graphite relation.

Graphene was first isolated as a 2D crystal by peeling it off from highly oriented pyrolytic graphite (HOPG) with Scotch tape and optically identify it by transferring to a $SiO_2$ layer on Si [39]. The method (often referred to as mechanical exfoliation or a scotch-tape technique) provides crystals of high structural and electronic quality [40] which can reach millimeter size (figure 2.5) However yields for this method are low and involve searching the substrates for single sheets and optical microscope, atomic force microscopy (AFM) and Raman techniques must be performed in order to provide existence of graphene sheets.

Although mechanical cleavage of graphite originally led to the discovery of graphene sheets and is the process currently used in most experimental studies, different methods other than mechanical exfoliation of 3D graphite crystals have been proposed to obtain graphene. These include epitaxial growth by thermal decomposition of SiC [41-46] or by

chemical vapor deposition of hydrocarbons on metal substrates [47-50], sonication in various solvents [51 52], intercalation [53] and chemical reduction of graphite to obtain few-layer graphite oxide (figure 2.6) [ 54-57].

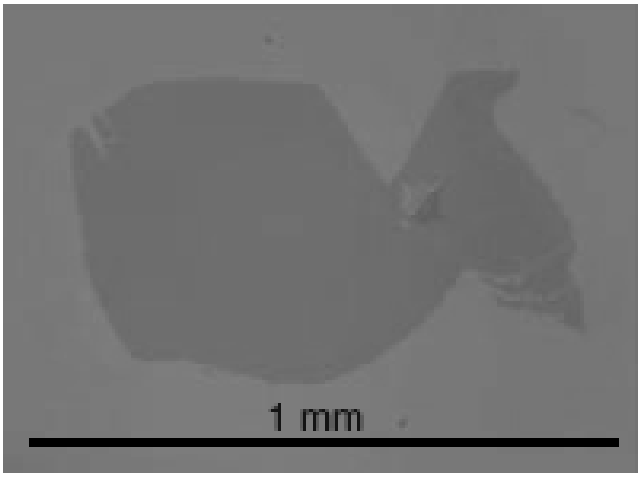


**Figure 2.5.** Large graphene crystal prepared on an oxidized Si wafer by the scotch tape technique. [Courtesy of Graphene Industries Ltd.]

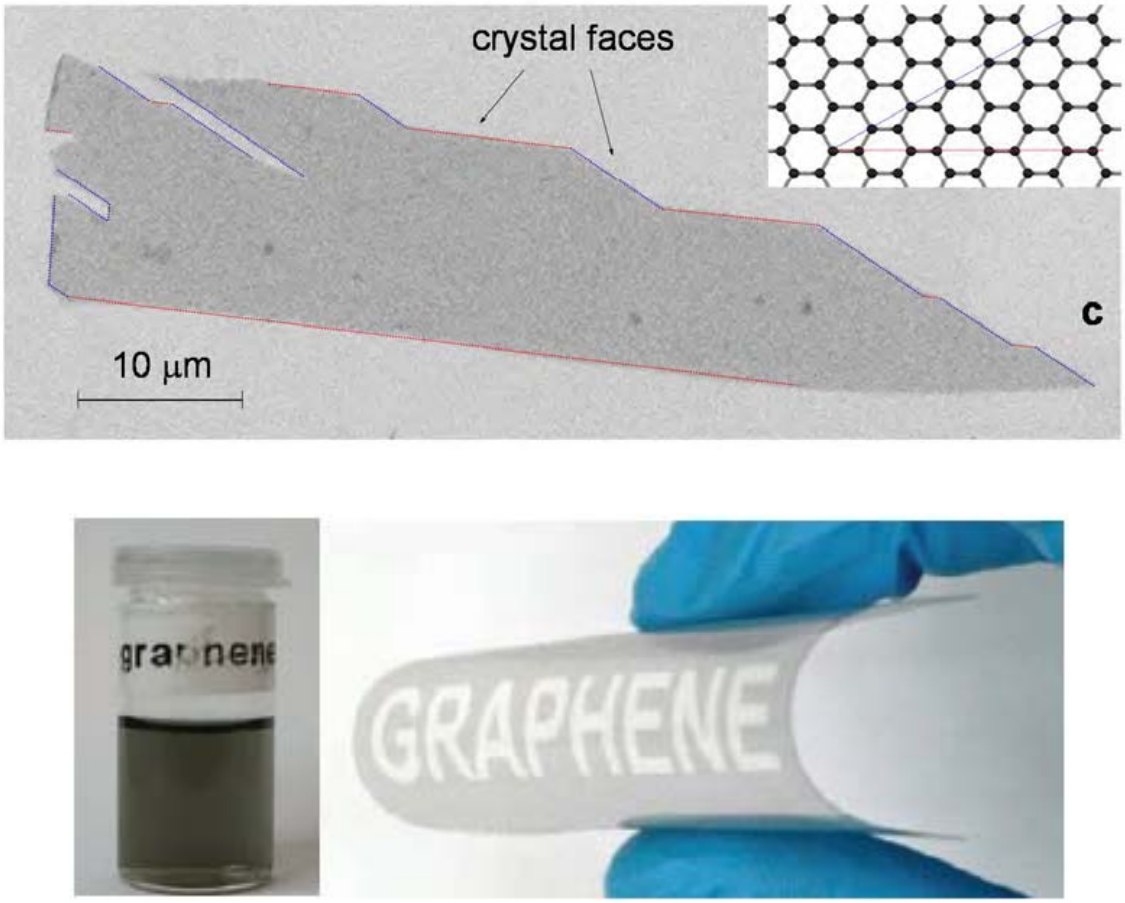


**Figure 2.6.** (a) Scanning-electron micrograph of a large graphene crystal showing armchair and zigzag edges [38] (b) Suspension of graphene microcrystals obtained by ultrasound cleavage of graphite in chloroform and printed graphene film on a substrate [Courtesy of R. Nair, University of Manchester]

A single atomic plane is considered as a 2D crystal, whereas 100 layers are considered as a thin film of a 3D material. For the case of graphene, the electronic structure gradually changes with the number of layers, approaching the 3D limit of graphite after 10 layers [58]. Therefore, according to the layer number, graphenes can be distinguished as single, double, and few (3–10) layer graphene. [38]. For practical applications, multilayer graphene sheets are preferable in terms of mechanical strength for supporting large- area

film structures, whereas thinner graphene films have higher optical transparency [59]. Graphene exhibits unusual electronic, mechanical, optical and chemical properties. The limit to mobility of electrons in graphene is about 200,000 $cm^2$/Vs at room temperature, compared to about 1,400 $cm^2$/Vs in silicon, 100,000 $cm^2$/Vs in carbon nanotubes [60] and 77,000 $cm^2$/Vs in indium antimonide, the highest mobility conventional semiconductor known [61] (see table 2.1)

**Table 2.1.** Comparison of electron mobility of materials at room temperature.

| Silicon | Indium antimonide | CNTs | Graphene |
|---|---|---|---|
| 1,400 $cm^2$/Vs | 77,000 $cm^2$/Vs | 100,000 $cm^2$/Vs | Over 200,000 $cm^2$/Vs |

Mobility can also be expressed as the conductivity of a material per electronic charge carrier, and so high mobility is also advantageous for chemical or bio-chemical sensing applications in which a charge signal from, for instance, a molecule adsorbed on the device, is translated into an electrical signal by changing the conductivity of the device [61, 62].

Graphene has very high room temperature thermal conductivity of up to 5300 W/mK [63-65]. Table 2.2 provides comparison of the thermal conductivity reported for graphene [66] with the experimental data reported for other carbon materials [67, 68]. Huge range of the thermal conductivities of carbon materials enables them to serve both as thermal

insulators (some of the diamond like carbons or amorphous carbons) as well as the “heat superconductors” such as graphene.

**Table 2.2.** Room temperature thermal conductivity of graphene and other carbon materials

| Diamond | Single Carbon Nanotube | CNT Bundles | Graphene |
|---|---|---|---|
| 0.2 W/mK | 3500 W/mK | 1750-5800 W/mK | 4840-5300 W/mK |

Recently, graphene has been reported to be the strongest material ever tested [69]. Mechanical properties of monolayer graphene membranes suspended over open holes can be measured by utilizing an atomic force microscope (AFM) nano indentation. Spring constant of graphene is in the range 1-5 N/m and the Young's modulus is 0.5 TPa, which differs from that of bulk graphite. These high values make graphene very strong and rigid material and raise the possibility of using graphene for nano-electro-mechanical systems (NEMS) applications such as pressure sensors, and resonators [70]

Overall, these outstanding properties of graphene make it a great candidate for applications in chemical sensing instruments [62], high-speed analogue electronics, spintronics [61], microchips, biosensors [71], ultracapacitance devices [72], flexible displays and other innovations [73,74]. Another significant advantage of graphene is its two-dimensionality, making it compatible with existing planar device architectures.

Much of the recent work focuses on controlling the geometry of graphene on a nano- or micrometer scale, so that one could obtain unique structures with well-defined physical and chemical properties.

### 2.2.2 Graphene Nanoribbons

Graphene nanoribbons (GNRs) are single layers of graphene that are cut in a particular pattern to give it certain electrical properties. When graphene is patterned into a narrow ribbon and the carriers are confined to a quasi-one-dimensional (1D) system and these charge carriers create an energy gap. Similar to CNTs, this energy gap depends on the width and crystallographic orientation of the graphene nanoribbon (GNR) [75,76]. Graphene ribbons with either metallic or semiconducting electronic structure are possible, depending on the crystallographic direction of the ribbon axis [77]. For instance, when a single graphite layer is terminated by zigzag edges on both sides, localized electronic states at each edge can be obtained [78]. Son et al. showed half-metallicity in nanometer-scale zigzag graphene ribbons (ZGNR) by controlling their magnetic properties if homogeneous electric fields are applied across the zigzag-shaped edges of the graphene nanoribbons. It has been shown that resistivity of a graphene nanoribbon increases as its width decreases, indicating the impact of size of the ribbons (Figure 2.7) [79]. The combination of lithography and etching is the most common procedure currently used to confine the width of graphene and thus to fabricate GNRs with various sizes. GNRs as narrow as 20 nm can be fabricated by e-beam lithography

and oxygen plasma etching [79,80], however there are difficulties in obtaining smooth edges and reaching the true nanometer scale ribbon width.

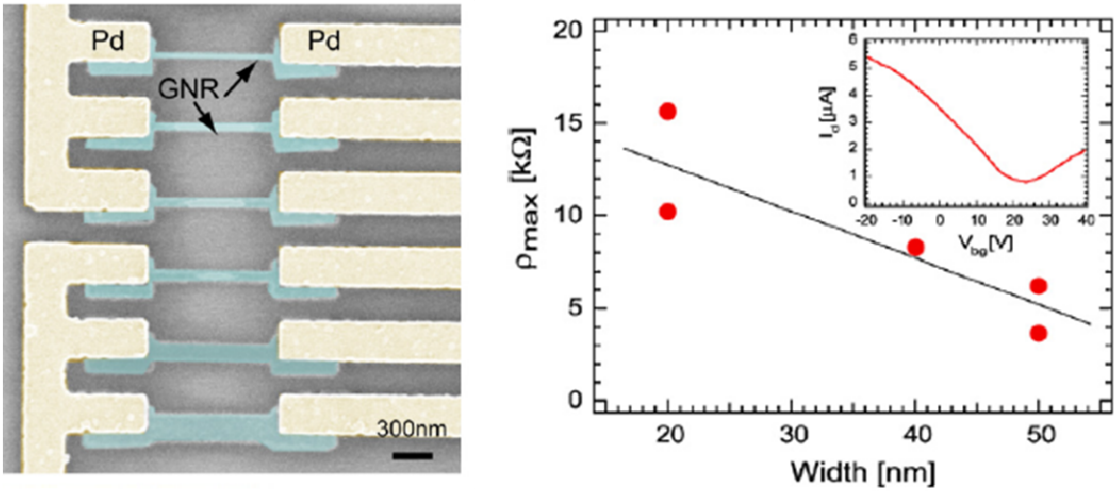


**Figure 2.7.** (a) SEM picture of GNR devices fabricated on a 200 nm $SiO_2$ substrate. The widths of the GNRs from top to bottom are 20, 30, 40, 50, 100 and 200 nm.(b) Maximum resistivity of GNRs as a function of ribbon width [79].

Chemical approaches and self assembly processes [56, 81,82] has also been proposed to make graphene structures with desired shape and dimensions for fundamental and practical applications. Li et al. [52] developed a chemical route to produce GNRs with varying widths along their lengths as well as single ribbons with widths down to 10 nanometers (figure 2.8).

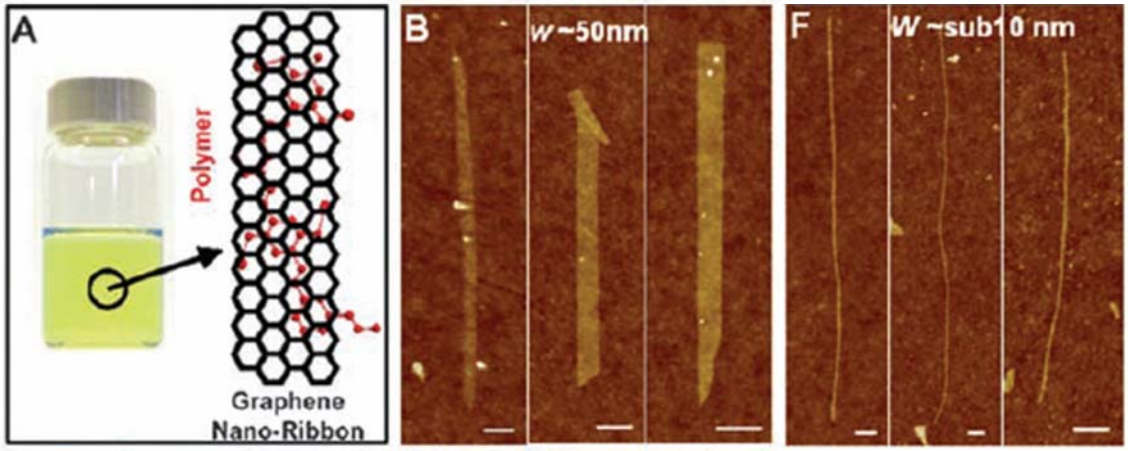


**Figure 2.8.** Chemically derived graphene nanoribbons down to sub-10-nm width [52].

## 2.3 Patterning Techniques for Carbon Thin Films and Graphene

The practical realization of micro- and nanoscale devices based on carbon materials requires precise engineering of carbon films, nanotubes or graphene layers on substrates. Patterning carbon materials has attracted considerable attention in the recent years because of their significant importance to many of the applications that range from electronic devices to solar cells to lubricants or to biocompatible coatings. Various techniques including standard lithography [79, 83-86], soft lithography [87, 88], and self-assembly [89], transfer printing [40,90], plasma etching [62, 91] or electrocatalysis [92] have been applied for systematically modifying the structure and fabricating carbon-based devices. Some of the examples of patterned carbon films, carbon nanotubes and graphene layers by different methods are provided in the next pages.

### 2.3.1 Lithography

#### 2.3.1.1 Selective Growth or Deposition on Pre-patterned Surfaces

Carbon black filled composite thin films have been patterned using a traditional photolithographic lift-off process [93] which includes several steps; spin coating a photoresist layer onto glass substrate, patterning the photoresist by ultraviolet light through a mask, layer-by-layer deposition of carbon film and removal of the underlying photoresist (Figure 2.9). The resolution that can be achieved using this procedure is around 5 μm.

Similarly, fabrication of 3D aligned carbon nanotube patterns by multi-step process based on photolithography and selective growth is outlined in Figure 2.10. Aligned carbon nanotube arrays on metal patterned substrates are obtained by pyrolysis of hydrocarbon and removal of metal pattern by chemical etching process [94]. However, morphology, length, density, and structure of the aligned CNT arrays are very sensitive to the varying experimental conditions.

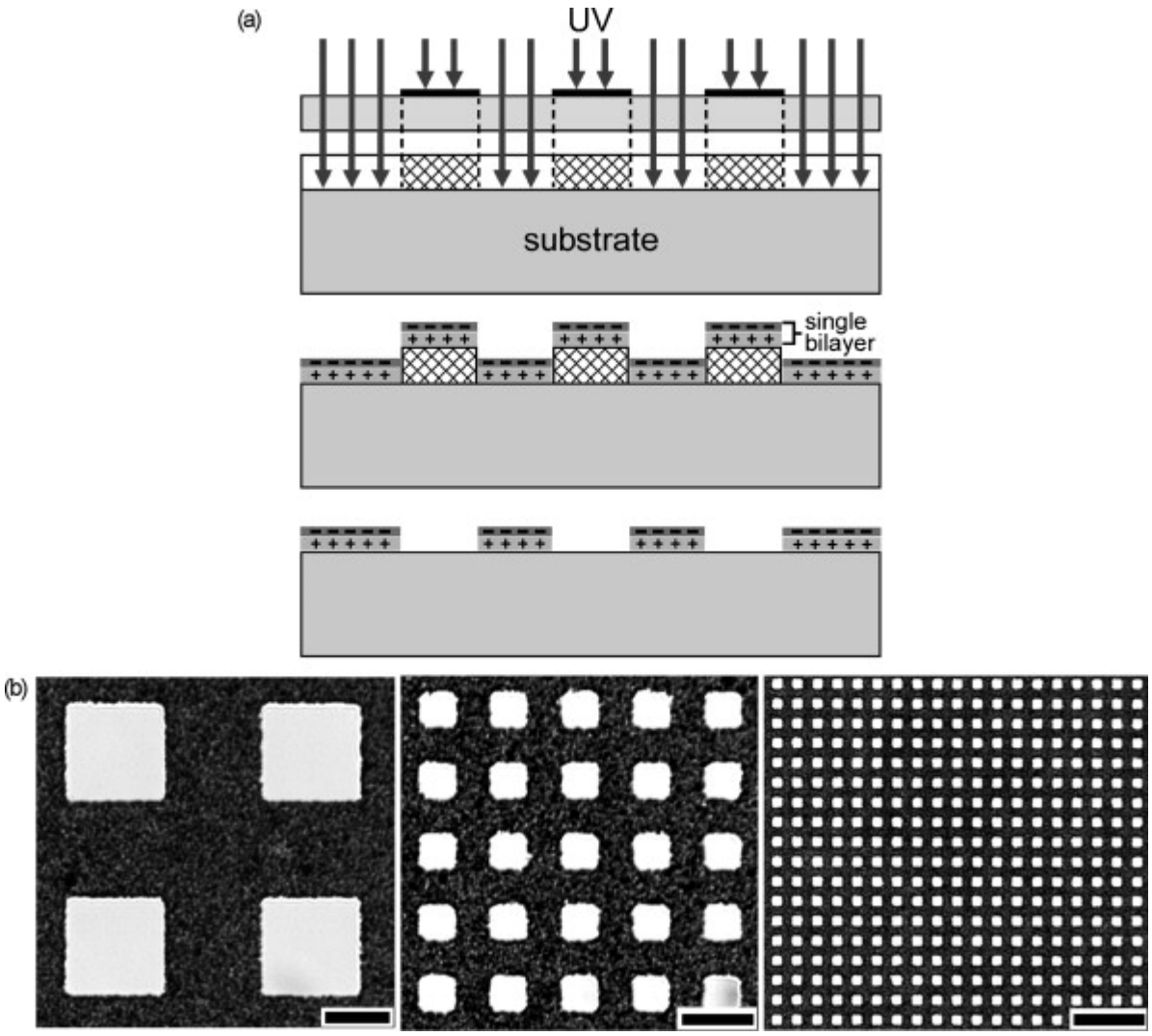


**Figure 2.9.** (a) Schematic of procedure used to pattern carbon black thin films (b) Optical micrographs of patterned carbon films. The scale bars are 20, 10, and 25 um moving from left to right [93]

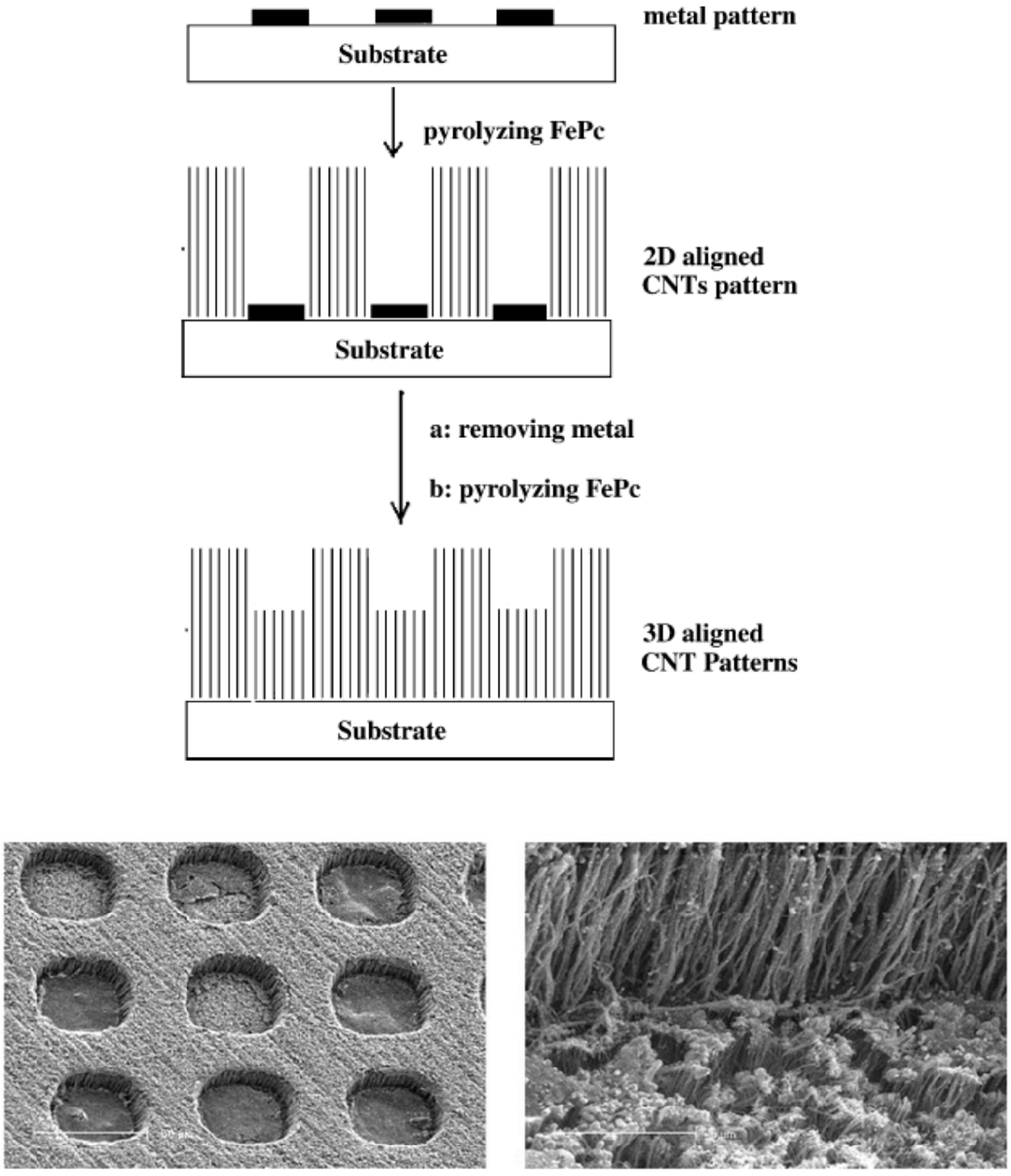


**Figure 2.10.** Top: Schematic illustration of the procedure for generating three-dimensional (3D) aligned CNTs. Bottom: SEM images of 3D aligned CNT arrays grow selectively on silver-patterned substrate [94]

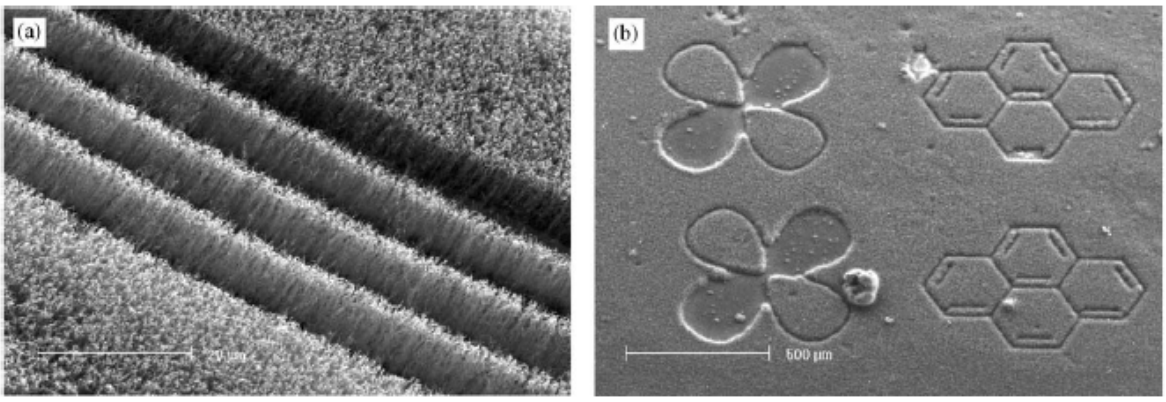


**Figure 2.11.** (a) Aligned carbon nanotube pattern fabricated by photolithography based on pyrolysis of FePc. (b) of acetylene [95]

Analogous to the carbon nanotube growth [96,97], single or multi layer graphene sheets are grown at particular locations and with desired geometries by controlling the catalyst morphology and position [48]. Figure 2.12 demonstrates the direct chemical vapor deposition growth of a graphene pattern using a pre-patterned Ni structure.

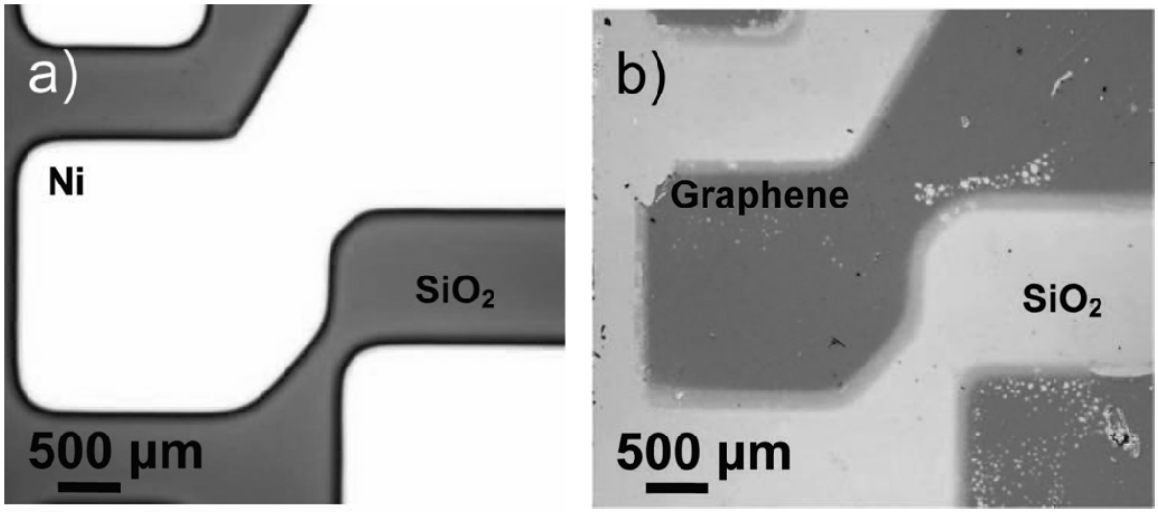


**Figure 2.12.** Direct growth of graphene patterns from pre-patterned Ni structures. (a) Optical image of a pre-patterned Ni film on $SiO_2$/ Si. (b) CVD graphene is grown on the surface of the Ni pattern [48].

#### 2.3.1.2 Transfer Printing

In this technique an elastomeric stamp or mold, usually a poly(dimethylsiloxane) (PDMS) block, with patterned relief structures on its surface is used to generate patterns. First the PDMS block is patterned by conventional photolithographic techniques. Then, these elastomeric stamps are used to cut and exfoliate a graphene piece from bulk graphite (see Figure 2.13.) and the quality of the graphene sheet that is attached on the stamp is inspected by microscope. Then, if the graphene printed on the stamp is good enough, the next step is to transfer the graphene sheet by establishing a direct contact with the substrate to be patterned [90, 98]. However, deformation and distortion of the elastomeric stamp/mold during printing need to be completely understood. Because the elasticity and thermal expansion of PDMS make it difficult to get high accuracy during applying across large areas, it may limit the utility of lithography in multilayer fabrication and/or nanofabrication. This technique requires precise control on transferring the graphene pattern in order to get good quality structures because resolution depends on the mechanical contact between PDMS stamp and the substrate.

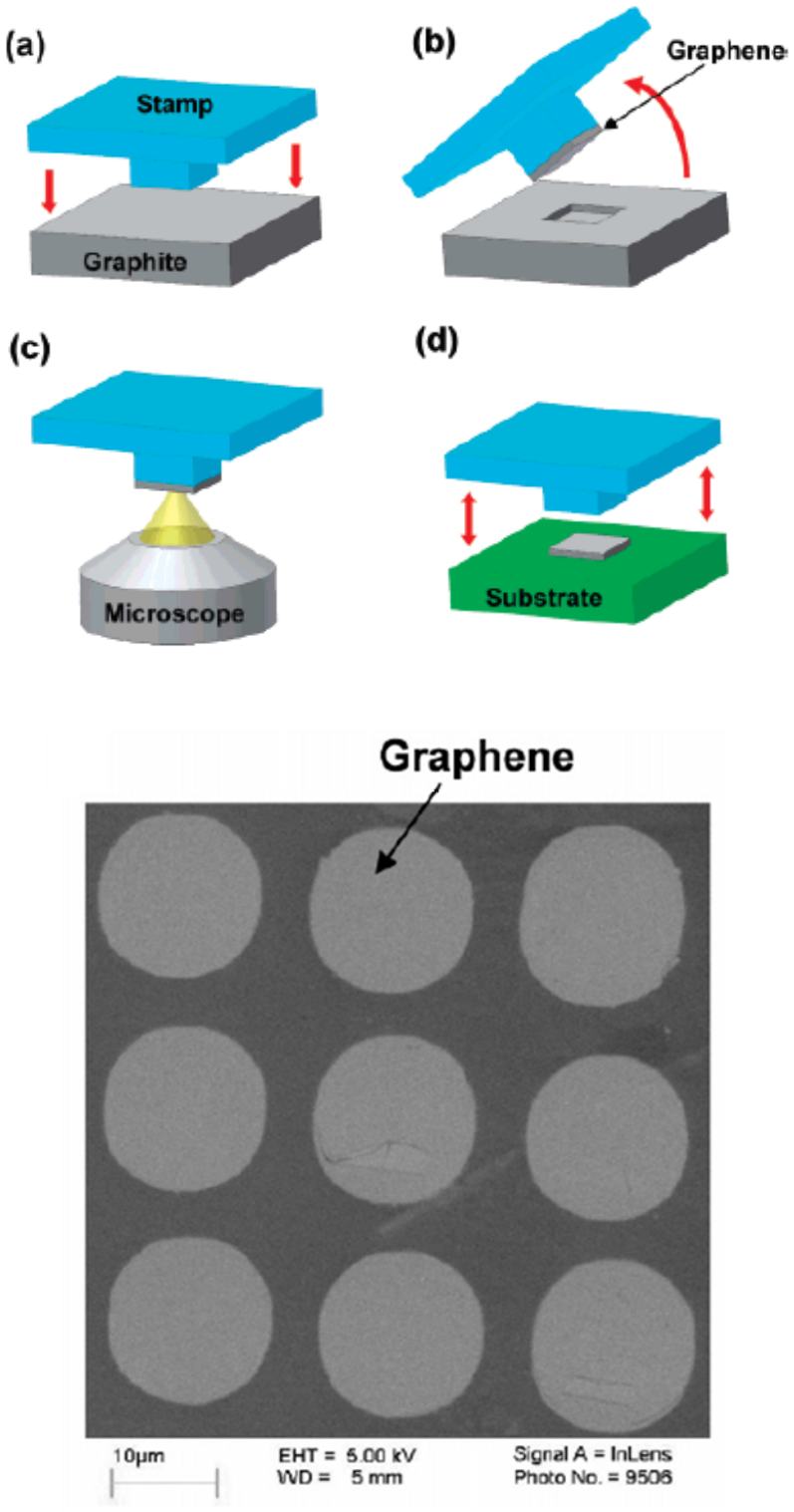


**Figure 2.13.** Schematic of transfer printing of graphene onto a substrate (top) and resulting graphene pattern on $SiO_2$ [90].

### 2.3.2 Electrocatalysis

The literature contains a few reports of pattern formation in carbon films by probe–based local modification. This technique typically involves using high voltages or currents across the tunneling junction or mechanical indentation of the carbon surface directly with the scanning probe tip [99, 100]. The voltage pulse height and length and also the height of the tip above the carbon surface when the pulse is applied have an effect on the results of patterning process. Eagle et al. reported writing nanoscale pits in amorphous carbon layers using a scanning tunneling microscope (STM) [100].

A similar method has been suggested by Muhl et al., for patterning carbon films based on either local graphitization of amorphous carbon films (a-C) in vacuum [101,102] or local oxidation [103] by using a scanning force microscope (SFM) tip. It is proposed that the local Joule heating due to the introduced power is the main reason for graphitization and raised features on the a-C film. However, in the presence of oxygen, applied voltage at the tip of a SFM induces local consumption of the carbon layer and results in trenches or pits on a-C surface (Figure 2.14). The main disadvantage of this technique is the slow patterning or writing speed. In addition to that, it is difficult to distinguish the written marks from the background surface due to surface roughness of the a-C layer.

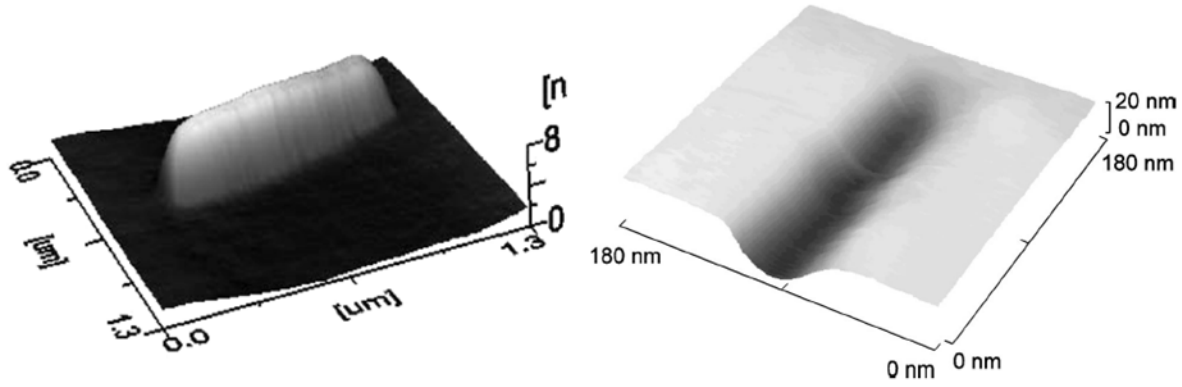


**Figure 2.14.** Raised feature of height 8nm (left) and trench of half width 35 nm (right) on a-C film by tip induced local modification in vacuum and in oxygen [101,103].

## 2.4 Motivation

The main obstacle in current patterning technology is inability to produce large amounts of identical carbon nanostructures. For example, nanotubes come in different sizes and structures and the same is true of many other carbon materials. There is no reliable way to directly produce a single CNT type such as will be needed in large integrated systems or no straightforward way exists of patterning even simple CNT based materials. Similarly patterning carbon thin films and graphene is limited by the resolution of current lithographic techniques.

For the case of graphene, it needs to be patterned with high precision down to nano level for the proposed next-generation devices. Such precision seems not possible through a combination of standard lithographic and chemical methods discussed so far. State-of-

the-art lithographic technology does not allow the formation of a uniquely defined graphene ribbon edge, such as, armchair or zigzag, but a mixture of edges may co-exist along the length of the graphene ribbon. This is likely the result of the present limitations of lithography rather than an intrinsic feature of graphene ribbons.

So, fabrication of precise graphene nanoribbons, graphene-based electronic devices/circuits or other patterned carbon film structures with well-defined geometry remains an important challenge. At present, it appears that revolutionary advances in process technology are needed to obtain reproducible characteristics for large-scale integration of carbon based devices.

Catalytic carbon combustion could be used for selectively removing material near strategically placed catalyst particles or films, and thus become a tool for shaping or patterning advanced carbon materials. This concept is especially attractive for carbon due to the lack of convenient liquid-phase etchants, such as those that exist for lithographic polymers and most other materials. Therefore, controlled oxidative etching to extract nanoscale graphitic structures (for example, cut-to-size carbon films, or nanosize graphene sheets) from larger domains of these materials would create extremely promising materials for all sorts of applications.

## References

**[1]** Kiema G.K., Brett M.J., *J. Electrochem. Soc.* 150 (2003) (7) E342–E347.

**[2]** Kim J., Song X., Kinoshita K., Madou M., White R., *J. Electrochem. Soc.* 145 (1998) (7) 2314–2319.

**[3]** Ranganathan S., McCreery R.L., Majji S.M., Madou M., *J. Electrochem. Soc.* 147 (2000) (1) 277–282.

**[4]** Sun J.Z., Gallagher W.J., Callegari A.C., Foglietti V., Koch R.H., *Appl. Phys. Lett*. 63 (1993) (11) 1561–1563.

**[5]** Yi H.R., Ivanov Z.G., Winkler D., Zhang Y.M., Olin H., Larsson P., Claeson T., *Appl. Phys. Lett*. 65 (1994) (9) 1177–1179.

**[6]** Yi H.R., Gustafsson M., Winkler D., Olsson E., Claeson T., *J. Appl. Phys.* 79 (1996) (12) 9213–9220.

**[7]** Fanchini G., Ray S.C., Tagliaferro A., Optical properties of disordered carbon-based materials , *Surface and Coatings Technology* 151 –152 (2002) 233–241

**[8]** Krishna K.M., Nukaya Y., Soga T., Jimbo T., Umeno M. Solar cells based on carbon thin films. *Solar Energy Mater Solar Cells* 65 (2001) (1–4):163–70.

**[9]** Kishore N, Sachan S, Rai KN, Kumar A. Synthesis and characterization of a nanofiltration carbon membrane derived from phenol-formaldehyde resin. *Carbon* 41 (2003) (15) 2961–72.

**[10]** Okpalugo T.I.T., Ogwu A.A, Maguire P.D, McLaughlin J.A.D. Platelet adhesion on silicon modified hydrogenated amorphous carbon films. *Biomaterials* 25 (2004) (2) 239–245.

**[11]** McLaughlin J.A., Meenan B., Maguire P., Jamieson N., *Diamond Relat. Mater.* 5 (1996) 486–491.

**[12]** Narayan R.J., *Int. Mater. Rev.* 51 (2006) (2) 127–143.

**[13]** Vanhulsel A., Velasco F., Jacobs R., Eersels L., Havermans D., Roberts E.W., Sherrington I., Anderson M.J., Gaillard L., *Tribol. Int.* 40 (2007) (7) 1186–1194.

**[14]** Harris S.J., Weiner A.M., Tung S.C., Simko S.J., Militello M.C., *Surf. Coat. Technol.* 62 x (1993) (1-3) 550–557.

**[15]** Sohn M.H., Ahn Y.O., Ko Y.W., Hah S.R., Fischer T.E., Kim S.I., J. *Vac. Sci. Technol. A* 16 (6) (1998) 3554–3558.

**[16]** Hollman P., Hedenqvist P., Hogmark S., Stenberg G., Boman M., *Surf. Coat. Technol.* 96 (2–3) (1997) 230–235.

**[17]** Aoqui S., Ikegami T., Yamagata Y., Ebihara K., *Thin Solid Films* 316 (1–2) (1998) 40 44.

**[18]** Li W.J., Song Z.R., Yu Y.H., Zou S.C., Shen D., *Nucl. Instrum. Methods Phys. Res. B* 206 (2003) 339–342

**[19 ]** Yamamoto K., Koga Y., Fujiwara S., Kokai F., *Jpn. J. Appl. Phy.*, (1997), 36, L1333-L1335

**[20]** Scheibe H.J., Schultrich B., *Thin Solid Films*, 246, (1994) 1-2, 92-102

**[21]** Chuang F.Y, Sun C.Y, Chen T.T, Lin I.N, *Appl. Phy. Lett.,* 69, (1996) 3504-3506

**[22]** Oh J.U, Lee K.R, Eun K.Y., Thin Solid Films, 270, (1995) 1-2, 173-176

**[ 23]** Palshin V., Meletis E.I, Ves S, Logothetidis S, Characterization of ion-beam-deposited diamond-like carbon films, *Thin Solid Films*, 270 (1995) 1-2,

**[ 24]** Savvides N, Window B*, J. Vac. Sci. Tec. A.,* 3, (1985) 6, 2386-2390

**[ 25]** Vogel M, Stenzel O, Petrich R, Schaarschmidt G, Scharff, *Thin Solid Films*, 227, (1993) 1, 74-89

**[26]** Uchida M, Tanaka H, Kotera K, *Jpn. J. Appl. Phy*., 35 (1996) 11, 5815-5819

**[27]** Yu H.A, Kaneko Y, Yoshimura S, Otani S, *Appl. Phys. Lett.,* 68, (1996) 4, 547-549

**[ 28]** Dischler B, Bubenzer A, Koidl P, *Appl. Phys. Lett*., 42, (1983) 8, 636-638

**[ 29]** Rusli G. A., Amaratunga J., Silva S. R. P., *Thin solid Films*, 270, (1995), 160

**[30]** Shing Y.H., Pool F.S., *Vacuum,* 41 (1990) 4-6, 1368-1370

**[31]** Jian K., Xianyu H., Eakin J., Gao Y., Crawford G.P., Hurt R.H., *Carbon* 43 (2) (2005) 407–415.

**[32]** Iverson I.K, Casey S.M, Seo W., Tam-Chang S., *Langmuir* (2002) 18 (9) 3510–3516.

**[33]** Dembo A, Ionov A, Lazarev P, Manko A, Nazarov V. Lyotropic dye-water mesophases formed by rod-like supramolecules. *Molec. Mater* (2001) 14 (4) 275–290.

**[34]** Bobrov Y.A., Dependence of the anisotropic absorption coefficient on the thickness of molecularly oriented organic dye films. *J Opt Technol* 1999 66 (6) 547–549.

**[35]** Mahan, John E. *Physical Vapor Deposition of Thin Films*. New York: John Wiley & Sons, 2000

**[36]** Bulut L., Yan A., Hurt R. H., *Combustion and Flame*, 154, (2008) 206-216.

**[37]** Yan A., Xiao X., Külaots I., Sheldon B. W., Hurt R. H., *Carbon* 44 (14) (2006) 3113–3120.

**[38]** Geim A. K., Novoselov K. S., The rise of graphene, *Nature Mater*., 6 (2007) 183-191

**[39]** Novoselov, K. S., Geim, A. K., Morozov, S. V., Jiang, D., Zhang, Y., Dubonos, S. V., Grigorieva, I. V. & Firsov, A. A. *Science* (2004), 306, 666–669.

**[40]** Geim A. K. et al., Graphene: Status and Prospect, *Science,* 324 (2009), 1530-1534

**[41]** Sutter P., How silicon leaves the scene, *Nature Materials*, 8 (2009), 171-172

**[42]** van Bommel, A.J., Crombeen, J. E., van Tooren, A. LEED and Auger electron observations of the SiC(0001) surface. *Surf. Sci.* 48, 463-472 (1975).

**[43]** Forbeaux, I., Themlin, J.-M., Debever, J.M. Heteroepitaxial graphite on 6H-SiC(0001): Interface formation through conduction-band electronic structure. *Phys. Rev. B* 58, 16396-16406 (1998).

**[44]** Berger, C. *et al*. Ultrathin epitaxial graphite: 2D electron gas properties and a route toward graphene-based nanoelectronics. *J. Phys. Chem. B*, 108*,* 19912-19916 (2004).

**[45]** Berger, C. *et al*. Electronic confinement and coherence in patterned epitaxial graphene. *Science* 312, 1191-1196 (2006).

**[46]** Ohta, T., Bostwick, A., Seyller, T., Horn, K., Rotenberg E. Controlling the electronic structure of bilayer graphene. *Science* 313, 951 - 954 (2006).

**[47]** Sutter, P. W., Flege, J.-I. & Sutter, E. A. *Nature Mater.*7, 406–411 (2008).

**[48]** Reina A., Jia X., Ho J., Nezich D., Son H., Bulovic V., Dresselhaus M. S., Kong J., *Nano Letters*, 9 (2009) 1, 30-35

**[49]** Land, T.A., Michely, T., Behm, R.J., Hemminger, J.C., Comsa, G. STM investigation of single layer graphite structures produced on Pt(111) by hydrocarbon decomposition. *Sur. Sci.* 264, 261-270 (1992).

**[50]** Nagashima, A. *et al*. Electronic states of monolayer graphite formed on TiC(111) surface. *Surf. Sci.* 291, 93-98 (1993).

**[51]** Hernandez Y., et al., High-yield production of graphene by liquid-phase exfoliation of graphite, *Nature Nanotech*., 3 (2008), 563-568

**[52]** Li X., Wang X., Zhang L., Lee S., Dai H., *Science* 319, (2008) 1229-1232

**[53]** Li X., Zhang G., Bai X., Sun X., Wang X., Wang E., Dai H., *Nature Nanotech*. 3 (2008), 538-542

**[54]** Tung V. C., Allen M. J., Yang Y., Kaner R. B., *Nature Nanotech.* 4 (2009) 25-29

**[55]** Stankovich, S. et al. Synthesis of graphene-based nanosheets via chemical reduction of exfoliated graphite oxide. *Carbon* 45, (2007) 1558–1565

**[56]** Stankovich, S., Piner, R. D., Nguyen, S. T. & Ruoff, R. S. Synthesis and exfoliation of isocyanate-treated graphene oxide nanoplatelets. *Carbon* 44, (2006) 3342–3347

**[57]** Li, D., Mueller, M. B., Gilje, S., Kaner, R. B. &Wallace, G. G. Processable aqueous dispersion of graphene nanosheets. *Nature Nanotech*. 3, (2008) 101–105

**[58]** Bartoens, B. and Peeters, F. M. From graphene to graphite: Electronic structure around the K point. *Phys. Rev. B* 74, 075404 (2006)

**[59]** Kim K. S., Zhao Y., Jang H., Lee S. Y., Kim J. M., Kim K. S., Ahn J. H., Kim P., Choi J. Y., Hong B. H., *Nature,* 457 (2009) 7230, 706-710

**[60]** Dürkop T., Getty S. A., Cobas E., and Fuhrer M. S., *Nano Letters* 4, 35 (2004)

**[61]** Chen J. H., Jang C., Xiao S., Ishigami M., Fuhrer M. S., *Nature Nanotech*., 3 (2008) 206-209

**[62]** Schedin F., A. K. Geim, S. V. Morozov, E. W. Hill, *Nat. Mater.* (2007), 6, 652

**[63]** Saito, K.; Nakamura, J.; Natori, A. *Phys. ReV. B* (2007), 76, 115409.

**[64]** Peres, N. M. R.; dos Santos, J.; Stauber, T. *Phys. ReV. B* (2007), 76,073412.

**[65]** Mingo, N.; Broido, D. A. *Phys. Re*V. *Lett.* (2005), 95, 096105.

**[66]** Balandin A. A., Ghosh S., Bao W., Calizo I., Teweldebrhan D., Miao F., and Lau C. N., Superior Thermal Conductivity of Single-Layer Graphene, *Nano Letters,* 8 (2008) 3, 902-907

**[67]** Pop, E., Mann, D., Wang, Q., Goodson, K., Dai, H., *Nano Lett.* (2006), 6, 96.

**[68]** Hone, J.; Whitney, M.; Piskoti, C.; Zettl, A., *Phys. ReV. B* 1999, *59*, R2514.

**[69]** Lee C., Wei X., Kysar J. W., Hone J., *Science,* 321 (2008) 385-388

**[70]** Frank, I. W., Tanenbaum, D. M., Van Der Zande, A.M., and McEuen, P. L. "Mechanical properties of suspended graphene sheets". *J. Vac. Sci. Technol. B* 25 (2007) 2558-2561.

**[71]** Mohanty N., Vikas B., *Nano Letters* 8 (2008) 4469-7446.

**[72]** Stoller, M. D., Park S., Zhu Y., An J., Ruoff R. S., *Nano Letters*, 8 (2008) 10, 3498-3502

**[73]** Eda G, Fanchini G, Chhowalla M., Large-area ultrathin films of reduced graphene oxide as a transparent and flexible electronic material". *Nature Nanotechnol* 3 (2008) 5 270–274.

**[74]** Wang, X.; et al. "Transparent, Conductive Graphene Electrodes for Dye-Sensitized Solar Cells". *Nano Letters* 8 (2007) 323

**[75]** Nakada K., Fujita M., Dresselhaus G., Dresselhaus M. S., *Phys. Rev. B* 54, 17 954 (1996).

**[76]** Wakabayashi K., Fujita M., Ajiki H., Sigrist M., *Phys. Rev. B* 59, 8271 (1999).

**[77]** Wakabayashi, K. *Phys. ReV. B* (2001), 64, 125428-1.

**[78]** Son Y., Cohen M., Louie S., *Phys. Rev. Lett.* (2006), 97, 216803.

**[79]** Chen Z., Lin Y., Rooks M., Avouris P., *Physica E* (2007), *40*, 228-232

**[80]** Han M., Ozyilmaz B., Zhang Y., Kim P., *Phys. Rev. Lett.* (2007), 98, 206805.

**[81]** Schniepp H.C., Li J. L., McAllister M.J., Sai H., Herrera-Alonso M., Adamson D.H., et al. *J Phys Chem B* (2006) 110 (17) 8535–8539.

**[82]**Yu A., Ramesh P., Itkis M. E., Bekyarova E., Haddon R. C., *J. Phys. Chem. Lett. C.,* 11 (2007) 7565-7569

**[83]** Fan S., Chapline M., Franklin N., Tombler T., Cassell A., Dai H., *Science* 283 (1999) 512.

**[84]** Yang Y., Huang S., He H., Mau A.W.H., Dai L., *J. Am. Chem. Soc.* 121 (1999) 10832.

**[85]** Huang S., Dai L., Mau A.W.H., *Adv. Mater.* 14 (2002) 1140.

**[86]** Wei B.Q., Vajtai R., Jung Y., Ward J., Zhang Y., Ramanath G., Ajayan P.M., *Nature* 416 (2002) 495.

**[87]** Xia Y. and WhitesidesG. M., *Annu. Rev. Mater. Sci.* (1998) 28:153–84

**[88]** Kind H., Bonard J.-M., Emmenegger C., Nilsson L.O., Hernadi K., Maillard-schaller E., Schlapbach L., Forro L., Kern K., *Adv. Mater.* 11 (1999) 1285.

**[89]** Burghard D., Duesberg G., Philipp G., Muster J., Roth S., *Adv. Mater*. 10 (1998) 584.

**[90]** Liang X., Fu Z., Chou S., *Nano Lett.* 2007, *7*, 3840-3844.

**[91]** Lu X., Huang H., Nemchuk N., and Ruoff R.S., Patterning of highly oriented pyrolytic graphite by oxygen plasma etching, *Appl. Phys. Lett.* 75, (1999) 2, 193-195

**[92]** Mühl T., Kretz J., Mönch I., Schneider C.M., Brückl H., Reiss G., *Appl. Phys. Lett.* (2000), *76*, 786-788.

**[93]** Walton M. D., Kim Y.S, C. Jason Jan, Ethan P. McConnel, W. Neil Everett, Jaime C. Grunlan, Deposition and patterning of conductive carbon black thin films, *Synthetic Metals*,157 (2007), 632-639

**[94]** Huang S., Controllable 3D architectures of aligned carbon nanotube arrays by multi-step processes, *Chem. Phys. Lett*.374 (2003) 157–163

**[95]** Huang S., Dai L., Mau A., Controlled fabrication of aligned carbon nanotube patterns, *Physica B* 323 (2002) 333–335

**[96]** Kong, J., Soh, H. T., Cassell, A. M., Quate, C. F., Dai, H. *Nature* 1998, *395* (6705), 878–881.

**[97]** Hayamizu, Y., Yamada, T., Mizuno, K., Davis, R. C., Futaba, D. N., Yumura, M., Hata, K. *Nat. Nanotechnol.* 2008, *3* (5), 289–294.

**[98]** Kim K. S. et al., Nature 457, 706 (2009)

**[99]** Albrecht T. R., Dovek M. M., Kirk M. D., Lang C. E., Quate C. F., Smith D. P. E., *Appl. Phys. Lett.* 55, 1727 (1989)

**[100]** Eagle S. C., Fedder G. K., *Appl. Phys. Lett*., 74 (1999) 25, 3902-3903

**[101]** Myhra S., Muhl T., *J. Phys. D: Appl. Phys.* 42 (2009) 035309

**[102]** Muhl T., *Appl. Phys. Lett.* 85 (2004) 5727

**[103]** Muhl T, Bruckl H, Weise G and Reiss G., *J. Appl. Phys.* 82 (1997) 5255

# Chapter 3

## *Catalytic Combustion of Carbon*

Carbons are quite resistant to solvents, acids, and bases and thus cannot easily be patterned by conventional techniques. Catalytic combustion may provide a way to exploit $O_2$ as a dry "etchant" for selective shaping or microstructural modification of a variety of carbon materials. In the following sections catalytic gasification of carbon, especially graphite, active catalysts for gasification of carbon and different catalyst behaviours on graphite surfaces will be explored. Selection of the catalyst, substrate, reactant and reaction temperature and their dependence on the reaction mode will be discussed in detailed.

### 3.1 Catalytic Gasification of Carbon

Carbon gasification reactions form the basis of many important processes such as combustion of coal and the production of synthesis gas, fuel gases and activated carbons. The most important gas carbon reactions involve reactions of carbon with $O_2$, $CO_2$, $H_2O$ or $H_2$. Gasification of carbon can take place by several reactions:

$$C + CO_2 \rightarrow 2CO$$

$$C+H_2O \rightarrow CO + H_2$$

$$C+2H_2 \rightarrow CH_4$$

$$C+O_2 \rightarrow CO/CO_2$$

It has been known for many years that small amounts of catalysts can have significant effect on the rates of these reactions, which have been analyzed in many studies from both experimental and theoretical viewpoints [1-4]. More recent literature focuses on catalyst regeneration for metallurgical processes and on the use of metals as additives for enhancing low-temperature soot burnout to remove carbon particulate from exhausts, especially in diesel engine applications [5-7].

The reactions of carbon with gases, especially with oxygen, are strongly affected by various catalytic agents and under some conditions a high degree of catalytic enhancement is observed. The carbon combustion reaction, $C(s) + O_2 \rightarrow CO/CO_2$ is catalyzed by a number of materials that have been shown to exhibit catalytic activity, the most active being transition metals, alkali metals and alkaline earth metals. In the following sections active catalysts for carbon gasification will be summarized.

### 3.1.1 Alkali Metals

Alkali metal salts are the oldest known additives that have been observed to increase the rate of oxidation of carbon materials and there have been many practical application of

their catalytic effect. In general, alkali carbonates are more active than sulfates or halides [8]. Addition of increasing amounts of sodium carbonate ($Na_2CO_3$), to coal gradually lowers the ignition temperature of coke in air [9, 10]. Also, potassium impurity introduced either electrochemically or from the vapor phase, leads to accelerated gasification of graphite by oxygen and higher combustion rates [11]. The catalytic activity of alkali and alkaline earth metal salts or oxides in gasification of coal is given in the following order: $K_2CO_3$ > $Na_2CO_3$ > KCl > NaCl > $CaCl_2$ [12]. Alkali metal monoxides such as $Na_2O$, when added to graphite showed very rapid acceleration in the rate of gasification in oxygen, the reaction being initiated at temperatures in the range of 450-500 $^oC$ [13]. K-Ca catalyst mixture has been observed to be much more active for the steam gasification of graphite at temperatures 577-627$^oC$ than potassium oxide or calcium oxide alone [14].

### 3.1.2 Alkaline Earth Metals

The strong catalytic effect of alkaline earth (group IIA) metals on carbon oxidation rates is also well known. When reactivity of coal towards air at 500 $^oC$ is measured, coal chars containing the highest amount of calcium and magnesium impurities show the most reactivity [15]. The order of the catalytic activity of alkaline earth metals is given as Na > Ba > Sr > Mg > Ca for graphite oxidation [16]. It has been observed that, the oxides of alkaline earth metals show only modest catalytic effects when added to graphite and then heated in air. Relative catalytic effects are given in the order BaO > CaO > MgO > SrO

and the effect of alkali and alkaline earth oxides on the oxidation of graphite in air is shown in Table 3.1. [13, 17]

**Table 3.1.** Effect of alkali and alkaline earth oxides on the oxidation of graphite in air

| Material | T ($^{o}$C) for 1% burnoff in air |
|---|---|
| Pure graphite (G) | 763 |
| G + MgO | 740 |
| G + CaO | 728 |
| G + SrO | 750 |
| G + BaO | 718 |
| G + $Li_2O$ | 568 |
| G + $Na_2O$ | 608 |

### 3.1.3 Transition Metals

Transition metals and their salts received much more attention than any other catalysts because they are known as the most active catalysts for the oxidation of carbon. Transition metals show different catalytic activities in different gas atmospheres [2,18]. They are only weakly active for the C + $CO_2$ and C + $H_2O$ reactions unless they are in reduced state whereas highest activity is seen for C + $O_2$ reaction. The magnitude of the catalytic effects of different metals for carbon gasification in oxygen are in the order Co > V > Fe > Mn > Cr [19]. Another reported catalytic rate order for metal doped carbon towards oxygen [20] is Ni > Co > Cu > Ag > Fe > Ca. For comparison, the effect of

different catalysts on the ignition temperature of graphite in oxygen is shown in Table 3.2 [21] and the order of activity for some metals is Pb > V > Mn > Co > Cr > Fe > Ni. Among all transition metals, Fe, Ni and Co are the most popular catalysts for graphite gasification reactions. Activity of metallic catalyst is very dependent on the nature of the oxidizing gas. For example Fe, is generally less active in air or $O_2$ than when the oxidation is carried out in $CO_2$ [22]

**Table 3.2.** Effect of catalysts on the ignition temperature of graphite in $O_2$

| **Catalyst** | **Ignition T ($^oC$) in $O_2$** |
|---|---|
| Pure graphite | 740 |
| Pb | 382 |
| V | 490 |
| Mn | 523 |
| Co | 525 |
| Cr | 540 |
| Cu | 570 |
| Mo | 572 |
| Ag | 585 |
| Cd | 590 |
| Fe | 593 |
| Pt | 602 |
| Ni | 613 |
| Ir | 638 |
| Rh | 622 |
| Ru | 640 |
| Pd | 659 |
| Ce | 692 |
| Zn | 700 |
| W | 718 |
| Hg | 720 |
| Sn | 738 |

## 3.2 Catalyst Behavior on Graphite

One of the most interesting subjects in the field of catalysts is the mechanism by which metallic particles influence the gasification of graphite reaction. Although there is no single mechanism which can describe all catalyzed carbon gasification reactions, two major mechanisms have been proposed: electron transfer and oxygen transfer [2,8,18,23,24]. In the electron transfer mechanism, carbon-carbon bonds attached to the edge or surface carbon are weakened because the carbon matrix transfers an electron to the metal ion in the catalyst and facilitates the gasification of carbon. In the oxygen transfer mechanism, the solid catalyst forms intermediates in the oxidizing atmosphere which are then transferred to the carbon surface from the catalyst particle and oxidize the carbon in its vicinity. Regardless of the mechanism, it is a well-established experimental fact that catalyst action is localized. It has been shown that enhanced local gasification rates are observed after gasification of carbon in $O_2$ with fine dispersions of active (e.g. Cu, Ni, Fe, Ag) metals [25]. Also, the areas of preferred attack of Ni metal on diamond correspond to the regions in the immediate vicinity of the catalyst particle [8]. Therefore, oxidation reaction takes place directly at the carbon/catalyst interface [26] and intense localized action of the catalyst particles is evident from these studies.

The most interesting phenomenon related with the catalyzed gas-carbon reactions is the motion of the catalyst on carbon or graphite which results in the catalytic activity. In the past years, a great deal of attention has been devoted to understanding of the catalytic behavior during the gasification reactions. The action of catalysts has been investigated by microscopic studies on the surfaces of graphite single crystals. A variety of catalyst

motions are observed, mostly by electron microscopy, including pitting [8, 27], channeling [8, 26, 28, 29] and deep edge recession [14, 30, 31].

### 3.2.1 Modes of Catalytic Attack

In the graphite oxygen reaction, catalysts operating by facilitating basal-plane penetration in imperfect regions are known as pitting catalysts and those operating by increasing the rate of removal of carbon atoms at the edges or steps are known as channeling catalysts. In general, for particles to become activated they must be located at the edges or steps on the graphite. Imperfections on the graphite basal plane, i.e. vacancies, can also serve as centers for catalytic attack. A schematic of the graphite basal plane with edges and steps is shown in Figure 3.1.

The mode by which a catalyst operates is governed to a large degree by the strength of the interaction between the metal and the graphite edge atoms. Although catalytic action is a complex phenomenon and has not been fully understood yet, the mode of the catalytic attack is known to depend on several factors such as chemical state of the catalyst, temperature of the reaction, vacancies and/or defects of the graphite surface, size of the catalyst particle and interaction between the metal and the graphite edge atoms [32]

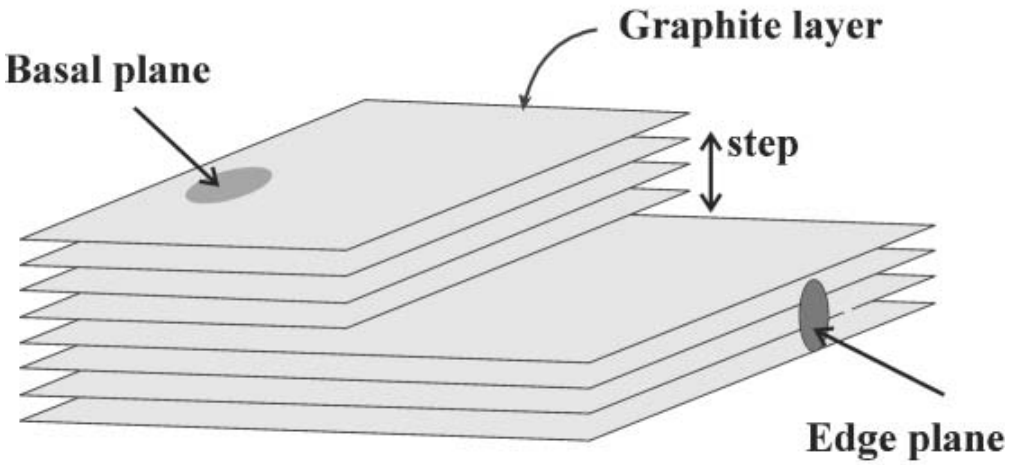


**Figure 3.1.** Schematic representation of graphite structure showing basal plane, edge plane and steps.

### 3.2.1.1 Catalytic Pitting

Pits are generally initiated when catalyst particles come into contact with surface defects, such as vacancies. An active catalyst particle proceeds to attack the graphite crystal in a direction perpendicular to the basal plane and produces a pit. With continued oxidation, pits increase in depth and take the form of hexagonally shaped holes which is believed to be due to uncatalyzed attack. It is well established that the rate of oxidation by pitting is slower than that which occurs by catalytic removal of carbon along the basal plane by channeling [26]. The behavior of metal particles on the surface of graphite single crystals during oxidation has been studied by Baker et al. [33] and an example of pitting action by platinum particles on graphite at 500 $^{o}$C is shown in Figure 3.2.

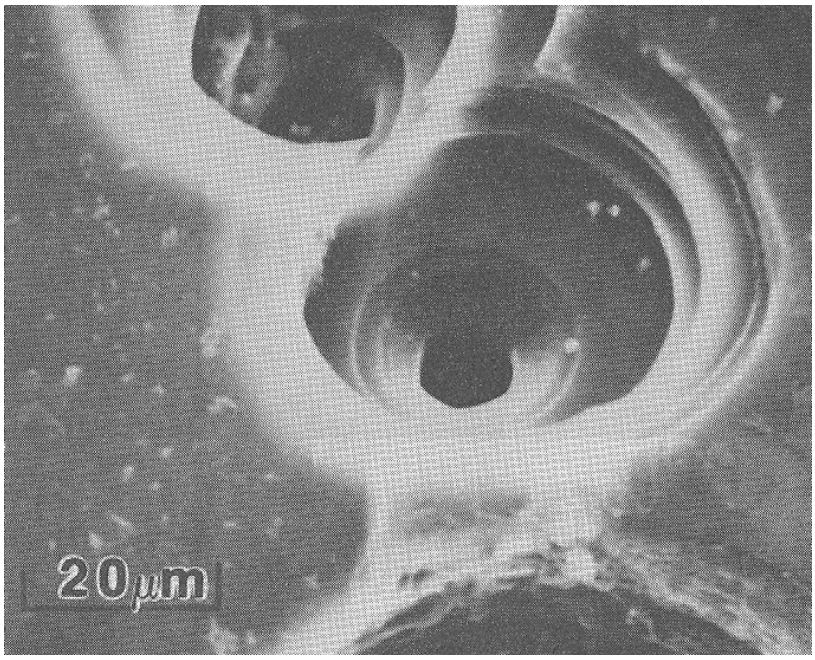


**Figure 3.2.** Scanning electron microscope image of a pit produced by platinum particles [33].

### 3.2.1.2 Catalytic Channeling

Mobility of catalyst particles and the channeling on the basal plane of graphite crystals are unique features of graphite gasification reactions and the reason for the particle motion during catalytic gasification has not been fully explored yet. However, it has been established primarily by Baker et al. [26] that channeling is initiated only when the catalyst particle comes into contact with a step on the graphite surface [26, 28]. The reaction takes place at the catalyst/graphite interface, and since the loss of carbon atoms is faster at the step, particles proceed to cut channels in the graphite crystal.

Some catalyst particles tend to move along steps and edges and resulting channels follow well-defined crystallographic directions in the graphite basal plane. On the other hand,

channeling is completely irregular in some instances, and the moving particles might perform frequent and random changes in direction [21].

Regardless of the direction of motion both types of channels share common features: 1) All channels originate from edges or steps on the surface, 2) The width of the channel is generally the same as that of the catalyst particle, 3) The linear rate of channel propagation is proportional to the depth of the channel and to the width of the catalyst particle. Small particles cutting shallow channels move at the fastest rate.

Catalytic channeling by potassium hydroxide has been observed during steam gasification of graphite at temperatures between 500-600$^{o}$C [34]. Catalyst particles indicated by arrows can be seen at the head of channels which have random orientation on the graphite surface (see Figure 3.3)

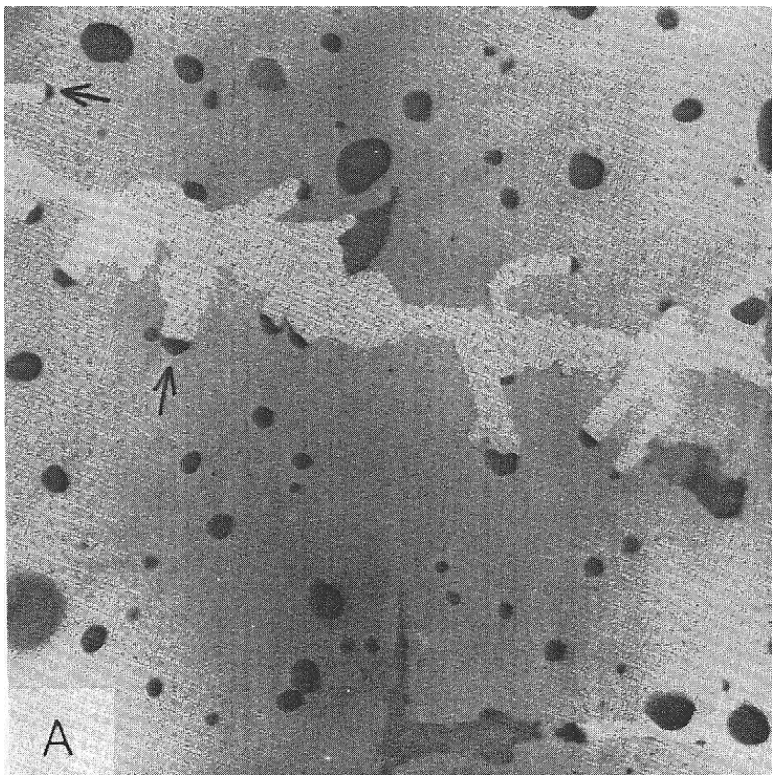


**Figure 3.3.** Catalytic channeling by KOH at 500$^{o}$C [34]

Another observation of catalytic attack by channeling reveals that catalyst particles may undergo random directional changes on the surface of graphite [33]. Pt particles larger than 100 nm in diameter formed irregular channels at higher temperatures between 735-850 $^{o}$C in $O_2$ (see Figure 3.4). Keep et al. gives the order of catalytic effect of different metals as Rh > Ru > Ir > Pt > Ni > Pd > Co > Fe and shows channeling of Ni particles during hydrogenation of single crystal graphite [29] (Figure 3.5). The majority of the channels are observed to exist parallel to the specific crystallographic directions.

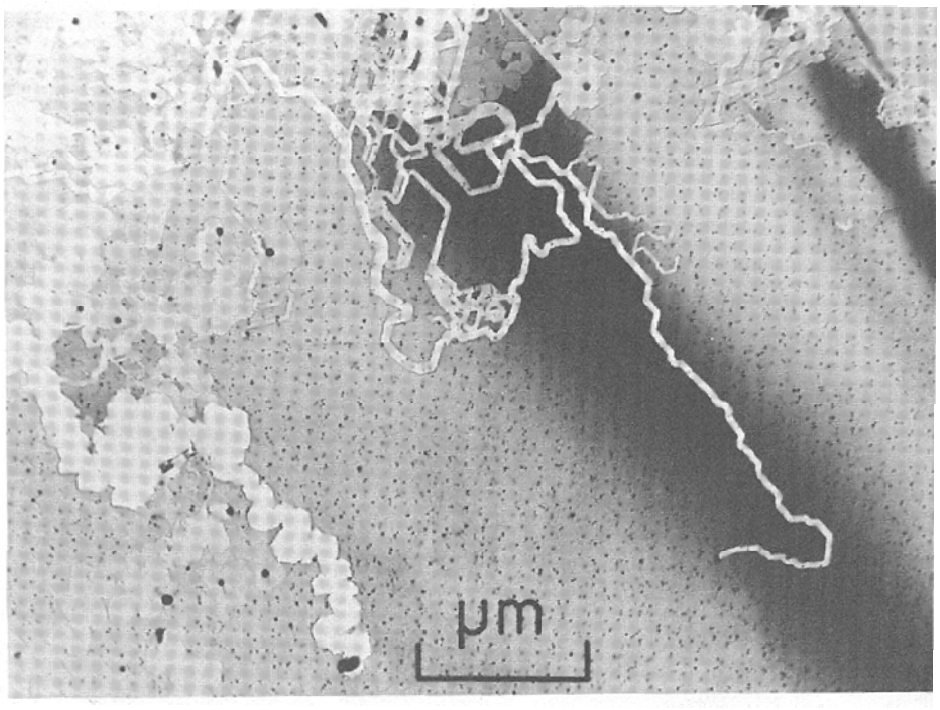


**Figure 3.4.** Catalytic channeling of Pt particles during graphite oxidation at 750°C [33].

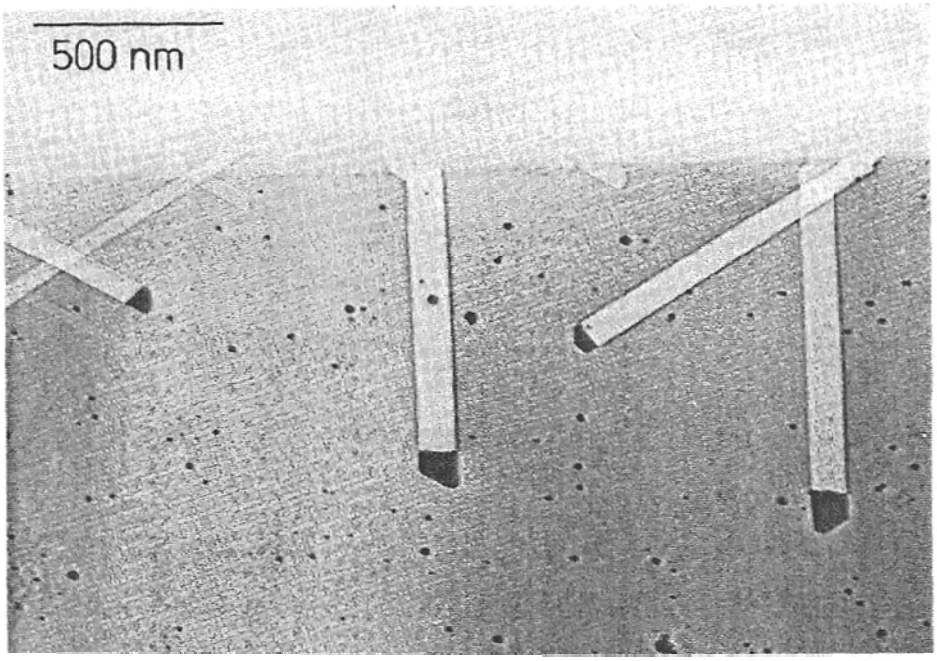


**Figure 3.5.** Channeling of Ni particles in $H_2$ at 800°C [29]

### 3.2.1.3 Edge Recession

When the catalyst particles show strong interaction with the graphite edge atoms and form a thin film, the mode of catalytic action is known as edge recession. Catalyst particles which adhere to edges and steps starts to spread along these regions and proceed to facilitate the removal of carbon. A schematic of catalyst spreading on the graphite surface is shown in Figure 3.6. The contact area between catalyst and graphite edge atoms is maximized when the catalyst spreads on the surface as a thin film. Edge recession was first presented by Harris et al. [31] by using controlled atmosphere electron microscopy. It has been shown that lead forms an extremely thin film on graphite at temperatures below 545$^{o}$C and rapid edge recession takes place during graphite-oxygen reaction. Catalytic edge recession has been observed by a number of catalyst including calcium and barium [35] during steam gasification of graphite at relatively high temperatures (see Figure 3.7).

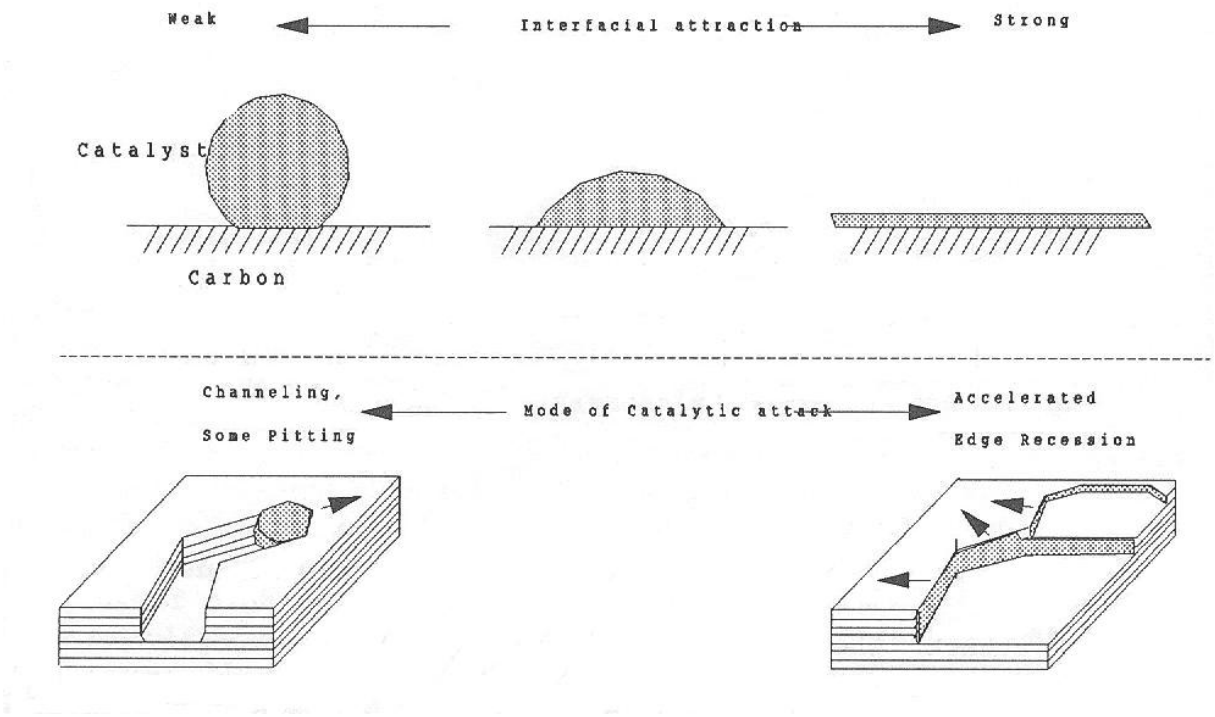


**Figure 3.6.** Relation between wetting tendency of a catalyst and the mode of catalytic attack [36]

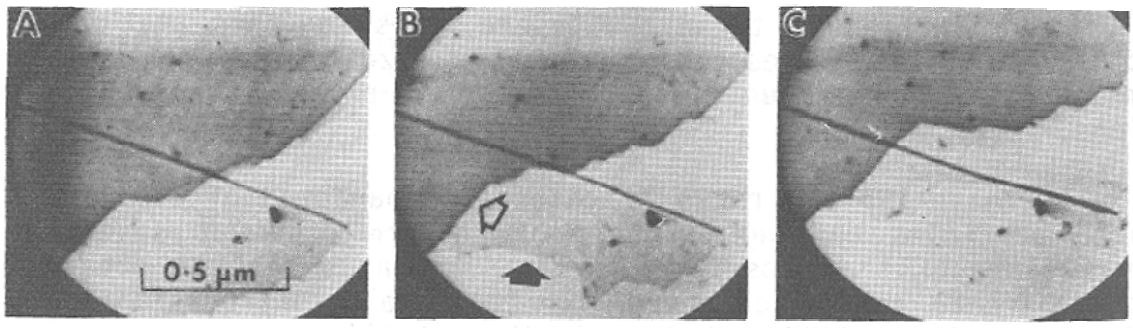


**Figure 3.7.** Catalyzed edge recession by calcium in steam at 715$^{o}$C [35]

In some cases, it may not be possible to predict whether catalytic attack will occur by channeling or edge recession because catalysts may show a transformation in wetting properties of graphite depending on the temperature or reactant gas, and as a consequence, both forms of catalytic attack can be observed. An example of how a minor change in the gas composition can change the catalyst action was shown by Baker et al. [35]. Nickel particles spread along the graphite edges as a thin film in steam gasification allowing the edge recession as the dominant mode of attack. However, addition of a small amount of hydrogen to the steam reduces the wettability of nickel on graphite and causes metal to remain in a particle form. So, in that case the catalyst action is restricted to channeling.

Reaction temperature, as well as the type of the catalyst, is also an important factor affecting the catalytic behavior. For example, metals such as molybdenum, platinum and palladium catalyze the oxidation of graphite by a pitting mode at lower temperatures and then switch over to channeling mode at higher temperatures [33, 35]. Silver and lead are very active catalysts at low temperatures whereas temperatures over 725$^{o}$C are required for zinc particles to be active for the graphite-oxidation reaction. [26, 31].

## References

**[1]** Walker P. L. Jr., Rusinko F. Jr., and Austin L.G., in "*Advances in Catalysis*" (D. D. Eley. P. W. Selwood, and P. B. Weisz. Eds.). Vol. 11, p.133. Academic Press, New York, 1959

**[2]** Walker P. L. Jr., Shelef M., and Anderson R. A., in "*Chemistry and Physics of Carbon*" (P. L. Walker, Ed.). Dekker, New York, 1968.

**[3]** Walker P. L. Jr., in "*Carbon and Coal Gasification*"( Figueiredo. J. L., Moulijn, J. A Eds.) NATO ASI Series, 1988

**[4]** Lizzio A. A., Jiang H., Radovic L. R., *Carbon*, 28, 1990

**[5]** Neeft J. P. A., Makkee M., Moulijn*. J. A., App. Catal. B: Env*, 8, 1996

**[6]** Ciambelli P., Corbo P., Gambino M., Palina V., Vaccaro S., *Catal. Today* 27, 1-2 1996

**[7]** Badini C., Saracco G., Russo N., *Specchia.Catal. Lett*. 69, 207, 2000

**[8]** McKee D. W., in "*Chemistry and Physics of Carbon*" (P. W. Walker, Jr., and P. A. Thrower, Eds.), Vol. 16, Dekker, New York, 1980.

**[9]** Patrick J. W., and Shaw F. H., *Fuel,* 51, 69, 1972

**[10]** Lee G. W., *Coke and Gas*, 23, 398, 442, 1961

**[11]** Harker H., Horsley J. B., and Robson. D., *J. Nucl. Mater*. 37, 331, 1970

**[12]** Liu Z. L., Zhu H. H., *Fuel*, 65, 1334, 1986

**[13]** McKee D. W., Chatterji D., *Carbon*, 13, 381, 1975

**[14]** Pereira P., Csencsits R., Somorjai G. A., and Heinemann H., *J. Catal*. 123, 463, 1990

**[15]** Jenkins R. G., Nandi S. P., Walker P. L. Jr., *Fuel,* 52, 288, 1973

**[16]** Amariglio H., Duval X., *Carbon,* 4, 323, 1966

**[17]** McKee D. W., *Carbon*, 17, 419, 1979

**[18]** Holstein W. L., and Boudart M., *Fuel*, 62, 162, 1983

**[19]** Marsh H., Taylor D. W., Abstract 13th Biennial Carbon Conf., 1977, p. 46

**[20]** Marsh H., Adair R. R., *Carbon,* 13, 327, 1975

**[21]** McKee D. W., *Carbon*, 8, 623, 1970

**[22]** Turkdogan E. T., Vinters J. V., *Carbon,* 10, 97, 1972

**[23]** Long F. J., and Sykes K. W., *Proc. R. Soc. London Ser. A* 215, 100, 111, 1952

**[24]** Lewis. J. B., in "*Modern Aspects of Graphite Technology*" (L. C. F. Blackman Ed.), Academic, New York, 1970,

**[25]** Adair R. R., Boult E. H., Freeman E. M., Jasienko S., and Marsh H., *Carbon,* 9, 763, 1971.

**[26]** Baker R.T.K., *Catal. Rev. Sci. Eng*. 19 (2) (1979) 161–209.

**[27]** Thomas J. M., in "*Chemistry and Physics of Carbon*" (P. L. Walker, Jr., Ed.), Vol.1, Dekker, New York, 1965.

**[28]** Hennig G. R., *J. Inorg. Nucl. Chem*. 24, 1129, 1962

**[29]** Keep C. W., Terry S., and Wells M.*, J. Catal.* 66, 451, 1980

**[30]** Baker R. T. K., *Carbon* 24, 715, 1986

**[31]** Harris P. S., Feates F. S., and Reuben B. G., *Carbon* 11, 565, 1973

**[32]** Figueiredo J. L., Moulijn J. A., NATO ASI Series E, No:105, 1985

**[33]** Baker R. T. K., France J. A., Rouse L., Waite R. J., *J. Catal.,* 41, 22, 1976

**[34]** Coates D. J., Evans J. W., Cabrera A. L., Somorjai G. A., Heinemann H., *J. Catal*., 80. 215, 1983

**[35]** Baker R. T. K., Lund C. R. F., Chludzinski J. J., *J. Catal*., 87, 255, 1984

**[36]** Mims C. A., in "Fundamental Issues in Control of Carbon Gasification Reactivity" ( Lahaye J. and Ehrburger P. Eds) NATO ASI Series Vol 192 383-407

# Chapter 4

# *Experimental Techniques*

## 4.1 Thermogravimetric Analyzer

The thermogravimetric analyzer (TGA) is a useful technique for quantifying kinetics. TGA measures weight changes in a material as a function of temperature (or time) under a controlled atmosphere. Its principal uses include measurement of a material's thermal stability. It can be used in isothermal conditions to determine reaction order by varying the reactant gas concentration or under various temperature conditions to determine activation energy with various partial pressure conditions or using a given heating rate to determine chemical reactivity. Oxidation reactivity of carbon samples was measured by non-isothermal thermogravimetric analysis in this work. The TGA (Dupont 951 TGA and CAHN TGA-2141 systems) consists of a high precision balance with a pan (usually Pt) loaded with the sample. The balance and the pan system are placed in a small electrically heated furnace, which is controlled by a temperature programmer, with thermocouple to accurately measure the temperature. Sample weight given by the microbalance and the temperature readings from S type thermocouple are recorded to a computer. Air is used

as a reactant gas and regulated at 300cc/min by the flow meters. Digital photographs of the TGA systems used in this work are shown in Figure 4.1. A carbon sample weighing about 3-10 mg is placed in a Pt pan and suspended by the microbalance. Then, samples are heated from room temperature to 900 $^{o}$C with a heating rate of 10 $^{o}$C/min. Most of the time heating is delayed at 100 $^{o}$C for 20 minutes to remove possible absorbed moisture from the sample. Sample weight and the temperature are continuously monitored and results are processed and expressed as reaction rate versus temperature for the samples.

**Figure 4.1.** Thermogravimetric analyzer systems with (a) vertical balance and furnace (b) horizontal balance and furnace.

## 4.2 Resistive Heat Treatment Device

The resistive heat treatment apparatus has been designed and built in our group previously [1] to quantify char deactivation by high temperature heating experiments in inert atmospheres. The heat treatment device is capable of 2700 $^{o}$C with a maximum heating rate of 1000 $^{o}$C/s. In order to perform controlled oxidation experiments together with magnetic actuation, we modified the heating apparatus to allow close-proximity access for high temperature resistant permanent magnet and CCD video recording. The heating device modified for catalytic oxidation experiments (see Figure 4.2), consists of a thin polycrystalline graphite sheet held at the end of brass electrodes connected to a low-voltage power supply. Natural graphite samples are placed onto the graphite sheet, which acts as an electrical resistance heater, so that there is a direct contact between the heat source and the sample. The surface of the graphite sheet is optically accessible from beneath for temperature measurements.

The temperature measurement system includes optical fiber thermometer from LUXTRON$^{TM}$ and optical pyrometer sensor. A high-speed one-color pyrometer focuses on a spot on the underside of the polycrystalline graphite and measures the temperature in real time. The graphite sheet electrode is vertically symmetrical and temperature gradients across the ultra-thin exfoliated natural graphite sample are small. The pyrometer is capable of measuring temperatures of 450 $^{o}$C-3000 $^{o}$C at 30 readings per second operating at 10 kHz and results are accurate within ±13 $^{o}$C.

High temperature resistant samarium-cobalt ($Sm_2Co_{17}$) permanent magnets from MMC Magnetics, NY are mounted to steer the magnetic catalyst particles during air oxidation experiments. Reaction is monitored with a long focal length refracting microscope (Infinity Photo-Optical, Model K2) with fiber optic illumination and CCD video recording [2].

**Figure 4.2.** Digital micrograph of the hot stage oxidizing microscope.

## 4.3 Optical Microscopy

Optical microscopy imaging is an attractive technique for convenient and large-scale investigation of macroscopic samples. The optical microscope basically uses visible light and a system of lenses to magnify images of small samples and information is obtained by light transmission through or reflected from the surface of a material. Magnification up to 1000X may be obtained, allowing the examination of structures to a limit of resolution on the order of 1 μm.

In order to characterize the surface of carbon thin films polarized light is often used. Crossed polarized mode enables one to observe the interference colors generated due to the orientation of the graphitic lamellae at the carbon surfaces. Carbon can show a unique series of microstructures depending on the range of shared orientations [3]. Optical microscopy is very useful in the observation of liquid crystal textures, due to the anisotropic properties of liquid crystals (see Figure 4.3). The interference colors, usually yellow, blue and purple can be used to determine the orientations of the lamellar planes. Yellow and blues are indicative of prismatic edges whereas purple regions indicate basal planes. The purple color represents an essentially isotropic surface and remains unchanged during the rotation of the specimen. However, the purple color of anisotropic carbon is generally darker in tone than that of glassy carbons and these two can be distinguished with careful investigation.

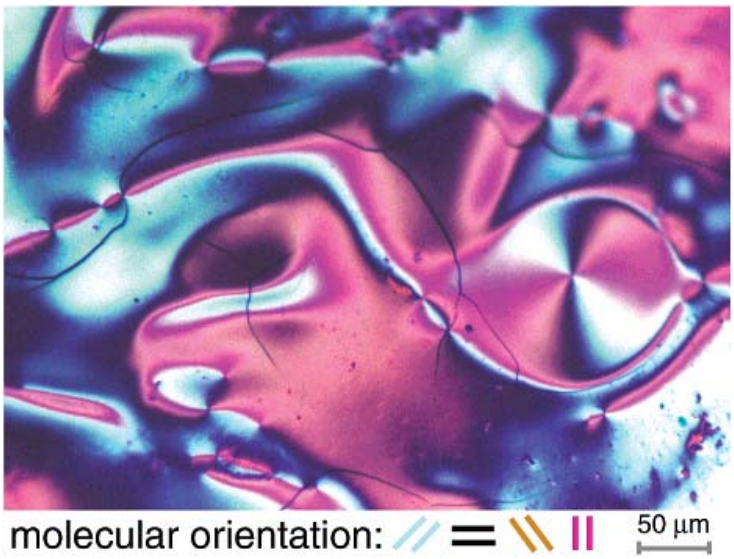


**Figure 4.3.** Example of a liquid crystal texture with different molecular orientations obtained by polarized optical microscopy [4]

Optical microscopy is also widely used to determine the thickness of graphene layers by looking at the color modulation on the substrate [5, 6]. The presence of thin graphite on the surface produces a phase shift on the interference in the reflection spectrum as a consequence of the additional optical length introduced in the system. These phase shifts in the interference color are sensitive to the number of graphene layers. As shown in Figure 4.4, there are color contrast changes in the samples with different thicknesses due to interference induced color shifts. Color shifts in region I and II indicates that graphene layer is thinner in region one compared to region II. In addition to optical microscopy, atomic force microscopy (AFM) can be used to obtain a detailed height profile of the graphene layers. Optical microscopy is rapid and nondestructive technique for reliable thickness evaluation and applicable to thin layers of wide variety of materials.

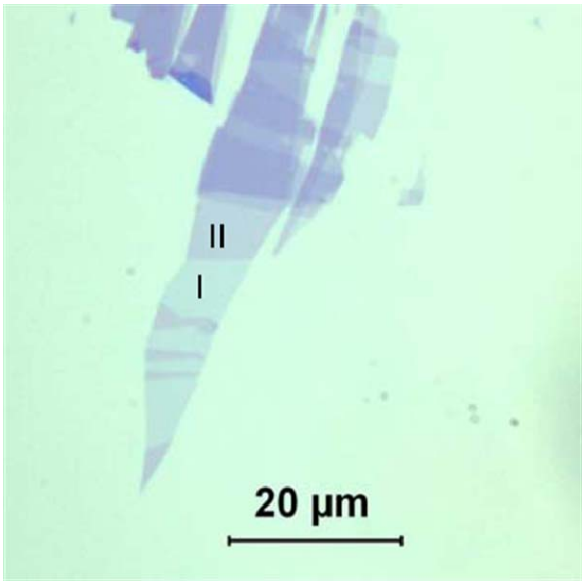


**Figure 4.4.** An optical microscope image of a cleaved graphite sample containing regions of many different thicknesses. Color shifts indicate a thinner graphene layer in region I compared to region II [6].

## 4.4 Scanning Electron Microscopy

Scanning electron microscope (SEM) is one of the most useful instruments for understanding the surface structure of various samples including carbon materials. SEM uses electrons instead of light to form a largely magnified image. Because the SEM uses electromagnets rather than lenses, there is much more control in the degree of magnification. SEM has a large depth of field, which allows more of a specimen to be in focus at one time yielding characteristic three-dimensional appearance. Therefore, closely spaced specimens can be magnified at much higher levels by SEM than is possible with a light microscope.

The schematic of the working principle of the SEM is shown in Figure 4.5. A beam of electrons is produced at the top of the microscope by an electron gun. The electron beam follows a vertical path through the microscope, which is held within a vacuum. The beam travels through electromagnetic fields and lenses, which focus the beam down toward the sample. Once the beam hits the sample, electrons and X-rays are ejected from the sample. Detectors collect these X-rays, backscattered electrons, and secondary electrons and convert them into a signal that is sent to a screen. This produces the final image. The images created without light waves are delivered black and white.

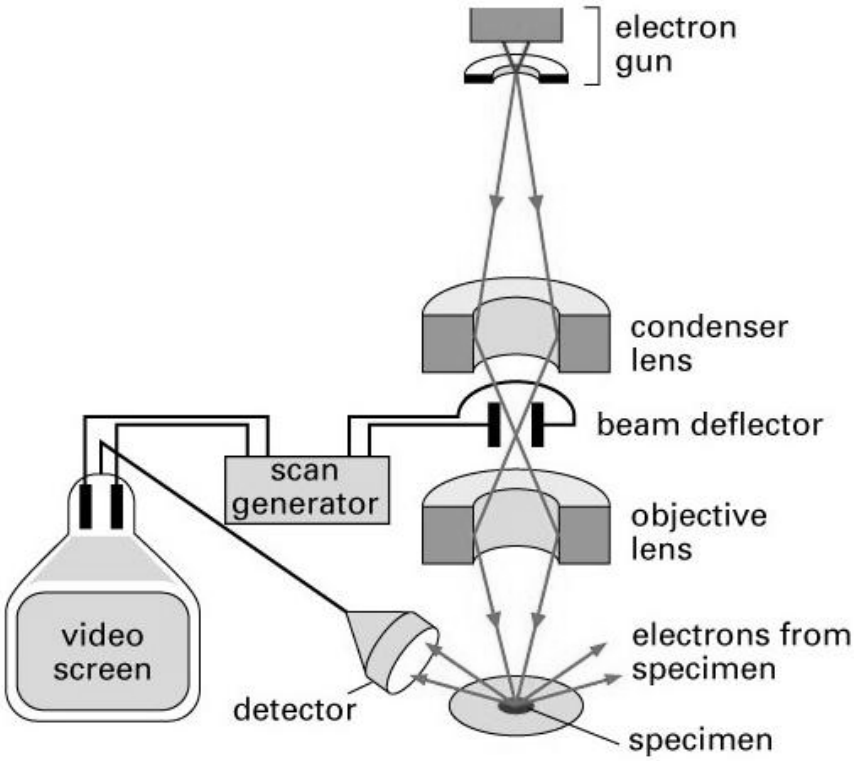


**Figure 4.5.** The schematic view of scanning process and image formation of the SEM.

Low acceleration voltage for electron beam is recommended for analyzing carbon materials because in materials that consist of low atomic number, such as carbon, the electron beam can penetrate and thus the images obtained are the accumulation of secondary electrons reflected from all parts along the depth of penetration. Therefore, in this work, we used low acceleration voltages, less than 5 kV to understand the exact surface of carbon thin films and graphite.

## References

**[1]** Hong Shig-Shim, Ph.D. thesis, Brown University, 1999

**[2]** Jian K, Shim HS, Tuhus-Dubrov D, Woodward C, Bernstein S, Pfeffer M, et al. *Carbon* (2003) 41(11):2073–83

**[3]** Jian K., Xianyu H., Eakin J., Gao Y., Crawford G. P., Hurt R. H., *Carbon* 43 (2005) 407–415

**[4]** Hurt R. H., Krammer G., Crawford G., Jian K., Rulison C., *Chem. Mater.* (2002) *14,* 4558-4565

**[5]** Roddaro S., Pingue P., Piazza V., Pellegrini V., Beltram F., *Nano Lett.* (2007) 7, 2707

**[6]** Zhang Y., Tan Y. W., Stormer H. L., Kim P., *Nature* (2005) 438, 201

**[7]** Ding W., Dikin D. A., Chen X., Piner R. D., Ruoff R. S., Zussman E., Wang X., Li X., *J. Appl. Phys.* (2005) *98*, 014905.

# Chapter 5

# *Catalytic Combustion as a Synthesis Tool for Micropatterned Carbon Materials*

## 5.1 Introduction

It has long been known that the carbon combustion reaction, $C(s) + O_2 \rightarrow CO/CO_2$, is catalyzed by metals, including metal-containing impurities in carbon materials derived from natural precursors. There is an extensive literature on the catalysis of carbon combustion [1–6], much of it from the 1960s and 1970s, motivated by the desire to predict the combustion rates of coal and biomass chars [7,8], cokes [9], and nuclear and structural graphites [10–12]. Al kali metal salts have been observed to markedly increase the rate of oxidation of carbonaceous materials.

Adding 0.5–5 wt% sodium carbonate to a coal resulted in a progressive increase in the reactivity of coke toward air [13]. Harker et al. showed that a potassium impurity had a significant catalytic effect on the gasification of graphite by oxygen [14]. When alkali-metal monoxides, such as $Na_2O$, are added to graphite powder, the temperature of the gasification reaction significantly drops [15]. In a study of coal char reactivity toward air, chars containing the greatest amounts of Ca and Mg impurities showed the highest reactivity at 500 $^oC$ [16]. Vanadium metal and vanadium oxide ($V_2O_5$) were observed to be extremely active catalysts for the oxidation of graphite at temperatures around 550 $^oC$ [17]. Chromium, in the form of $Cr_2O_3$, has been reported as an active catalyst for graphite oxidation [18], as have Pt, Fe, Ni [19], Ag, and Cu [20]. A series of metals and oxides were examined as catalysts for oxidation of powdered graphite and lead oxide showed the highest catalytic activity [19].

In some of these cases, especially for relatively pure carbons at low combustion temperatures, significant rate enhancements ($R_{cat}/R_{non\text{-}cat}$) are observed upon only ppm-level addition of well-dispersed active catalysts. More recent literature on the catalytic combustion of carbon has focused on the use of metals as additives for enhancing low-temperature soot burnout to remove carbon particulate from exhausts, especially in diesel engine applications. Several catalysts have been developed for diesel particulate combustion [21–23]. Ciambelli et al. [24] showed that a Cu/V/K based catalyst is very active in the combustion of various carbonaceous materials. The vanadate-based catalyst $Cs_4V_2O_7$, which still stands as the most active catalyst for diesel soot combustion, resulted in a 50% decrease of the activation energy compared to noncatalytic combustion [25].

Catalytic carbon combustion is a three-phase (solid/solid/gas) reaction system whose fundamental mode of catalytic action has been postulated to involve (1) alteration of the electronic structure of the carbon substrate by catalyst particles and/or (2) oxygen transfer to the carbon surface from the catalyst particle, which serves as a dissociation center for the $O_2$ reactant. Regardless of the mechanism, it is a well established experimental fact that the catalyst action is *local* [6,26]—the accelerated combustion reaction is observed in the immediate vicinity of the catalyst particle or directly at the carbon/catalyst interface, as observed directly by in situ TEM [26].

The combination of local action and high selectivity (large *R*cat/*R*non-cat) suggests to us that catalytic carbon combustion could be used for selectively removing material near strategically placed catalyst particles or films, and thus become a tool for shaping or patterning advanced carbon materials. This concept may be especially attractive for carbon due to the lack of convenient liquid-phase etchants, such as those that exist for lithographic polymers and most other materials. Carbons are quite resistant to solvents, acids, and bases and thus cannot easily be micropatterned by conventional techniques. Catalytic combustion may provide a way to exploit $O_2$ as a dry "etchant" for selective shaping or microstructural modification of a variety of carbon materials. To our knowledge, however, there have not been systematic studies along these lines, and the potential of catalytic carbon combustion as a materials synthesis tool remains largely unexplored. The goal of this chapter is to demonstrate the concept of catalytic combustion as a synthesis tool for shape/structure control in advanced carbon materials using a convenient model material and reaction system.

For the first demonstration of this concept, we chose to work with carbon thin films as simple two dimensional materials and to attempt the formation of parallel microfeatures (a circle micropattern) using liquid transfer of water-soluble metal salts as location-specific catalysts. Carbon thin films find application as electrodes [27–31], lithographic masks [32–35], or material coatings designed for biocompatibility [36,37], lubrication [38,39], abrasion resistance [40,41], or thermal and electrical conductivity [42,43]. For organic materials there are established patterning techniques that include lithography, replica molding (REM), microcontact printing (μCP), and micromolding in capillaries (reviewed in [44]), but these techniques cannot be applied to carbons because of the lack of suitable liquid etchants. The literature contains one report of pattern formation in carbon films produced by the tip of a scanning probe microscope in the presence of oxygen. That study is an example of electrocatalysis, in which the applied voltage at the probe tip induces local consumption of the carbon layer [45]. A second study from the same group shows the possibility of creating 3D structures on amorphous carbon films by local carbon oxidation under the prepatterned tip of a scanning tunneling microscope [46].

For the oxidation catalyst we chose liquid transfer, as it allows us to use established microprinting techniques and is applicable to a wide variety of metals in the form of water-soluble salts. The literature provides some guidance for the selection of the catalyst. Letort and Martin (reviewed in Walker et al. [1]) studied the combustion of graphite in air at 500 ◦C with 0.12% catalyst addition and found the following order of activity: Au > Na > Ca > Ag > Cu > Pb > Ni > Mn > Co > Fe. Amariglio (also reviewed in [1]) impregnated nuclear graphite with 110 ppm of water-soluble salt and

studied the combustion in air at 600 ◦C. This study reported relative activities as in Letort and Martin, but also the catalyst enhancement factors (*R*cat/*R*non-cat): Pb, $4.7\times10^{6}$; Mn, $8.6\times10^{4}$; Ag, $1.34 \times 10^{5}$; Cu, 500; Au, 240; Na, 230; Ba, 100; Cd, 90; Sr, 8; Mg, 6; Co, 4; Al, 3; Be, 1; and B, 1. These enhancement factors are particularly useful for the present study, as they become the "selectivity ratio" that is a key parameter in pattern formation. Other reported rank sequences are from Amariglio and Duval [10] for graphite oxidation, Na > Ba > Sr >Mg > Ca, and Marsh and Taylor [47] for oxidation of metal doped polymer carbon, Co > V > Fe > Mn > Cr. For pure graphite powder in oxygen, McKee obtained the order of catalytic activity as Pb > V > Mn > Co > Cr > Fe > Ni [19].

These data provide only initial guidance for our chosen experiment, since the rank orders are not always consistent and because the catalytic carbon combustion rate is known to depend in a complex way on the properties of the carbon substrate, the doping level, the catalyst dispersion, and to some extent the anion associated with the salt delivery system.

For the anion effect on catalytic activity see for example, Lang [48]. For this reason, a significant experimental effort was spent on testing and optimizing the catalyst formulation.

In the remainder of this chapter we describe the screening of potential catalysts, the behavior of salt solution microdroplets during liquid transfer and drying, and the optimization of catalyst concentration and carbon substrate and then integrate these aspects in the demonstration of simultaneous parallel microfeature formation. This demonstration uses a polydimethylsiloxane (PDMS) stamp to transfer 200-μm diameter catalyst salt solutions as ordered droplet microarrays onto a carbon thin film. Under the

correct drying and reaction conditions, we demonstrate that it is possible to convert these microdroplet arrays into well-defined micropatterned carbon films by controlled catalytic combustion.

## 5.2 Experimental

This study used carbon thin film fabricated by two methods: physical vapor deposition (PVD) and spin coating/carbonization of an organic liquid-crystalline dye [49]. The PVD films were made by using thin carbon thread (1.3 mm nominal diameter) as a source of coating material for evaporation. Quartz substrates were coated by flash evaporation of the carbon thread under high vacuum conditions (CED 030 Carbon Coater, Bal-Tec). The resulting carbon films were annealed at 1000 ◦C for 30 min. The thickness of the PVD films can be preselected by using the film thickness curve and adjusting the height of the sample holder in the evaporator.

The spin-coating process involved depositing an aqueous solution of the aromatic precursor indanthrone disulfonate (Optiva Inc., South San Francisco) [49] onto the center of a quartz substrate and then spinning the substrate at 500 rpm for 20 sec and then 5000 rpm for 30 s in a CEE 200 spin coater from Brewer Science Equipment. After drying, the organic thin film was carbonized by slow heating (4 $^{o}$C/min) in nitrogen to 700 $^{o}$C for 1 h and then annealed at 1000 ◦C for 10 min for further improvement of the film structure. The thickness of the films were estimated by scanning electron microscopy at high tilt and found to be typically 120 nm for PVD films and 1.9 μm for the liquid-crystal-derived

films. In many experiments the carbon thin films were treated with 2 wt% ozone gas in oxygen at room temperature for 10 min to impart oxygen surface groups [50], which improves the droplet wetting and salt deposition patterns.

After ozonation, both drying patterns and combustion results improved for Na and Cr salts. When non-ozonated films were used, the Cr salt formed a high-density catalyst deposit, which blocked oxygen during combustion. By comparison, on ozonated films the same salt produced thinner catalytic films and resulted in quality combustion patterns.

Thermal gravimetric analysis (TGA) is a useful technique for quantifying kinetics, but the very low mass of the carbon thin films make them poor subjects for TGA experiments. We therefore carried out TGA experiments on model carbon nanoparticles with dimensions similar to the film thickness (300–1000 nm) and fabricated from the same precursor and under similar carbonization conditions [51]. These liquid-crystal-derived "supramolecular" carbon nanoparticles were studied as prepared [51] and after doping with 8 mol% NaCl added by incipient wetting of saturated NaCl solutions in air from room temperature to 900 ◦C with a heating rate of 10 ◦C/min in TGA. The reaction temperature was selected by comparing the reactivity plots of as-produced and catalyst-doped carbon nanoparticles in air.

Carbon films were loaded with aqueous solutions of catalytic metal using 10-µl micropipettes. After drying at room temperature, the samples were examined under an optical microscope and the dried droplet pattern was documented by photography prior to combustion. Preliminary combustion experiments were performed at a predetermined reaction temperature in air to eliminate the catalysts that give an inefficient combustion

pattern. To measure selectivity ratios, the times required to completely remove carbon from the as-produced and catalyst-loaded films were determined visually after combustion in a tube furnace.

For the full micropatterning demonstration, aqueous salt solutions were transferred onto carbon thin films using a PDMS microstamping technique. An elastomeric PDMS stamp (see Figure 5.1) with 200-μm diameter circle features was first prepared by casting a prepolymer against a silicon master patterned by conventional lithographic techniques. The catalytic salt solutions were deposited on a glass slide and then spread into uniform thin films by Meyer-bar coating (RD Specialties Inc.) [49]. Meyer bars are wire-wound rods that leave a liquid film of calibrated thickness when scraped over smooth substrates. Here the 20-mil Meyer bar was chosen to give 46-μm thick films, chosen to be much less than the circles' feature depth of 225 μm to prevent filling of the intercircle spaces. After the hemispherical droplet arrays formed on PDMS, the stamps were brought into direct contact with the carbon surface and lifted off to produce similar hemispherical droplet microarrays that were allowed to dry into salt patterns on carbon (see Figure 5.1).

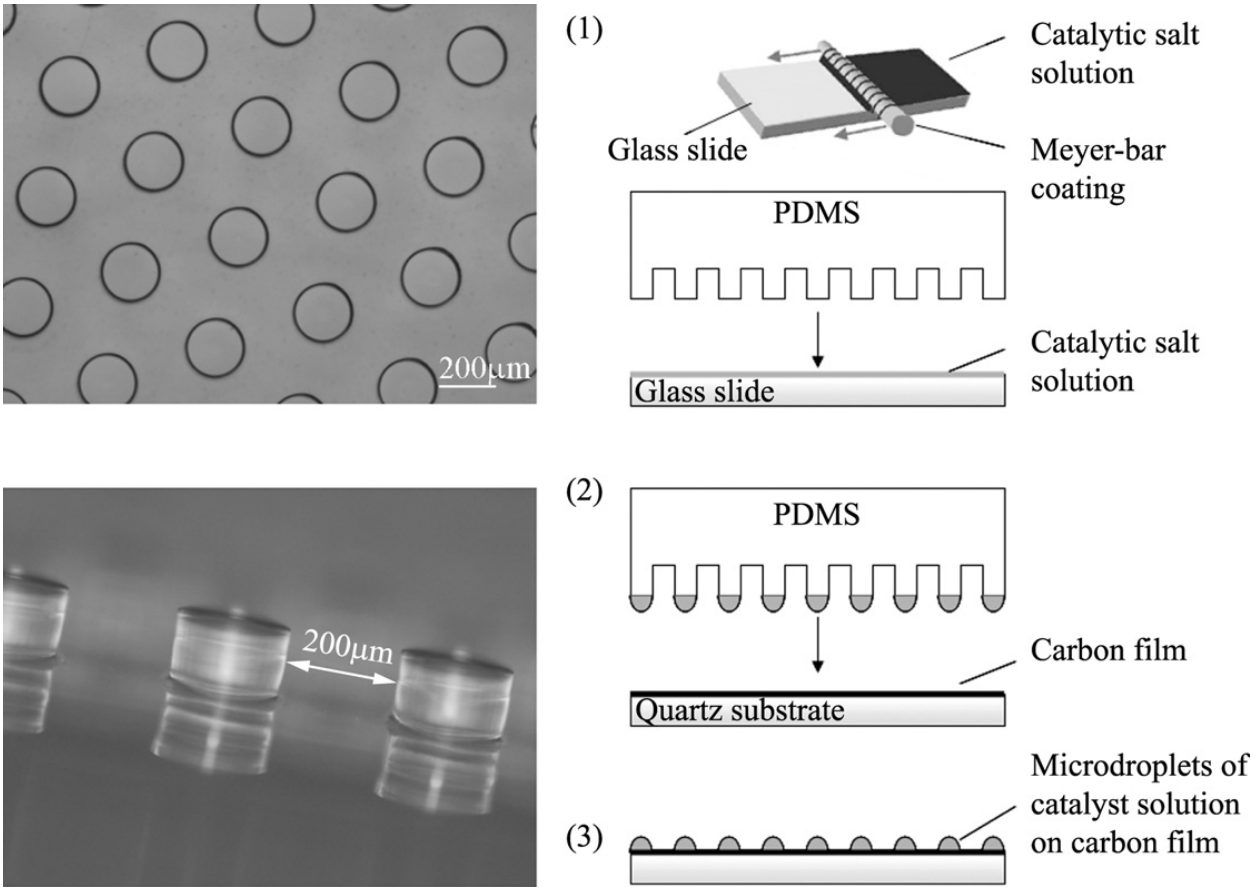


**Figure 5.1.** Optical microscope images of PDMS stamp with feature size 200 μm (left), PDMS stamping technique (right). The microprinting technique consists of (1) PDMS stamp fabrication and Meyer-bar preparation of thin liquid films of catalytic salt solution, (2) microdroplet lift-off and transfer to carbon film, and (3) drying of the microdroplet array and combustion of the carbon with patterned salt films.

After drying at room temperature, the samples were examined by optical and/or electron microscopy and then placed on a ceramic dish and inserted into a quartz tube furnace. After purging with nitrogen gas, the furnace was ramped to 400 ◦C and the gas supply switched to 300 $cm^3$/min of air for controlled oxidation times. The reaction was quenched by switching back to nitrogen flow and cooling and the samples were subjected to microscopic examination.

## 5.3 Results

### 5.3.1 Catalyst Screening

Saturated solutions of $CdCl_2$, $CoCl_2$, $CrCl_3$, $FeCl_3$, KCl, $MgCl_2$, NaCl, and $NiCl_2$ were screened as potential catalysts in the early phase of this study. It quickly became clear that the drying pattern of the salt solutions was the key to obtaining high-quality micropatterns. The Cd, K, Mg, and Ni salts were observed to give irregular drying patterns that deviated significantly from the desired circular footprint of the original microdroplet (see Figure 5.2). These are pipetted droplets of saturated solutions of metal salts dried on liquid-crystal-derived carbon thin films. Compared to salt free droplets, these solutions spread, suggesting some active interaction between the solute and the substrate that altered surface free energies and wetting behavior. Note that these irregular patterns all arise upon drying, as the original pipette drop is observed to be initially circular.

The dendritic structures of potassium salt deposits are particularly noteworthy and beautiful (Figure 5.2). The Co salt showed a coffee drop drying pattern—one in which a

dense ring of solids forms at the outer edge of the original droplet footprint, usually attributed to internal convective flow that transports fine particles (here precipitate particles) from the center to the contact line perimeter, where they deposit [52]. The NaCl solution dries to give a small number of visible salt crystals, which bear no resemblance to the original droplet footprint (Figure 5.2). The chromium salt gave regular circular patterns, which appear promising for micropatterning.

Initial combustion experiments were performed on these samples in air using 400$^{o}$C for short periods of time with 10-s increments to observe the combustion pattern of catalysts. Cd, Mg, and Ni salts did not burn through the carbon and Co and K salts gave undesirable patterns, as expected, because of irregular salt film formation during drying. Although the Fe salt produced a circular drying pattern, burning of larger areas than the original droplet footprint was observed after the preliminary combustion tests. The combustion results for NaCl were surprisingly positive, despite the odd drying pattern (see Figure 5.2), which deviated greatly from the ideal circular footprint. Progressive combustion of NaCl-doped samples gradually gave rise to well-defined circular etch patterns (see Figure 5.3) at the location of the original droplets.

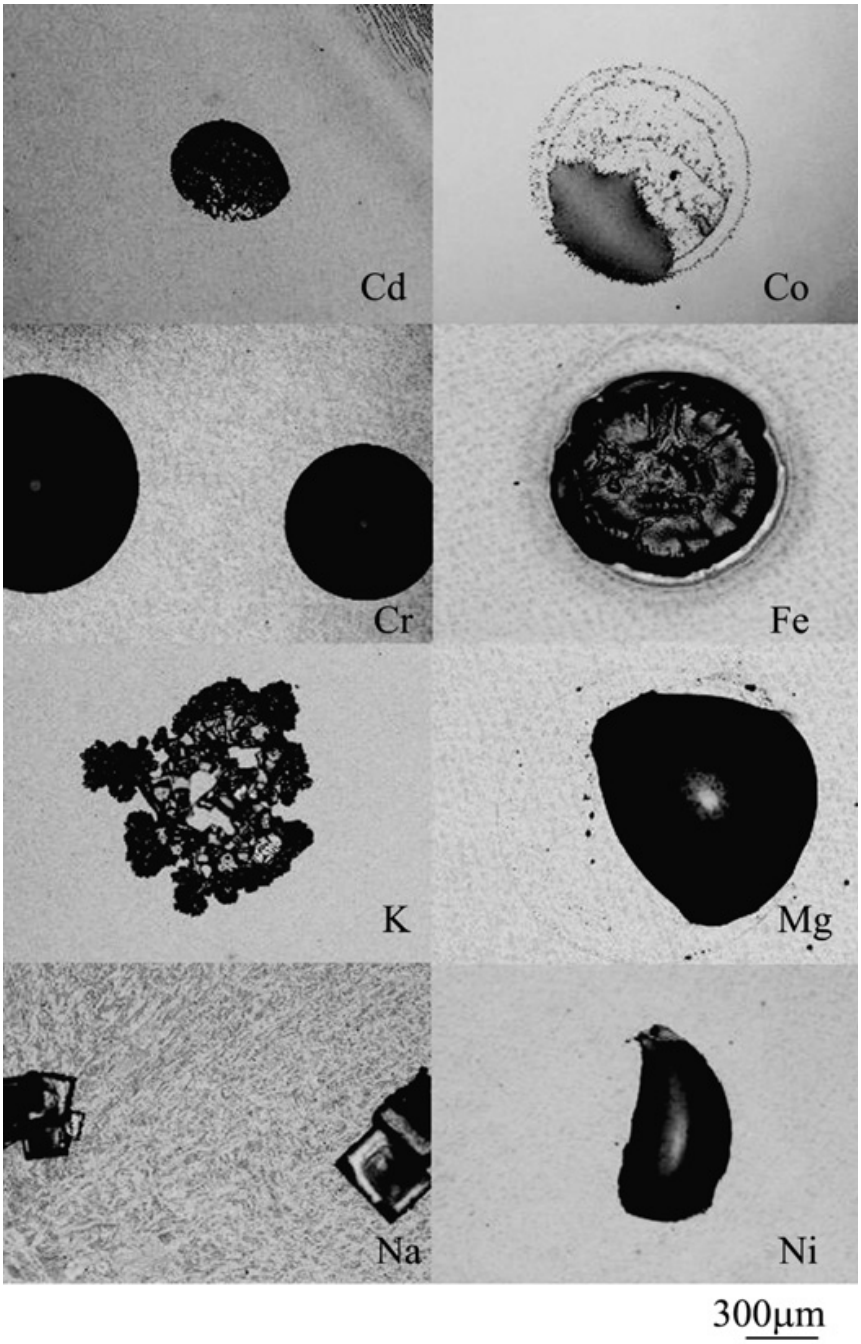


**Figure 5.2.** Optical microscope images of metal salt deposits on carbon thin films following microdroplet deposition and drying.

It became clear that there is a transparent circular film on the original droplet footprint that is catalytically active, and the large crystals are excess salt above that needed to form the adsorbed film. The existence of this circular thin NaCl film in the unreacted sample was confirmed by SEM (see Figure 5.3), and surprisingly, NaCl was one of the best catalysts, judged by the quality of the final circular etch features. Sodium chloride catalysis occurs through an active but optically invisible salt layer (Fig. 5.3 left), which is gradually revealed (Fig. 5.3 center and right) through its selective combustion at 400 ◦C in air of the underlying carbon thin film.

Based on the time for the catalytic reaction to completely consume the underlying carbon (see Section 5.3.4), one can define a dimensionless reaction time or Damköhler number as,

$$Da \equiv \frac{t_{process}}{t_{cat-rxn}}$$

In Figure 5.3, Da = 0 (left), 0.11 (center), and 0.5 (right).

In general, both the drying pattern and the subsequent combustion pattern need to be evaluated to choose the best catalyst formulation. Based on both sets of experiments, Na and Cr were chosen for further development as micropatterning catalysts.

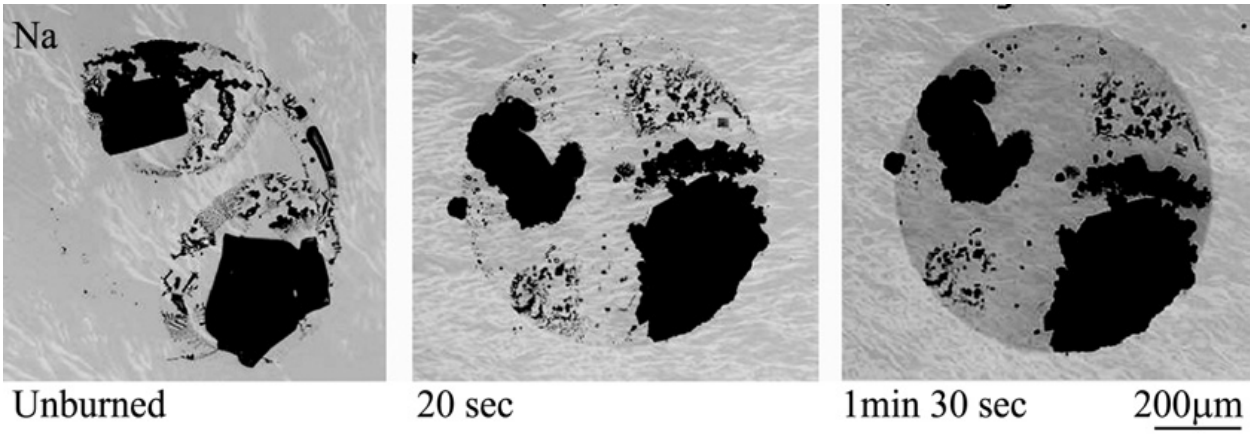


**Figure 5.3.** Optical microscope images of gradual appearance of sodium chloride catalysis which at first forms an active but optically invisible thin film.

### 5.3.2 Effect of Carbon Substrate

The effect of the carbon substrate was examined by comparing the combustion pattern of NaCl on PVD and spin coated films. After 5 min combustion of the PVD carbon thin film at 400 ◦C with Na salt in air, we observed peeling of the carbon on the outer edge of the original droplet (see Figure 5.4), which may be due to residual tensile stress in the films.

The carbon thin films prepared by spin coating of an aromatic aqueous solution followed by carbonization at 700 ◦C show liquid crystalline structure under polarized light [49]. The surface is uniform, dense, and entirely anisotropic. After combustion in the presence of Na or Cr salts, no secondary fracture or detachment was observed, so further work concentrated on these films. The spin coated carbon films were ozone treated at room temperature for 10 min. Cr forms a solid drop of a catalytic film on as produced carbon

film (Figure 5.5a left) , which blocks oxygen and results in inefficient combustion (Figure 5.5a right).

However, ozonated films show a better combustion pattern (Figure 5.5b right) due to formation of a thinner catalytic film showing optical interference patterns that indicate a thickness on the order of a wavelength of visible light (Figure 5.5b left). Significant improvement in the fidelity of the combustion pattern was observed as a result of better salt film deposition on the more hydrophilic film.

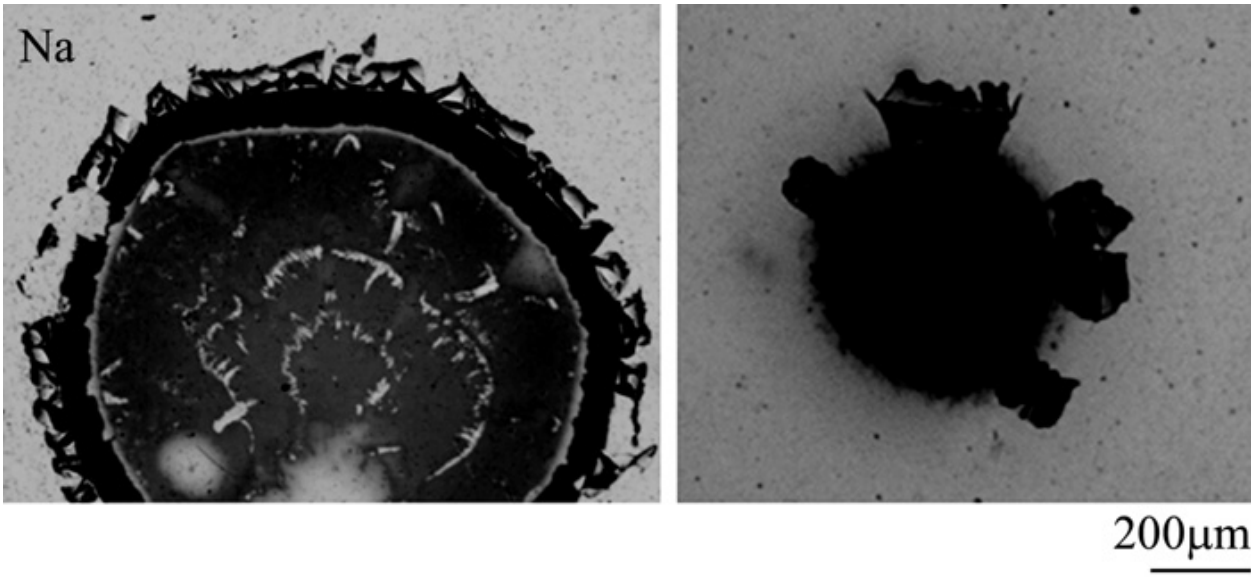


**Figure 5.4.** Combustion pattern of Na salt on PVD carbon films. Cracking, detachment, and curl-up of the carbon film occurs on the edges of a large (left) and small (right) circular combustion zone, likely due to residual stress in this type of film.

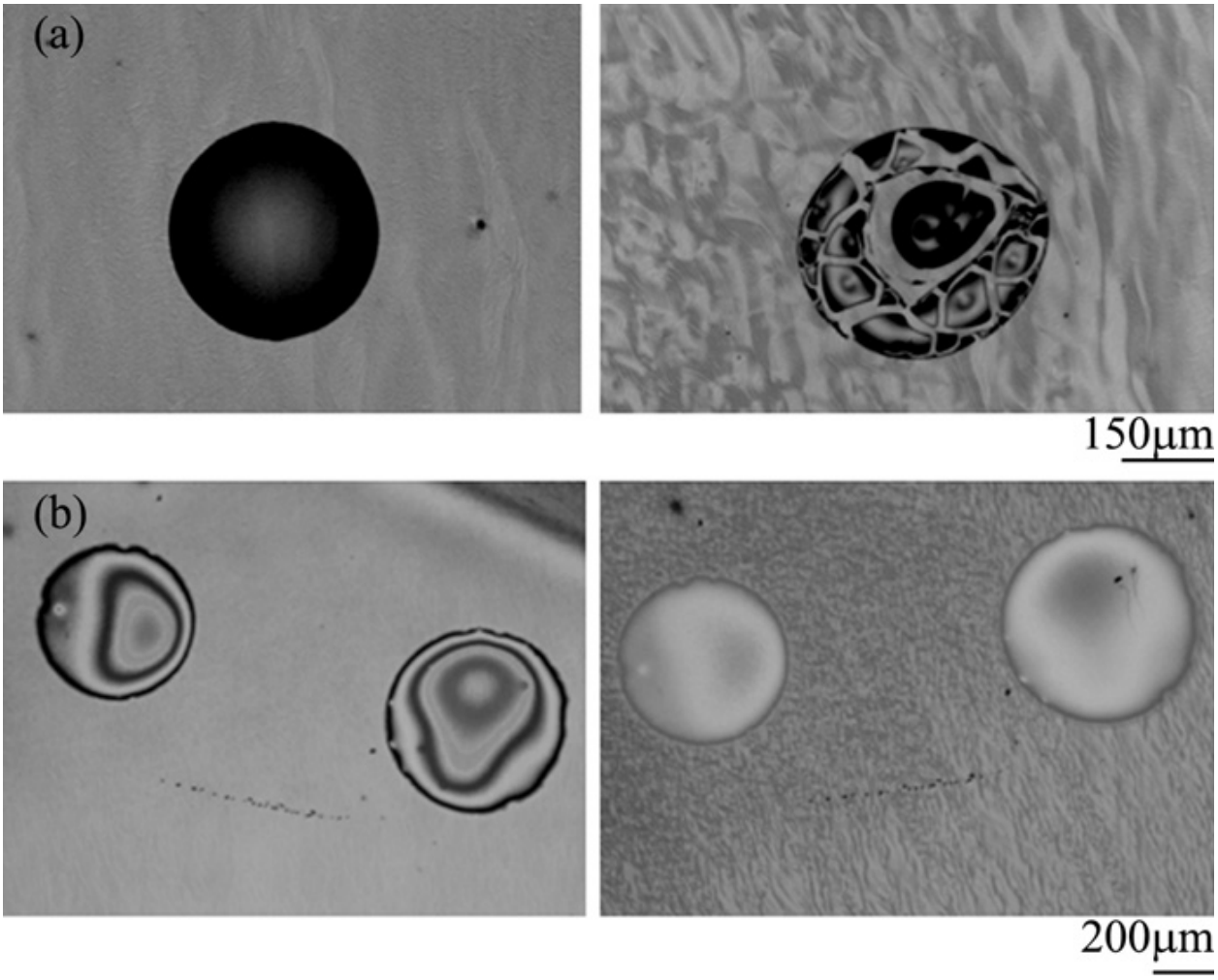


**Figure 5.5.** Drying (left) and combustion patterns (right) of Cr salt on as-produced (a) and ozonated (b) spin-coated carbon films.

### 5.3.3 Effect of Salt Concentration

After Na and Cr were chosen as catalysts for detailed study, the role of solution concentration was investigated by repeating the screening experiments after various dilutions of the original saturated NaCl solution. Figure 5.6 shows the result for NaCl, which shows improved performance at the highest concentration used. Optical

microscope images of NaCl-doped carbon films before (top row) and after combustion at 400 ◦C in air for 3 min (bottom row) demonstrate the effect of increasing NaCl concentrations. Concentrations used with the left-to-right sequence are: (a) 0.01 mol% or 1/1000 saturation; (b) 0.1 mol% or 1/100 saturation; and (c) 5 mol% or 1/2 saturation.

Examination of these films from below indicates that at lower concentrations the reaction is confined to the zone directly beneath the large NaCl crystals. As the salt concentration increases, larger Na crystals form on the film and the combustion results suggest the formation of a better salt film (Figure 5.6c).

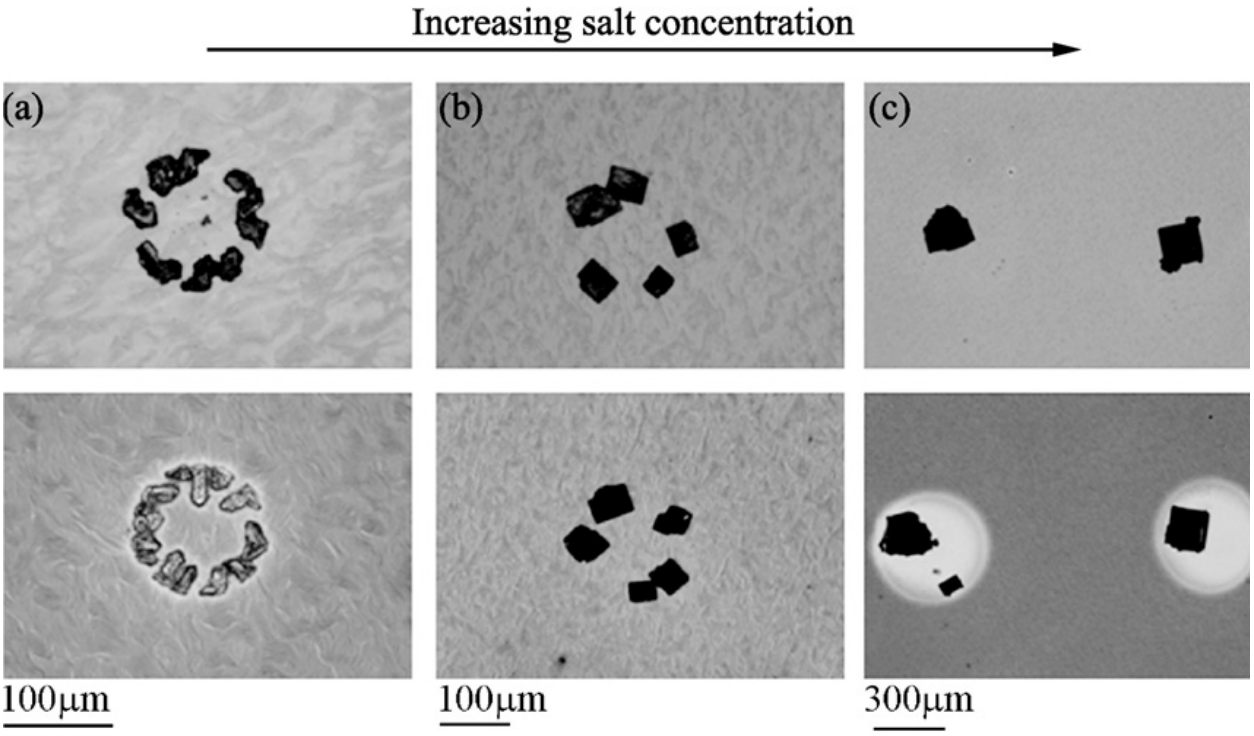


**Figure 5.6.** Effect of salt concentration on the generation of features by selective combustion.

### 5.3.4 Kinetics and Selectivity

Regarding catalytic combustion as an etching process, we can define selectivity as the ratio of the catalytic to the noncatalytic (undoped) rate: $R_{cat}/ R_{non\text{-}cat}$. Selectivity ratios were measured as the inverse ratios of the total combustion time in the presence and absence of catalyst and were determined optically as the times required to reveal the underlying quartz (see Table 5.1). The total catalytic combustion time was determined optically as the time required at 400 ◦C in air to completely remove the carbon film in the doped areas and reveal a circle of underlying quartz. The total combustion time of the as-produced (non-catalytic) carbon film at 400 ◦C is 170 min and selectivity ratios are summarized in Table 5.1.

Figure 5.7 gives the nonisothermal TGA data as an alternative way to quantify the catalytic rate enhancement. The as-produced carbon nanoparticles used as model material begin to lose mass by oxidation around 550 $^{o}$C, compared to about 400 ◦C for the 8 mol% NaCl doped nanoparticles. A temperature of 400 ◦C was selected for the micropatterning process, since the TGA data in Figure 5.7 indicate that the non-catalytic rate is very slow, but the temperature is just above the reaction initiation point where the catalytic rate begins to proceed quickly.

**Table 5.1.** Selectivity ratios[a] measured for carbon thin fims[b] doped with saturated solutions of various catalytic salts

| Material | Time (min) | $R_{cat}/ R_{non\text{-}cat}$[c] |
|---|---|---|
| Raw carbon film | 170 | - |
| NaCl | 3 | 57 |
| $CrCl_3$ | 0.5 | 329 |
| $CoCl_2$ | 1.5 | 113 |

[a] Selectivity ratios are special for conditions of this experiment (T, $P_{O2}$, solution concentration, droplet size)

[b] Liquid-crystal derived carbon films with an average salt film diameter of 500 μm.

[c] Combustion in air at 400°C

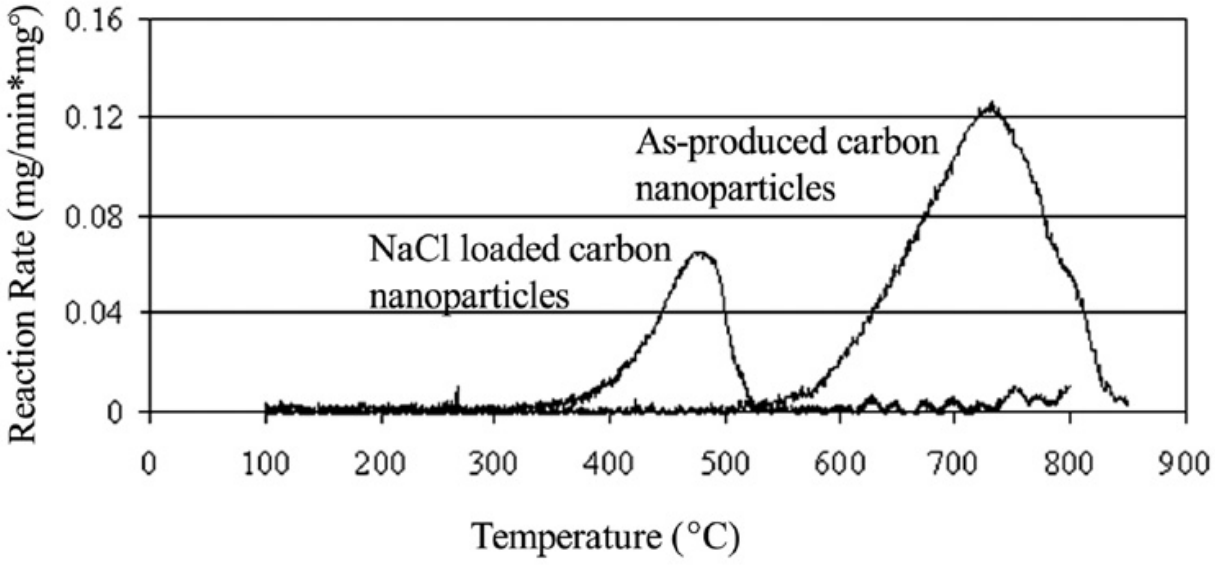


**Figure 5.7.** Comparison of catalytic and noncatalytic rates on carbon nanoparticles [50,51] prepared from the same precursor and carbonization conditions as the liquid-crystal-derived films. Rates are measured by nonisothermal TGA at $10^{o}$C/min in air. Catalyst is 8 mol% NaCl added by incipient wetness from saturated NaCl solutions. On the $Y$-axis, $mg_o$ refers to the initial unreacted weight of the sample.

### 5.3.5 Micropatterning

The full micropatterning experiment was carried out for both the sodium and chromium salts using saturated solutions on the liquid-crystal-derived thin films. Following the Meyer-bar spreading of solution films, microdroplet arrays were transferred to carbon via the PDMS stamp followed by drying and oxidation (10 and 3 min for sodium and chromium respectively) at 400$^{o}$C. A selection of results is shown in Figure. 5.8. For the sodium salt case, an ordered array of polygonal crystals is seen prior to combustion and a surrounding circular salt film is visible by SEM (b) but not optical microscopy (a). Combustion is selective on the catalytic regions, and Figure 5.8 shows examples of circle features in various stages of formation (c, d, f). Exceeding the minimum time for complete carbon consumption under the catalyst footprint (3 min, based on Figure 5.6c) leads to "blooming" of the combustion front beyond the circle boundaries.

This does not appear to be due to non-catalytic reaction (which is slow), but rather to horizontal migration of the catalytic reaction front occurring during or after the formation of the primary pattern. These larger area arrays are sometimes vulnerable to temperature and oxygen gradients and corresponding gradients in conversion, as seen in the example in panel (d).

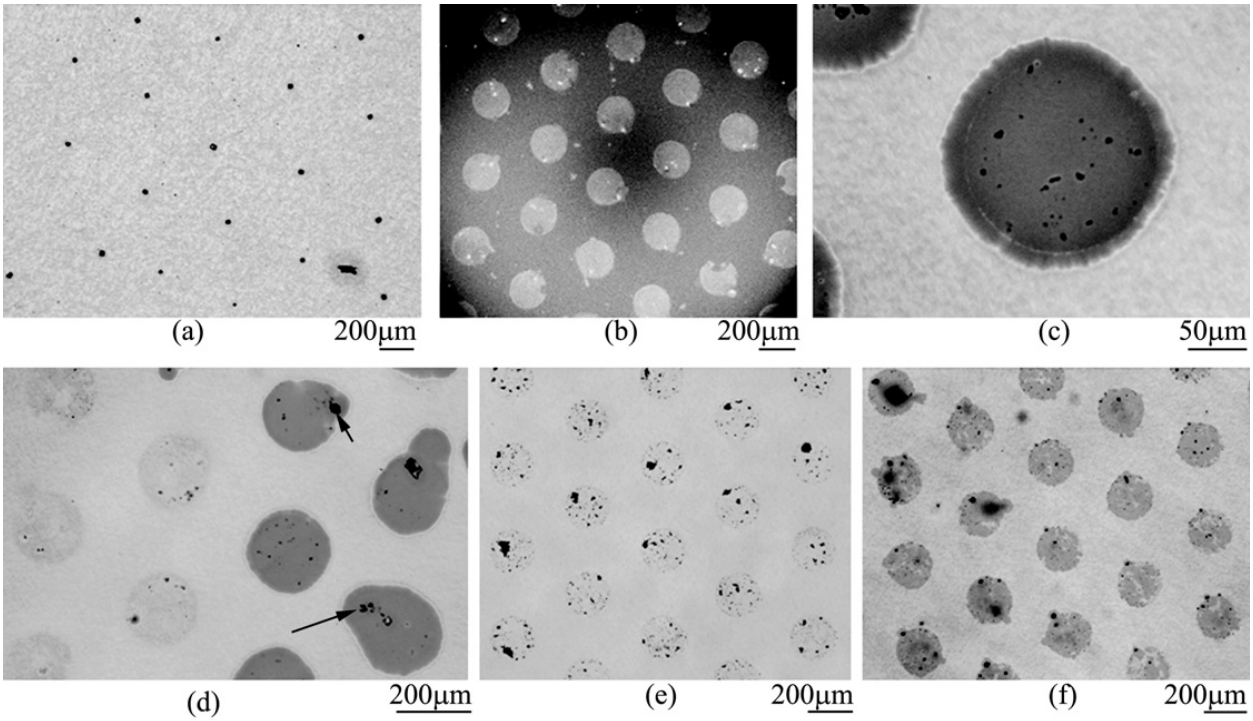


**Figure 5.8.** Selection of micropatterning behaviors. (a) Optical micrograph of NaCl micropattern showing excess salt crystals but no visible salt film, (b) same array with salt film visible by SEM, (c) NaCl-catalyzed single-circle feature at high magnification postcombustion (10 min), (d) example of circle features at different stages of combustion in a single sample due to spatial gradients where arrows indicate probable sites of horizontal catalyst migration (10 min), (e) $CrCl_3$ array after drying, and (f) $CrCl_3$ array after partial combustion (3 min).

## 5.4 Discussion

The combined results successfully demonstrate the concept of selective etching using catalytic combustion for the chosen example of micropatterned carbon thin films. Measured selectivity ratios ($R_{cat}/ R_{non\text{-}cat}$) are high, ranging from about 50 to 300, so the larger challenge is to create well-defined metal doping patterns prior to combustion. Here

we focused on liquid-phase delivery of soluble salts, which works sufficiently well for some catalysts (NaCl and $CrCl_3$) but is problematic for others due to irregular drying patterns. Beyond uniform deposition, there is also the challenge of controlling metal surface density in the desired range. Insufficient density does not lead to a uniform catalytically active salt film, while very high densities produce excess deposits, which in some cases block access of oxygen to the carbon surface and/or are difficult to remove following combustion. Similar behavior has been reported in other studies of catalytic carbon gasification, where rates are proportional to metal content at low doping levels, but reach saturation at higher levels [1, 8, 12, 13] and eventually cause rate decreases by physical blockage of carbon surface area. For both NaCl and $CrCl_3$ a catalyst formulation was found and optimized that is capable of producing patterned microfeatures in carbons after PDMS microprinting, drying, and low-temperature combustion at 400$^{o}$C. The condition that leads to successful microfeature production in Figure 5.8c corresponds to a surface NaCl density of about 2 mg/cm$^2$, which for a 1.9-μm-thick carbon film of density 1.7 g/cm$^3$ corresponds to a NaCl/C mass ratio of 6.5:1 or 57 mol% catalyst within the doped circles.

Finally, it will be useful to examine any fundamental limitations on feature size that arise from the scaling relationship between droplet size and salt film density (see Figure. 4.9).

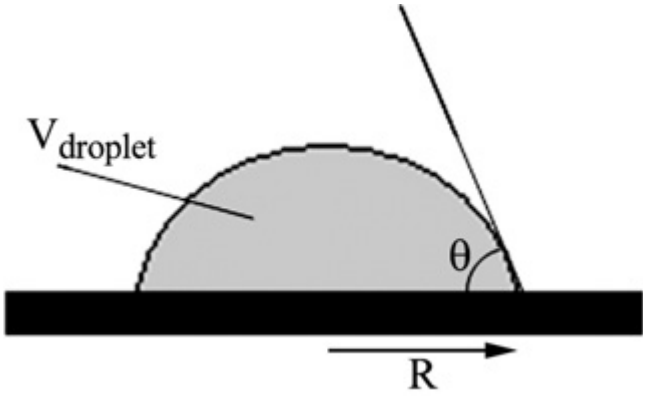


**Figure 5.9.** Schematic diagram of the salt film droplet on carbon film.

Dried salt film density depends on the contact angle, $\theta$, the feature size, $R$, and the concentration, $[C]$, of the initial salt solution. The combustion behavior is governed by the *dried* salt film, so we are interested in predicting the dried salt surface density, $\sigma \equiv m_{salt}/A_{droplet}$, as a function of droplet radius, $R$, solution contact angle, $\theta$, and mass concentration (mg/ml) of salt, $[C]$, in the initial solution. The main mass balance is,

$$m_{salt} = V_{drop} \times [C], \tag{1}$$

where $V_{drop}$ is the volume of the droplet determined by the geometric relation.

For spherical curvature in the liquid (see Fig. 5.9),

$$V_{drop} = \frac{\pi}{3} \times \frac{R^3}{\cos^3(90-\theta)} \times [1-\sin(90-\theta)]^2 \times [2+\sin(90-\theta)]. \tag{2}$$

This condition is strictly fulfilled in the limit of small drops where gravity effects are negligible and the Laplace equation predicts uniform 2D curvature at the droplet/gas interface.

Combining, the dried salt film density, $\sigma$, becomes

$$\sigma = \frac{1}{3} \times [C] \times R \times \frac{[1 - \sin(90 - \theta)]^2 \times [2 + \sin(90 - \theta)]}{\cos^3(90 - \theta)} \quad (3)$$

For the simple case of θ = 90◦,

$$\sigma = \frac{2}{3} \times [C] \times R \quad (4)$$

Figure 5.10 shows the effect of solution wetting (contact angle) at fixed concentration. As expected, decreasing contact angle (improved wetting) leads to larger feature sizes and lowered salt film densities. Figure 5.11 examines the effect of droplet size for the simple case of 90◦ solution contact angle, which is similar to that for pure water on highly oriented pyrolytic graphite often used as model of the ideal graphite basal surface [50]. (Other smooth carbon surfaces have lower contact angles that range from 30◦ to 80◦ depending on surface functional groups [50].)

At a fixed salt concentration in solution and fixed contact angle, increasing droplet size leads to higher salt film surface densities due to the $\sim R^1$ scaling in Eq. (3). The data from the present study are also shown on this plot, along with a rough indication of the salt film density ranges that led to good feature production. One of the consequences of this plot is the need to use higher salt concentrations as droplet (feature) size is reduced in order to remain in the favorable range of salt film density. Another consequence of this scaling behavior will be the difficulty of extending the technique to nanoscale features (<100 nm) (using dip-pen lithography, for example [53]) due to reduced salt film density

at small scales. Extension of this technique to nanoscale features may require another method of metal delivery such as physical vapor deposition or sputtering.

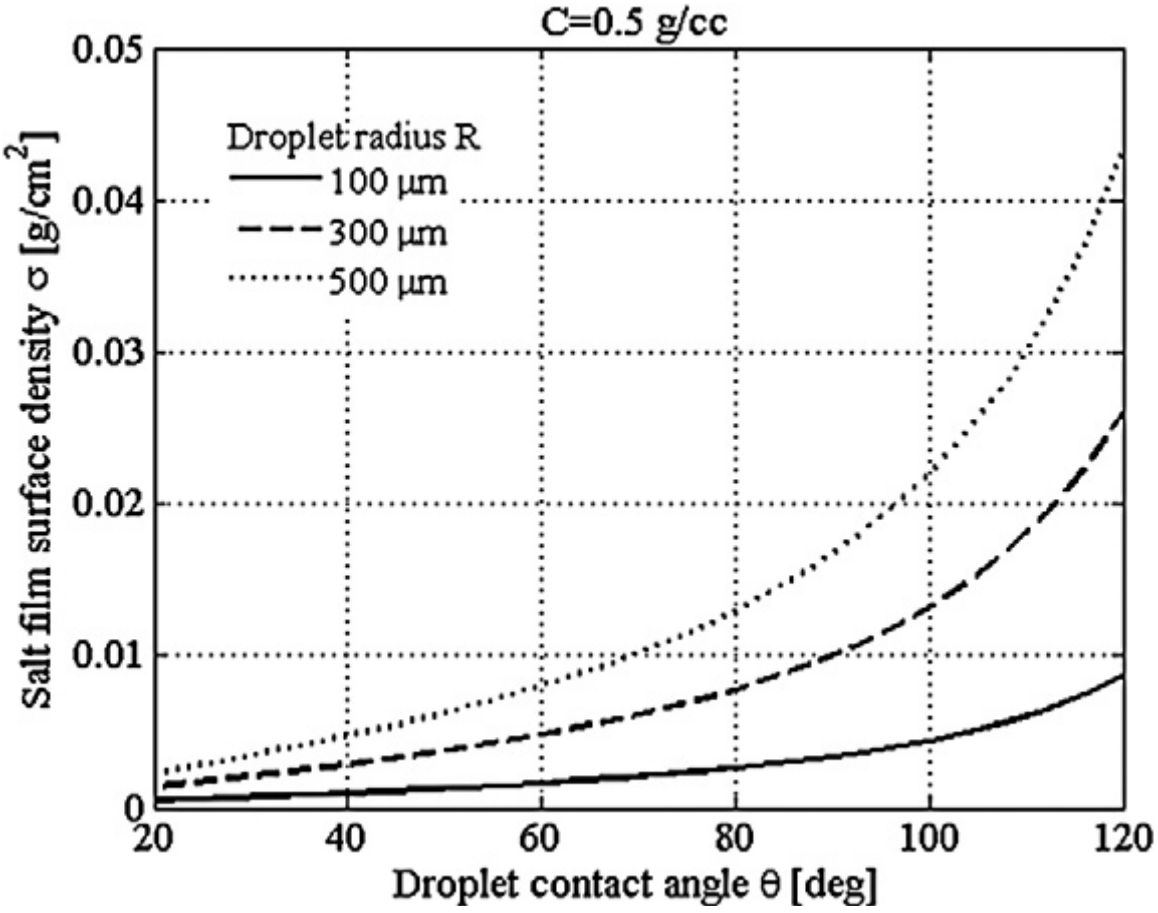


**Figure 5.10.** Salt film surface density predicted by Eq. (3) as a function of feature size and water contact angle. All calculations are for the high concentration case, [*C*] = 0.5 g/cm3. Poor wetting solvents (high $\theta$ ) are more effective at delivering patterns with high salt film densities.

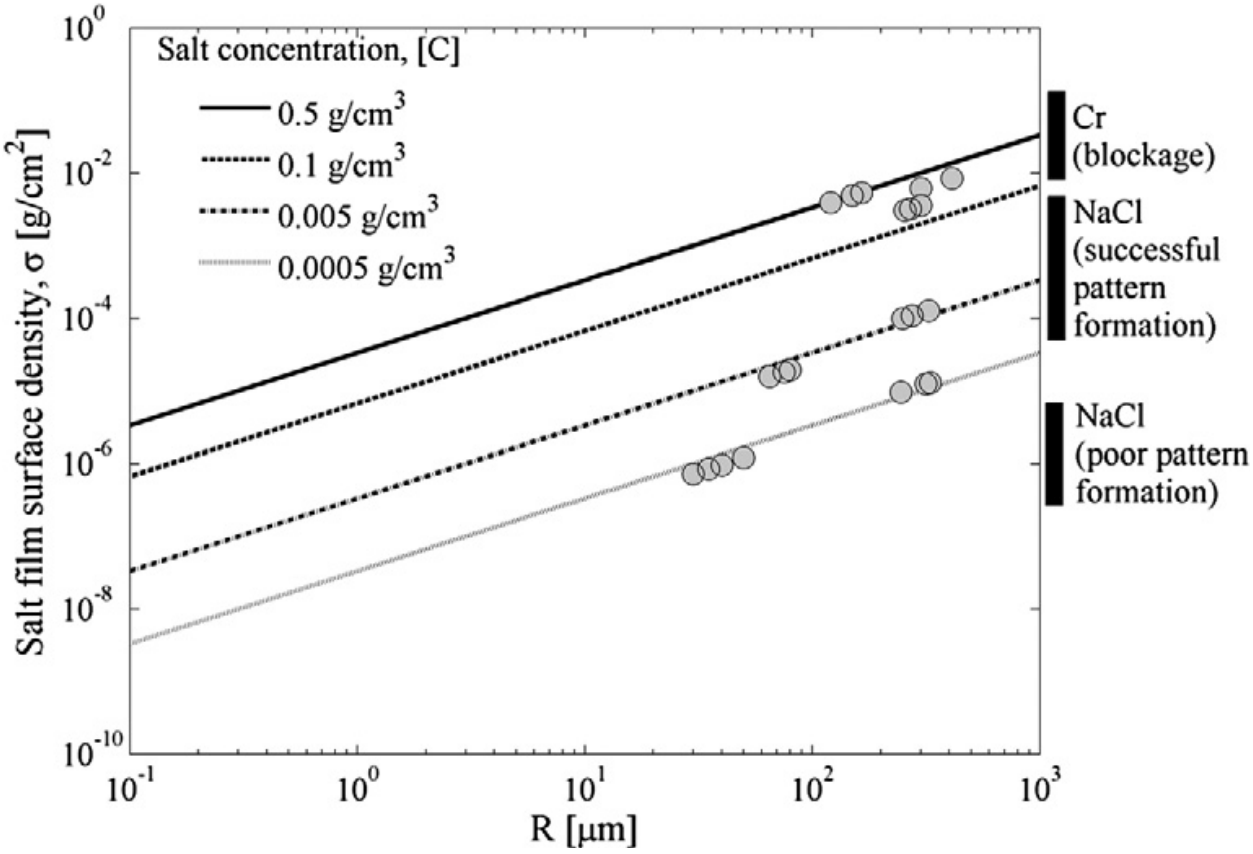


**Figure 5.11.** Salt film surface density predicted by Eq. (3) as a function of feature radius, *R*, and initial salt concentration, [*C*].

Circles show the experimental data (*R*, [*C*] values) and the vertical bars indicate the approximate ranges where combustion patterning was observed to be successful or not. Figure 5.11 suggests a fundamental limitation on the minimal feature size obtainable by this technique. Below about 1 μm, even the most concentrated solutions (0.5 g/cm$^3$) give salt films of lower surface density than is needed to make reliable patterns.

## 5.5 Conclusions

These results demonstrate that catalytic combustion can be used to selectively shape or pattern carbon materials. Common metals give catalytic selectivity factors (*R*cat/*R*non-cat) that are clearly large enough for high-fidelity patterning, so the more significant challenge is the accurate positioning of the catalyst and prevention of its migration during drying and combustion. Among the metal salts examined, sodium and chromium chlorides are most suited overall for microfeature formation by selective catalytic combustion. PDMS microstamping provides a route for one step generation of large area arrays. Droplet footprints of 300 μm and larger can be reproduced in carbon with reasonable fidelity, but smaller features become more challenging due to the effects of horizontal catalyst migration and/or the intrinsic scaling law for droplet drying which predicts reduced salt film surface density as droplet size decreases.

We imagine a variety of other applications for this basic concept including the shaping of carbon monoliths, the use of catalytic single particles, fibers, nanoparticles, or nanorods to make controlled pores or nanoscale features, or three-dimensional contouring of vertical carbon nanotube/fiber arrays within alumina templates, which is not easily accomplished by existing patterning techniques. Combustion methods in general are making increasing contributions to advanced materials synthesis and processing [54–58], and the present work offers a new approach within this emerging interdisciplinary field.

## References

**[1]** P.L. Walker Jr., M. Shelef, R.A. Anderson, in: P.L. Walker Jr. (Ed.), Chemistry and Physics of Carbon, vol. 4, Dekker, New York, 1968, p. 287.

**[2]** P.L. Walker Jr., F. Rusinko Jr., L.G. Austin, Adv. Catal. 11 (1959) 133.

**[3]** G.D. Blackwood, Coke Gas 22 (190) (1960) 250–293.

**[4]** T.J. Clark, R.E. Woodley, D.R. De Halas, Nuclear Graphite, Academic Press, New York, 1962, pp. 387–437.

**[5]** S. Ergun, M. Menster, in: P.L. Walker Jr. (Ed.), Chemistry and Physics of Carbon, vol. 1, Dekker, New York, 1966, pp. 203–263.

**[6]** D.W. Mckee, in: P.L. Walker Jr., P.A. Thrower (Eds.), Chemistry and Physics of Carbon, vol. 16, Dekker, New York, 1981, pp. 1–118.

**[7]** J.T. Gallagher, H. Harker, Carbon 2 (2) (1964) 163– 173.

**[8]** H. Harker, in: Proceedings of the Fourth Conference on Carbon, Buffalo, 1959, Pergamon, New York, 1960, pp. 125–139.

**[9]** G.W. Lee, Coke Gas 23 (398) (1961) 442.

**[10]** H. Amariglio, X. Duval, Carbon 4 (3) (1966) 323–332.

**[11]** H. Hering, S. Keraudy, F.M. Lang, S. May, in: Proceedings of the Fourth Conference on Carbon, Buffalo, 1959, Pergamon, New York, 1960, pp. 115–122.

**[12]** H. Amariglio, These Docteur Science, Université de Nancy, 1960.

**[13]** J.W. Patrick, F.H. Shaw, Fuel 51 (1) (1972) 69–75.

**[14]** H. Harker, J.B. Horsley, D. Robson, J. Nucl. Mater. 37 (3) (1970) 331–339.

**[15]** D.W. McKee, D. Chatterji, Carbon 13 (5) (1975) 381–390.

**[16]** R.G. Jenkins, S.P. Nandi, P.L. Walker Jr., Fuel 52 (4) (1973) 288–293.

**[17]** R.T.K. Baker, R.B. Thomas, M. Wells, Carbon 13 (2) (1975) 141–145.

**[18]** P. Magne, X. Duval, Bull. Soc. Chim. Fr. 5 (1971) 1585–1593.

**[19]** D.W. McKee, Carbon 8 (5) (1970) 623–626.

**[20]** E.T. Turkdogan, J.V. Vinters, Carbon 10 (1) (1972) 97–106.

**[21]** P. Ciambelli, P. Corbo, M. Gambino, V. Palma, S. Vaccaro, Catal. Today 27 (1–2) (1996) 99–106.

**[22]** P. Ciambelli, P. Corbo, P. Parrella, M. Scialò, S. Vaccaro, Thermochim. Acta 162 (1) (1990) 83–89.

**[23]** C. Badini, G. Saracco, V. Serra, V. Specchia, Appl. Catal. B Environ. 18 (1–2) (1998) 137-150.

**[24]** P. Ciambelli, V. Palma, S. Vaccaro, Catal. Today 17 (1–2) (1993) 71–78.

**[25]** C. Badini, G. Saracco, N. Russo, V. Specchia, Catal. Lett. 69 (2000) 207–215.

**[26]** R.T.K. Baker, Catal. Rev. Sci. Eng. 19 (2) (1979) 161–209.

**[27]** G.K. Kiema, M.J. Brett, J. Electrochem. Soc. 150 (7) (2003) E342–E347.

**[28]** J. Kim, X. Song, K. Kinoshita, M. Madou, R. White, J. Electrochem. Soc. 145 (7) (1998) 2314–2319.

**[29]** S. Ranganathan, R.L. McCreery, S.M. Majji, M. Madou, J. Electrochem. Soc. 147 (1) (2000) 277–282.

**[30]** S. Ranganathan, R.L. McCreery, Anal. Chem. 73 (5) (2001) 893–900.

**[31]** R. Schlesinger, M. Bruns, H.-J. Ache, J. Electrochem. Soc. 144 (1) (1997) 6–15.

**[32]** J.Z. Sun, W.J. Gallagher, A.C. Callegari, V. Foglietti, R.H. Koch, Appl. Phys. Lett. 63 (11) (1993) 1561–1563.

**[33]** H.R. Yi, Z.G. Ivanov, D.Winkler, Y.M. Zhang, H. Olin,P. Larsson, T. Claeson, Appl. Phys. Lett. 65 (9) (1994)1177–1179.

**[34]** H.R. Yi, M. Gustafsson, D.Winkler, E. Olsson, T. Claeson, J. Appl. Phys. 79 (12) (1996) 9213–9220.

**[35]** S. Park, T. Lim, D. Yang, J. Jeong, K. Kim, K. Lee, H. Kong, Appl. Phys. Lett. 88 (20) (2006) 203105.

**[36]** J.A. McLaughlin, B.Meenan, P.Maguire, N. Jamieson, Diamond Relat. Mater. 5 (1996) 486–491.

**[37]** R.J. Narayan, Int. Mater. Rev. 51 (2) (2006) 127–143.

**[38]** A. Vanhulsel, F. Velasco, R. Jacobs, L. Eersels, D. Havermans, E.W. Roberts, I. Sherrington, M.J. Anderson, L. Gaillard, Tribol. Int. 40 (7) (2007) 1186–1194.

**[39]** S.J. Harris, A.M. Weiner, S.C. Tung, S.J. Simko, M.C. Militello, Surf. Coat. Technol. 62 (1–3) (1993) 550–557.

**[40]** M.H. Sohn, Y.O. Ahn, Y.W. Ko, S.R. Hah, T.E. Fischer, S.I. Kim, J. Vac. Sci. Technol. A 16 (6) (1998) 3554–3558.

**[41]** P. Hollman, P. Hedenqvist, S. Hogmark, G. Stenberg, M. Boman, Surf. Coat. Technol. 96 (2–3) (1997) 230–235.

**[42]** S. Aoqui, T. Ikegami, Y. Yamagata, K. Ebihara, Thin Solid Films 316 (1–2) (1998) 40–44.

**[43]** W.J. Li, Z.R. Song, Y.H. Yu, S.C. Zou, D. Shen, Nucl. Instrum. Methods Phys. Res. B 206 (2003) 339–342.

**[44]** Y. Xia, G.M. Whitesides, Annu. Rev. Mater. Sci. 28 (1998) 153–184.

**[45]** T. Mühl, H. Brückl, G. Weise, G. Reiss, J. Appl.Phys. 82 (10) (1997) 5255–5258.

**[46]** T. Mühl, J. Kretz, I.Mönch, C.M. Schneider, H. Brückl, G. Reiss, Appl. Phys. Lett. 76 (6) (2000) 786–788.

**[47]** H. Marsh, D.W. Taylor, in: Abstracts 13th Biennial Carbon Conf., 1977, p. 46.

**[48]** R.J. Lang, Fuel 65 (1986) 1324–1329.

**[49]** K. Jian, H. Xianyu, J. Eakin, Y. Gao, G.P. Crawford, R.H. Hurt, Carbon 43 (2) (2005) 407 415.

**[50]** A. Yan, X. Xiao, I. Külaots, B.W. Sheldon, R.H. Hurt, Carbon 44 (14) (2006) 3113–3120.

**[51]** A. Yan, B.W. Lau, B.S. Weissman, I. Külaots, N.Y.C. Yang, A.B. Kane, R.H. Hurt, Adv. Mater. 18 (18) (2006) 2373–2378.

**[52]** R.D. Deegan, O. Bakajin, T.F. Dupont, G. Huber, S.R. Nagel, T.A. Witten, Nature 389 (6653) (1997) 827–829.

**[53]** R.D. Piner, J. Zhu, F. Xu, S. Hong, C.A. Mirkin, Science 283 (5402) (1999) 661–663.

**[54]** F.S. Xu, X.F. Liu, S.D. Tse, Carbon 44 (3) (2006) 570–577.

**[55]** M.J. Height, J.B. Howard, J.W. Tester, J.B.V. Sande, Carbon 42 (11) (2004) 2295–2307.

**[56]** R.L. Vander Wal, Combust. Flame 130 (1–2) (2002) 37–47.

**[57]** R.A. Ayers, D.E. Burkes, G. Gottoli, H.C. Yi, F. Zhim, L. Yahia, J.J. Moore, J. Biomed. Mater. Res. Part A 81 (3) (2007) 634–643.

**[58]** Y.S. Zhang, G.C. Stangle, J. Mater. Res. 9 (8) (1994) 1997–2004.

# Chapter 6

# *A Magneto-Catalytic Writing Technique for Etching Complex Channel Patterns In Multi-Layer Graphene*

## 6.1 Introduction

Graphene, single layer of graphite sheet, has a two-dimensional (2D) honeycomb structure and forms the basis of all other graphitic materials of different dimensionalities such as 0D fullerenes, 1D nanotubes or 3D graphite. Although graphene has been studied for more than 60 years as 2D crystals of graphite [1-3], the number of studies has increased significantly after the discovery of one-atomic-thick free standing graphene [4]. Graphene shows remarkable electronic, mechanical and chemical [5-8] properties making it a potential material for semiconductors, microprocessors, electric batteries and novel

electronic devices. Several methods have been reported to produce graphene sheets based on chemical oxidation of graphite [9-11] or thermal decomposition of silicon carbide [12-14] or mechanical exfoliation of graphite [4]. Recently, many researchers have focused on the ability to control the geometry of graphene, since it would be more promising for nanostructured devices with well-defined electronic properties.

There is tremendous interest in the patterning of graphene and other carbon films for applications that range from electrodes [15,16] to integrated electronic circuits [17**]** to lithographic masks [18, 19] to material coatings designed for biocompatibility, [20] or lubrication, [21] or thermal and electrical conductivity [22] Proposed patterning methods include lithography, [23,24] , transfer printing [25,26], plasma etching, [27,28] and electrocatalysis [29]. Lithographic patterning of graphene sheets [24,25,30] has produced graphene nanoribbons (GNRs), quasi-one dimensional structures. Their charge carrier ability [31] and high thermal conductivity [32] makes them great candidates for room temperature transistor operations [33, 34]. However, due to the limitations of the lithographic techniques, fabrication of precise graphene nanoribbons, graphene-based electronic devices/circuits, or other patterned carbon film structures with well-defined geometry remains an important challenge.

In addition to lithographic methods, graphene and carbon film patterning may be possible through selective etching by catalytic gasification. It has long been known that gas/carbon reactions are catalyzed by metals, [35-40] and the specific gasification reactants include steam [41], carbon dioxide and hydrogen, [42-44] and dioxygen [45, 46]. Few layer graphene, three and more layers of graphite sheet, has shown similar etching results to bulk natural graphite [47]. Catalytic gasification of natural graphite has

been studied extensively in the literature [35]; much of it focused on the effect of catalysts on the rate of gasification reactions. Vanadium metal, vanadium oxide [36] and chromium, in the form of $Cr_2O_3$ [37] have been reported as active catalysts for the oxidation of graphite, as well as Pt, Fe, Ni, [38] Ag and Cu [39]. Transition metal oxides have been known to be the most active catalysts for the $C+O_2$ reaction [40] as opposed to $C+H_2O$ and $C+CO_2$ reactions, where they are only weakly active.

Also, a significant amount of work has been published for the behavior of catalyst particles on graphite surfaces during gas-carbon reactions when the reactants are $O_2$, $CO_2$, $H_2O$ and $H_2$. Different catalyst behavior has been observed depending on the catalysts' activity and mobility, as well as the gasification agent. The dominant mode of the catalyst action depends on the wetting condition, which depends on the gas environment and temperature [48].

Gasification reactions typically occur in the immediate vicinity of the catalyst particle and result in pitting [49] (catalyst motion perpendicular to the basal plane), deep channeling [50] (catalyst motion along the basal plane transverse to step edges), or uniform edge recession [51]. The selection of reaction mode depends in a complex manner on catalyst, substrate, temperature, and reactant by rules that are only partially understood [38,52-55]. Catalytic pitting and channeling occurs naturally during the gasification of impure or doped carbon materials, [38,42,45,56-61] and only recently has this well-known solid/solid/gas reaction phenomenon been explored as a synthesis or patterning tool [62-66]. The channeling of graphite by various metal and oxide particles has been found in atmospheres of oxygen [45, 46] carbon dioxide and hydrogen [42-44] and steam [41]. Tamai and his coworkers [67] showed that series of transition metal

oxides created channels across the graphite basal planes in hydrogen environment. Mckee also found that the reaction between graphite and hydrogen was strongly catalyzed by iron, cobalt and nickel [68] resulting in random channels on graphite surface.

We recently reported that catalytic oxidation could be used as a tool for micropattern formation in carbon thin films [62] in which dioxygen serves as a dry etchant acting selectively on catalyst particles positioned by controlled metal salt deposition using microcontact printing followed by drying. Also, single-particle channels have recently been demonstrated in highly oriented pyrolytic graphite (HOPG) using hydrogen gasification catalyzed by cobalt nanoparticles [63]. For graphene patterning, Ci et al.[64] have used Ni nanoparticles in catalytic hydrogenation to create single-particle etch patterns in HOPG, and Severin et al.[65] have used silver as a channeling catalyst for the dioxygen reaction. Datta et al.[66] have reported the use of iron to obtain nanotrenches in few layer graphene through catalytic hydrogenation. It has been reported that channeling catalyst particles follow preferred crystallographic directions, [64-66, 69] which if fully understood could lead to precise patterning through rule-based etching protocols. Such direct writing methods may offer advantages over static methods in terms of line resolution, but this class of technique would be much more powerful and flexible if one had a method to explicitly control the channeling directions, or to change direction dynamically to produce complex and preselected channel patterns.

Here we explore the possibility of creating arbitrarily complex patterns in multi-layer graphene or graphite films through magnetic steering of single catalyst particles. The immediate challenge was to find a material that is both an active channeling catalyst and a ferromagnet at reaction temperature.

### 6.1.1 Catalyst Selection

Ferromagnetism is lost above the Curie temperature, which for common magnetic phases occurs at temperatures near or below those of the graphite/hydrogen reaction (Ni: 354 $^{o}$C, Fe: 770 $^{o}$C). To improve the chances of magnetic steering, we attempted to reduce reaction temperature to below 600 $^{o}$C using the dioxygen reaction ($C + O_2 \rightarrow CO/CO_2$). There is a substantial literature on this reaction. Letort and Martin [55] studied the combustion of graphite in air at 500 $^{o}$C with 0.12% catalyst addition and found the following order of activity: Au > Na > Ca > Ag > Cu >Pb > Ni > Mn > Co > Fe. Other reported rank sequences are from Marsh and Taylor [70] for oxidation of metal-doped carbon, Co > V > Fe > Mn > Cr and McKee for pure graphite powder in oxygen, Pb > V > Mn > Co >Cr > Fe > Ni [38]. Holstein and Boudard [40] report that transition metal oxides are among the most active catalysts as opposed to $C+H_2O$ and $C+CO_2$ reactions, where they are only weakly active. Overall, Co (Curie pt: 1100 $^{o}$C) appears to be a particularly promising candidate if uniform catalytic channeling can be demonstrated in the range of 400-600 $^{o}$C.

Here we show that cobalt micro- and nano-particles can produce complex, preset patterns by catalytic channeling through graphene multi-layers on the surface of natural graphite in the presence of external magnetic fields. Other metals (Ni, Fe, Ni-Cr alloy, Nb, Ag) under the same conditions show a variety of interesting etch patterns, but no evidence of active steering due to weak or non-existent ferromagnetism at the elevated reaction temperature. We demonstrate our ability to dynamically steer these magneto-catalytic particles by producing four uniform and distinct reaction modes (pitting, unidirectional

channeling, bidirectional channeling, and tridirectional channeling) by varying only the position and motion of an external, permanent magnet while keeping reaction conditions constant.

## 6.2 Experimental Details

Much of the work reported in this article has been performed with natural single crystal graphite found in Ticonderoga, New York. These crystals have a well-defined crystalline structure (Figure 6.1a) and can be cleaved into thin specimens while maintaining large and smooth basal plane surfaces [57]. Clean and fresh surfaces (Figure 6.1b) were obtained through simple mechanical exfoliation, in which successive layers were removed by using an adhesive tape [4]. Such thin graphite films vary in thickness from 20 to 50 um which are suitable for Scanning Electron Microscopy (SEM) analysis. Excessive cleavages were not required since reactions on basal plane are of primary interest.

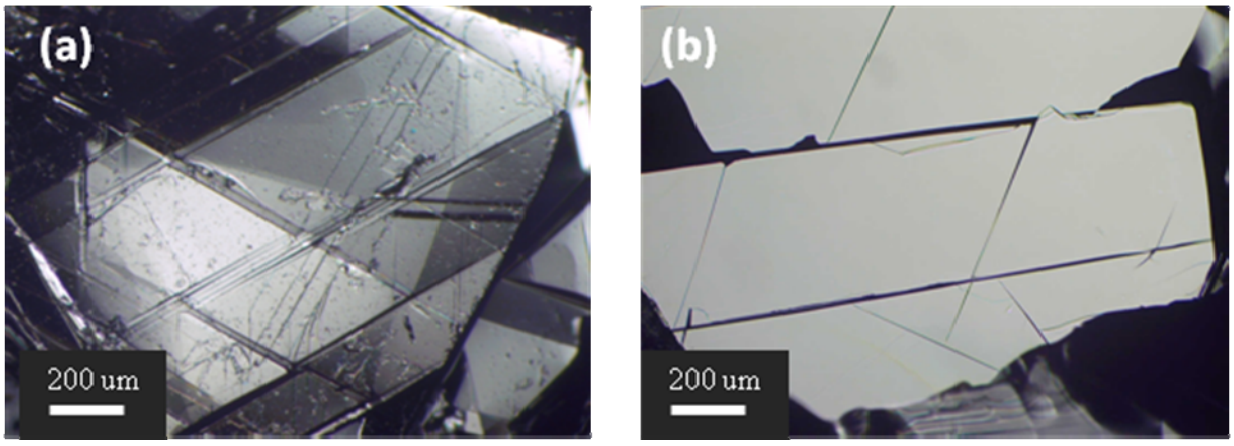


**Figure 6.1.** Optical microscope images of natural graphite surface before (a) and after mechanical exfoliation (b).

Magnetic cobalt microparticles (<2 um) from SigmaAldrich and nanoparticles (0.5-1.5 um) from Strem Chemicals, MA were deposited on freshly cleaved surfaces from aqueous solutions or as dry powders. Catalyst loaded samples were then dried at room temperature and subjected to oxidation in air at temperatures between 550-580 $^{o}$C. The catalytic oxidation was carried out in a custom resistive heat treatment device which consists of a thin polycrystalline graphite sheet held at the ends by brass electrodes connected to a low-voltage power supply. The device is capable of 2700 $^{o}$C with a maximum heating rate of 1000 $^{o}$C/s [71]. The temperature of the graphite sheet was measured in real time with a Luxtron high-speed one-color pyrometer focused on a spot on the underside of the polycrystalline graphite. The graphite sheet electrode is vertically symmetrical and temperature gradients across the ultra-thin exfoliated graphite sample are small. The sample is in direct contact with the resistively heated polycrystalline graphite sheet spanning brass electrodes. The pyrometer results are accurate within ±13 $^{o}$C.(see Figure 6.2). High-temperature-resistant $Sm_2Co_{17}$ magnets (MMC Magnetics, NY) were mounted to steer the Co catalyst particles during air oxidation while the reaction was monitored with a long-focal-length refracting microscope (Infinity Photo-Optical, Model K2) with fiber optic illumination and CCD video recording [72]. The long focal-length microscope allows *in situ* hot stage video imaging of the behavior of magnetic particles during hot catalytic oxidation and magnetic steering from below. A schematic of the experimental setup is shown in Figure 6.2.

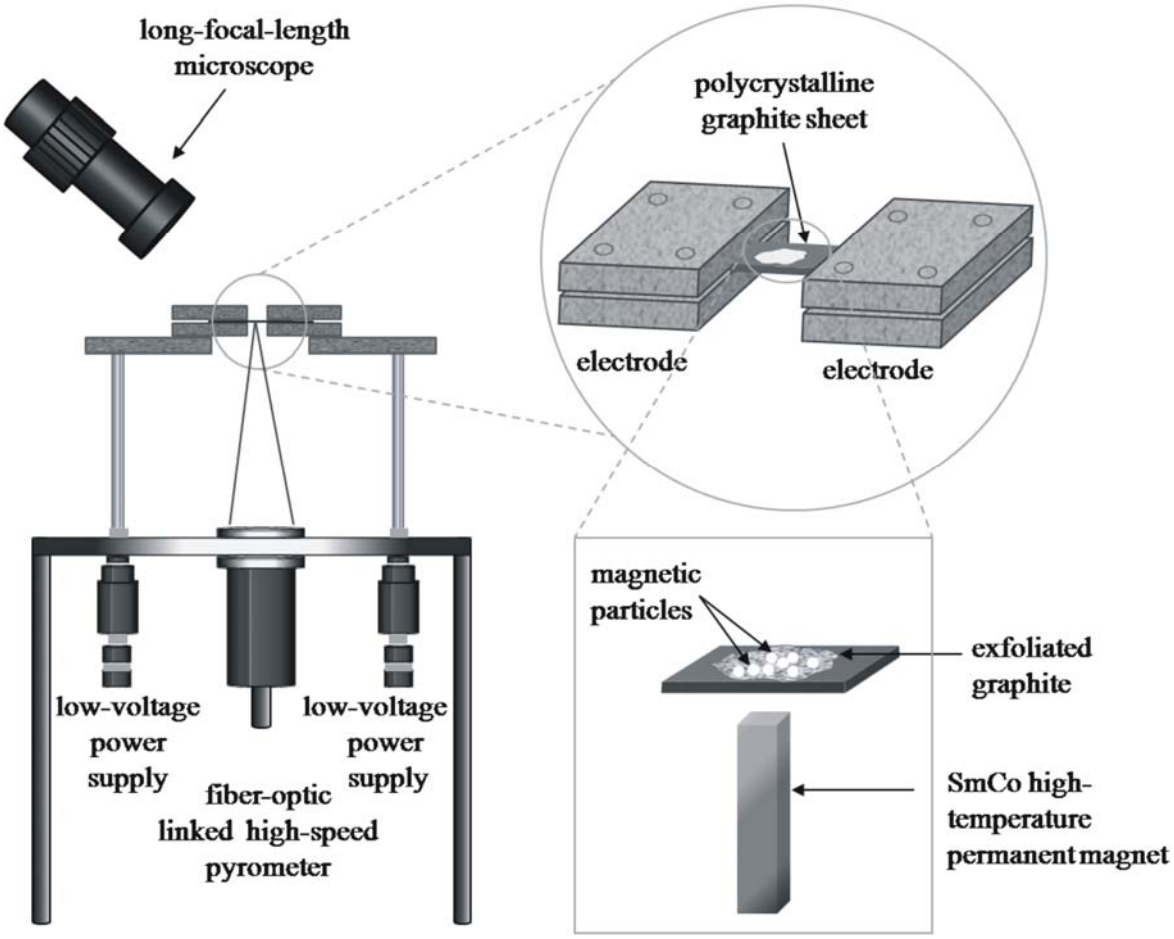


**Figure 6.2.** Hot stage oxidizing microscope modified for close-proximity ferromagnetic actuation.

After the oxidation reactions, samples were examined in detail by optical microscopy and SEM. Preliminary studies were also done with other catalysts, including nickel (3-7 um, Alfa Aeser, MA), iron (<10 um, Alfa Aeser, MA), $Fe_2O_3$ (<50 nm, SigmaAldrich), $Fe_3O_4$ (7-10 nm, supplied from Prof. Sun, Brown University), nickel-chromium (<100 um, Alfa

Aeser, MA), niobium (1-5 um, Alfa Aeser, MA) and citrate-stabilized silver (10-100 nm) provided courtesy of Jingyu Liu at Brown University. The thermal and phase behavior of the cobalt catalyst and and its mixtures with graphite were studied by Thermal Gravimetric Analysis in air from room temperature to 700$^{o}$ C with a heating rate of 10$^{o}$C/min, and by X-ray diffraction (Bruker AXS D8 Advance XRD).

## 6.3 Results

Early experiments with Ni, Fe, Ni-Cr, Nb and Ag showed a variety of interesting graphene etch patterns, many of which have been reported previously [63-66,69]. Even with the catalysts that are ferromagnetic phases at room temperature we did not see any evidence that an external magnetic field could influence behavior or set a preferred channeling direction. Successful magnetic steering was only observed for Co catalysts, which became the focus for detailed study.

### 6.3.1 Pitting

Figure 6.3(a) shows cobalt particles on the graphite surface after air oxidation at 560 $^{o}$C without magnetic actuation. It is seen that without the $Sm_2Co_{17}$ permanent magnet, fine cobalt particles (<2 um) on freshly cleaved graphite surfaces are apparently inactive and immobile in air at 560 $^{o}$C, not forming visible pits or channels (Figure 6.3(a)). In contrast, when the high temperature $Sm_2Co_{17}$ magnet was positioned underneath the sample during reaction, vertical pits were observed associated with single catalyst particles (Figure 6.3(b)). Etching occurs at each location where Co particle lies/stays on the surface as

some of them are indicated by arrows in Figure 6.3(b). We believe the difference between Figs. 6.3(a) and 6.3(b) reflect the need for close contact between the catalyst and the graphite surface, which in this and some other cases appears necessary to initiate the gas/solid/solid reaction process. It has been suggested previously,[49] that etch pit formation requires good bonding between the metal and carbon, though ours is the first evidence that this bonding can be enhanced by application of an external magnetic force perpendicular to the substrate. Figure 6.3(b) shows that Co particles progressively penetrate each layer of graphite in the area of contact between metal and graphite and catalyze the perpendicular reaction of oxygen.

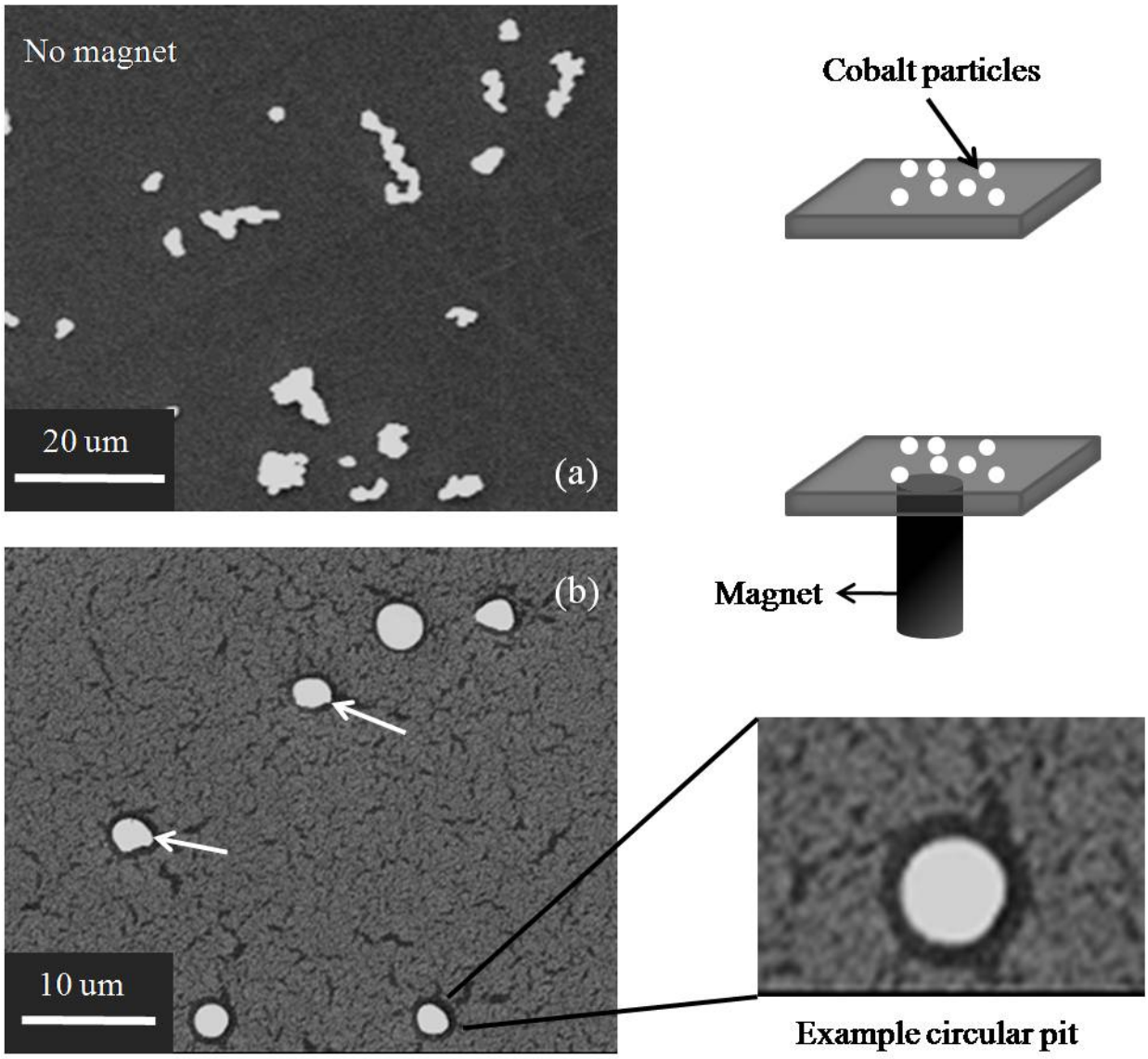


**Figure 6.3.** SEM images of (a) cobalt particles on natural graphite surface after air oxidation at 560$^{o}$C. (b) Vertical pitting (only in presence of the permanent magnet mounted in fixed position below the substrate)

### 6.3.2 Channeling and Complex Pattern Formation

Figure 6.4(a) shows the second reaction model (unidirectional channeling) caused by translational displacement of the $Sm_2Co_{17}$ magnet at the start of the reaction process (air oxidation, 570 $^oC$, 20 min.). We observe that the cobalt particles (between 0-2 um size in diameter) move in the same direction as the magnet and linear channels with catalyst particles at their tips are shown in Fig 6.4(a). Fixed orientation SEM (in which the sample is marked and mounted in the chamber in known orientation relative to the reaction experiment) clearly shows that these uniform channels are produced by particle motion along the same directional vector as the magnet translation. These first results suggested that the direction of motion of the metal particles was being controlled/restricted by the magnet, opening the possibility for controlled directional etching of complex patterns.

To confirm the hypothesis that the particles were being actively steered, further experiments were performed to create complex patterns that could not reasonably occur as natural (unguided) etch tracks. Figure 6.4(b) shows etch patterns produced by two translations of the $Sm_2Co_{17}$ magnet. (In all of these experiments, the $Sm_2Co_{17}$ magnet begins directly below the substrate to create the close metal/carbon contact that appears to be necessary for reliable channel or pit formation). After two translational motions (10 min in each of three locations for a total oxidation time of 30 min.), a complex, uniform etch pattern is seen in parallel for many particles (Figure 6.4(b)). The primary long etch track from lower left to upper right follows the vector of the first magnet translation, followed by an abrupt change in direction and a shorter etch track along the vector of the second translation. Schematic representation of the manipulation of the magnet is shown in Figure 6.4(b) inset. For some particles only, there is also a short initial track segment,

which we believe is associated with the original magnet position, which was not strictly below these particles and likely exerted some small horizontal magnetic force component during the initial 10 minutes. Co particles located at the end of each channel tip can be seen in higher magnification image of the selected area (see Figure 6.4(b) right), and the width of the channels are the same as the diameter of the particles. All the channels produced on this sample are oriented in the same direction regardless of the size of the catalyst particle. Larger Co particles appear to create longer channels (Figure 6.4(b)), and the primary etch track is much longer than the secondary though both were produced in 10 min reaction segments. This provides some evidence that the catalytic rate decreases over the course of the reaction (vida infra).

As a final and more rigorous test to confirm active steering, we attempted to produce tridirectional channeling through three translations of the $Sm_2Co_{17}$ magnet during one reaction period. Figure 6.4(c) shows the behavior when the magnet was translated to a new position every 10 minutes in a horse-shoe or U–shaped pattern. The uniform U-shaped etch patterns cannot reasonably be random, nor can they reflect preferred crystallographic directions in graphene – these complex shapes seen in parallel for many single particles, clearly demonstrate magnetic control.

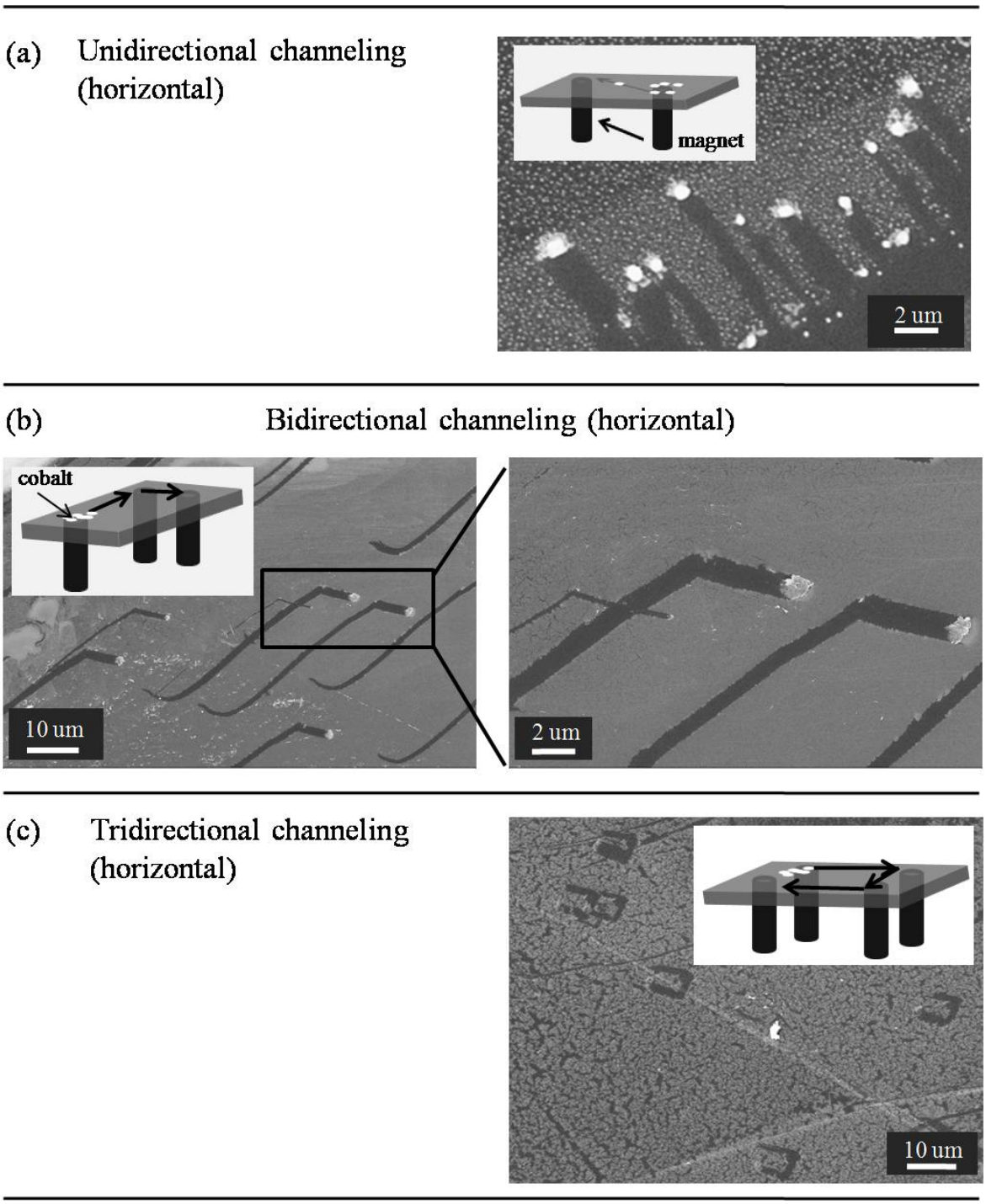


**Figure 6.4.** Demonstration of controlled reactive etching of freshly cleaved natural graphite by magnetic steering. Reaction conditions are 550-580 $^{o}$C in air and $Sm_2Co_{17}$ permanent magnet. (a) Unidirectional etching (1 translation of magnet); (b) Bidirectional

etching (2 translational motions of the magnet); Close up image of the selected area in image (b) showing individual channels with cobalt particles at the end of the channel tips; (c) Tridirectional etching (3 translational motions of the magnet). A schematic of the manipulation of the magnet during etching process is shown in insets.

## 6.4 Characterization

### 6.4.1 Thermagravimetric Analysis

Additional characterization was carried out to obtain insight into the etch mechanism. Figure 6.5 and Figure 6.6 show the thermal and phase behavior of Co, graphite, and Co/graphite mixtures under these reaction conditions. During non-isothermal thermo-gravimetric analysis in air, cobalt/graphite mixtures (33 wt% Co, metal basis) begin to lose mass by oxidation around 400 $^{o}$C, compared to about 650 $^{o}$C for graphite alone confirming the ability of Co to catalyze graphite oxidation in this temperature range. Pure cobalt particles under these conditions show mass gains beginning at 300 $^{o}$C and reaching completion at 520 $^{o}$C indicating gradual formation of cobalt oxides (see Figure 6.5). The mass gain of about 35 % is consistent with the ultimate formation of $Co_3O_4$ as also suggested by X-ray diffraction (vida infra).

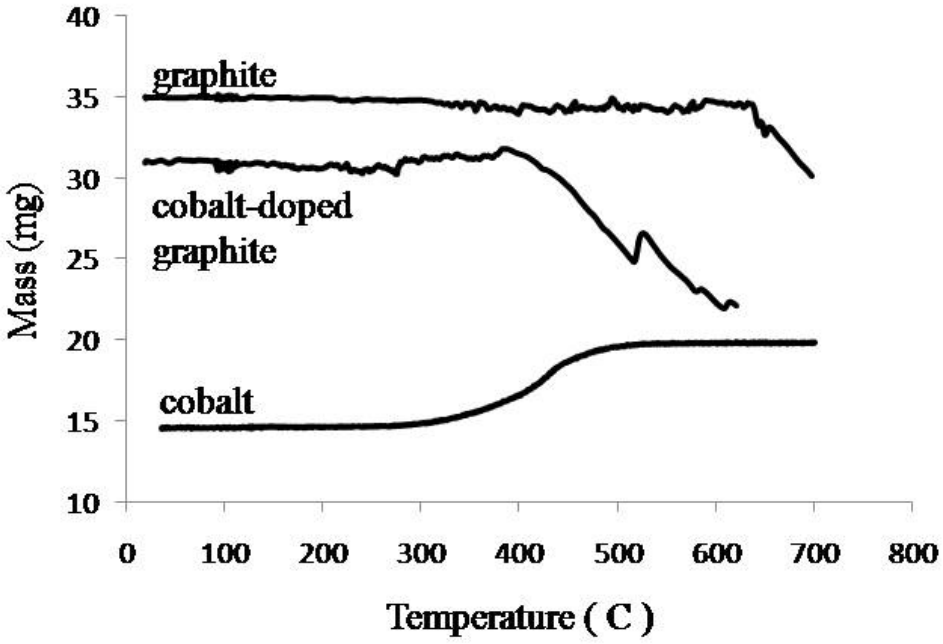


**Figure 6.5.** Oxidation behavior of cobalt, graphite and cobalt/graphite mixture by non-isothermal TGA in air at heating rate of 10 $^{o}$C/min.

Under our reaction conditions the stable phases of Co are clearly oxides, consistent with equilibrium thermodynamics ($\Delta G_f^0$ =-214.2 kJ/mol for CoO and -808.2 kJ/mol for $Co_3O_4$) [73, 74]. In the simultaneous presence of cobalt, carbon and dioxygen, one has an intrinsically non-equilibrium system, since carbon and dioxygen cannot coexist at equilibrium. The preferred cobalt phase in this Co/C/O system is a question of competing oxidation and reduction kinetics.

### 6.4.2 XRD analysis

The preferred cobalt phase is not apparent from the thermogravimetry data, because the large mass losses from catalyzed carbon gasification mask any mass changes associated with cobalt oxide formation.

We therefore used X-ray to better understand the phase behavior (see Figure 6.6). Spectrum (A) characterizes the phases produced by exposing Co particles alone to air at 400 $^{o}$C from 10 min, representing the early stages of the reaction, while (B) corresponds to Co particles alone in air at 550 $^{o}$C after 30 min, representing the end stages of the reaction. Comparison of these two spectra shows a gradual conversion of Co to CoO and then to $Co_3O_4$ as the primary phase. The early oxidation product (400 $^{o}$C, 10 min) still responds to the $Sm_2Co_{17}$ magnet, but much more weakly than the starting Co. The late oxidation product, (550 $^{o}$C, 30 min, giving almost entirely $Co_3O_4$) no longer responds to the $Sm_2Co_{17}$ magnet, even at very close proximity. The end stage of cobalt oxidation under our conditions appears to be much less effective as a magneto-catalyst, and this is a likely explanation for the decrease in etching speed as the reaction progress (see shorter final etch track in Figure 6.4(b)). McKee [38] report that iron, cobalt, and manganese gradually lose their catalytic activity through the course of reaction due to the formation of metal oxides, which may also be the case here.

Interestingly when cobalt is air oxidized (550 $^{o}$C, 30 min) but *in situ* on a graphite surface (spectrum C) it shows a small unique diffraction peak (200) for face centered cubic (fcc) metallic cobalt located at 53.16$^{o}$. The phases are otherwise similar to the pure Co case

under the end stage conditions (550 $^{o}$C, 30 min). This result suggests the presence of a minority cobalt-zero phase in intimate contact with the carbon, possibly engaged in a catalytic redox cycle where oxygen is shuttled to the graphene step edge sites through cyclic formation and decomposition of cobalt oxide. The proportion of Co metal is undoubtedly small, and it is not surprising that this phase would be only very weakly ferromagnetic.

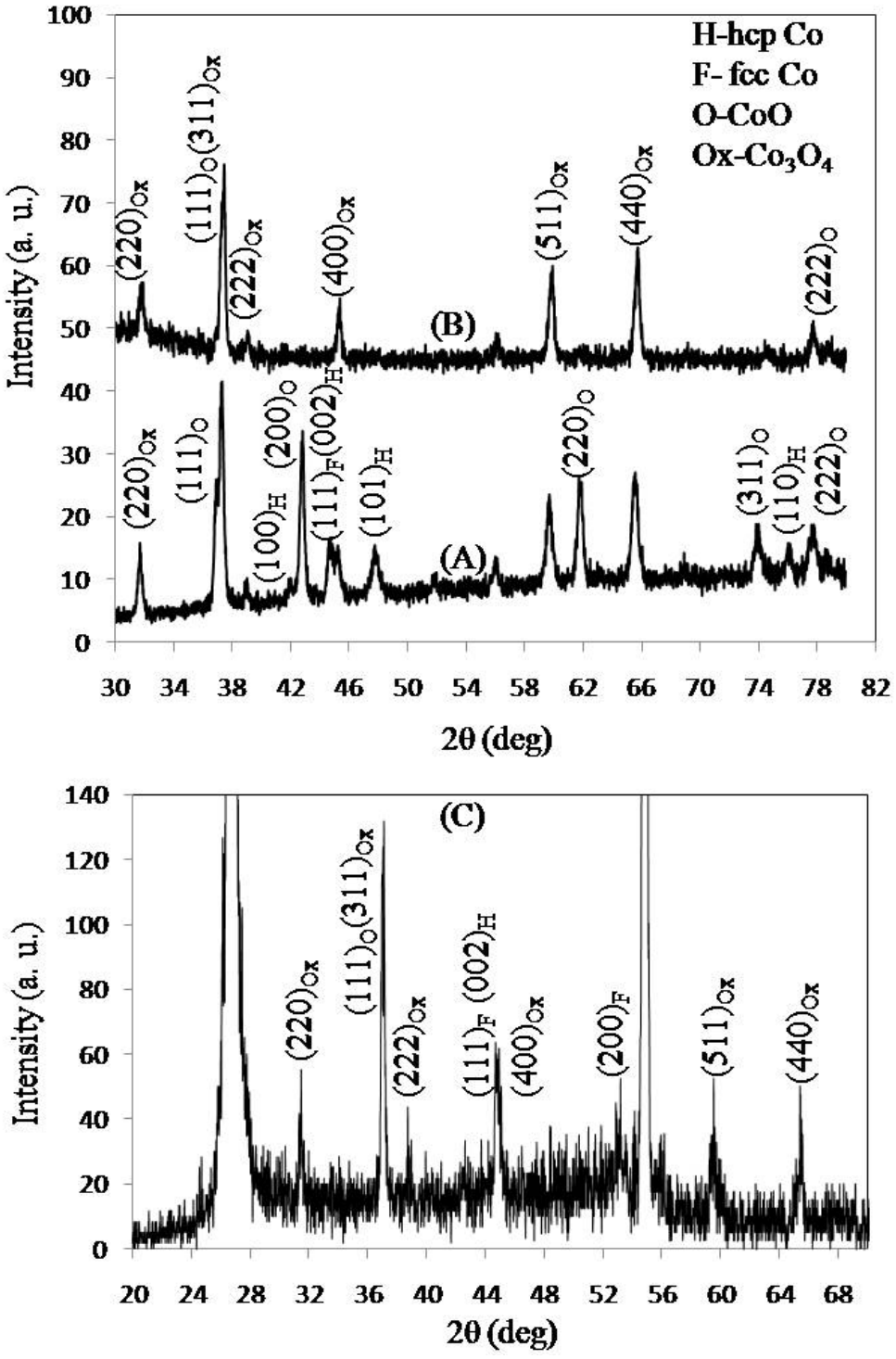


**Figure 6.6.** XRD spectra of cobalt particles after: (A): air oxidation for 10 min at 400 $^{o}$C (representing early-stage reaction); (B) air oxidation for 30 min at 550 $^{o}$C (representing late-stage reaction); (C) air oxidation for 30 min at 550$^{o}$C in contact with exfoliated

graphite with $Sm_2Co_{17}$ permanent magnet below substrate to improve catalyst/ carbon contact ( to characterize the effect of carbon on Co phase behavior).

Under these reaction conditions, and in the absence of carbon (A, B) Co is gradually converted to oxides on the time scales of our etching reaction. At the end stage of reaction (B), there is a mixture of $Co_3O_4$ and CoO (minority phase) and no detectable metal. In the presence of carbon, the end-stage products are $Co_3O_4$ with a trace of Co metal, likely located in intimate contact with the substrate allowing carbothermal reduction.

## 6.5 Conclusions

Overall, we have demonstrated that multi-layer graphene can be etched into arbitrarily complex and preset channel patterns by using cobalt-based catalyst particles for the dioxygen reaction ($C + O_2 \rightarrow CO/CO_2$) at temperatures near 550 $^oC$ using externally applied magnetic fields. Use of other catalyst formulations (Ni, Fe, Ni-Cr, Nb, Ag) produce interesting etch patterns but in random or multiple directions that cannot be dynamically controlled through field steering. Etch rates as high as 2 um/min are achieved and the etch tracks and XRD studies suggest the gradual decrease in magneto-catalytic activity over the course of the reaction through cobalt oxide formation. The results suffice to demonstrate active steering for particles/channels down to about 200 nm. For multi-domain particles, the effect of particle size on the magnetic steering force is complex, as are the surface forces that influence crystallographic etch directions, so the ultimate lower size limit for this technique requires additional experimentation. This is to

our knowledge the first demonstration of a magneto-catalytic writing technique for carbon materials, and it may find application in the massively parallel production of uniform flow channels, pores, wells, or ribbons. The present study focused on directional multi-layer graphene channeling parallel to the basal plane, and more work is needed to identify fundamental limitations on layer number, particle (feature) size, and feature precision, and to extend the technique if possible to nanopore fabrication or complex nanoscale channeling in few-layer or single-layer graphene.

## References

**[1]** P. Wallace, Phys. Rev. 71 (1947) 622-634.

**[2]** L. McClure, Phys. Rev. 104 (1956) 666-671.

**[3]** J. Slonczewski, P. Weiss, Phys. Rev. 109 (1958) 272-279.

**[4]** K. Novoselov, A. Geim, S. Morozov, D. Jiang, Y. Zhang, S. Dubonos, I. Grigorieva, A. Firsov, Science 306 (5296) (2004) 666-669.

**[5]** A. Geim, K. Novoselov, Nature Materials 6 (3) (2007) 183-191.

**[6]** J. Meyer, A. Geim, M. Katsnelson, K. Novoselov, Nature 446 (7131) (2007) 60-63.

**[7]** J. Fernandez-Rossier, J. Palacios, Phys. Rev. Lett. 99 (17) (2007) 177204.

**[8]** P. Shemella, Y. Zhang, M. Mailman, P. Ajayan, S. Nayak, Appl. Phys. Lett. 91 (4) (2007) 042101.

**[9]** R. P. S. Stankovich, D.A. Dikin, K. Kohlhaas, A. Klein-hammes, Y. Jia, Y.Wu, S. Nguyen, R. Ruo, Carbon 45 (7) (2007) 1558-1565.

**[10]** H. Schniepp, J. Li, M. McAllister, M. Herrera-Alonso, D. Adamson, R. Prud'homme, R. Car, D. Saville, I. Aksay, J. Phys. Chem. B 110 (17) (2006) 8535-8539.

**[11]** X. Li, X. Wang, L. Zhang, S. Li, H. Dai, Science 319 (5867) (2008) 1229-1232.

**[12]** M. McAllister, J. Li, D. Adamson, H. Schniepp, A. Abdala, J. Liu, M. Herrera-Alonso, D. Millus, R. CarO, R. Prud'homme, I. Aksay, Chem. Mater 19 (18) (2007) 4396-4404.

**[13]** T. Ohta, A. Bostwick, T. Seyller, K. Horn, E. Rotenberg, Science 313 (5789) (2006) 951-954.

**[14]** C. Berger, Z. Song, X. Li, X. Wu, N. Brown, C. Naud, D. Mayau, T. Li, J. Hass, A. Marchenkov, E. Conrad, P. First, W. de Heer, Science 312 (5777) (2006) 1191-1196.

**[15]** G. K. Kiema, M. J. Brett, *J. Electrochem. Soc*. 2003, *150*, E342-E347.

**[16]** K. S. Kim, Y. Zhao, H. Jang, S. Y. Lee, J. M. Kim, K. S. Kim, J. H. Ahn, P. Kim, J. Y. Choi and B. H. Hong, *Nature* 2009, *457*, 706-710.

**[17]** D. A. Areshkin, C. T. White, *Nano Lett*. 2007, *7*, 3253-3259.

**[18]** S. Park, T. Lim, D. Yang, J. Jeong, K. Kim, K. Lee, H.Kong, *Appl. Phys. Lett*. 2006, *88*, 203105.

**[19]** D. Li, W. Windl, N. P. Padture, *Adv. Mater*. 2009, *21*, 1243-1246.

**[20]** R. J. Narayan, *Int. Mater. Rev.* 2006, *51*, 127-143.

**[21]** S. J. Harris, A. M. Weiner, S. C. Tung, S. J. Simko, M. C. Militello, *Surf. Coat. Technol.* 1993, *62*, 550-557.

**[22]** S. Aoqui, T. Ikegami, Y. Yamagata, K. Ebihara, *Thin Solid Films* 1998, *316*, 40-44.

**[23]** Y. Xia, G. M. Whitesides, *Annu. Rev. Mater. Sci.* 1998, *28*, 153-184.

**[24]** Z. Chen, Y. Lin, M. Rooks, P. Avouris, *Physica E* 2007, *40*, 228-232.

**[25]** X. Liang, Z. Fu, S. Chou, *Nano Lett.* 2007, *7*, 3840-3844.

**[26]** A.K. Geim, *Science*, 2009, 324 1530-1534.

**[27]** F. Schedin, A. K. Geim, S. V. Morozov, E. W. Hill, P. Blake, M. I. Katsnelson, K. S. Novoselov, *Nat.Mater*. 2007, *6*, 652-655.

**[28]** S. Pang, H. N. Tsao, X. Feng, K. Mullen, *Adv. Mater*. 2009, *21*, 1.

**[29]** T. Mühl, J. Kretz, I.Mönch, C.M. Schneider, H. Brückl, G. Reiss, *Appl. Phys. Lett.* 2000, *76*, 786-788.

**[30]** L. Tapaszto, G. Dobrik, P. Lambin, L. Biro, Nature Nanotech 3 (7) (2008) 397-401.

**[31]** M. Han, B. Ozyilmaz, Y. Zhang, P. Kim, Phys. Rev. Lett. 98 (20) (2007) 206805.

**[32]** A. Balandin, S. Ghosh, W. Bao, I. Calizo, D. Teweldebrhan, F. Miao, C. Lau, Nano Lett. 8 (3) (2008) 902 907.

**[33]** Y. Son, M. Cohen, S. Louie, Phys. Rev. Lett. 97 (21) (2006) 216803.

**[34]** D. Areshkin, D. Gunlycke, C. White, Nano Lett. 7 (1) (2007) 204-210.

**[35]** J. Thomas, in *Chemistry and Physics of Carbon*, Vol. 1, Dekker, New York 1966, p.121.

**[36]** R. T. K. Baker, R. Thomas, M. Wells, *Carbon* 1975, *13*, 141-145.

**[37]** P. Magne, X. Duval, *Bull. Soc. Chim. Fr.* 1971, *5*, 1585-1592.

**[38]** D. McKee, *Carbon* 1970, *8*, 623-635.

**[39]** E. T. Turkdogan, J. V. Vinters, *Carbon* 1972, *10*, 97-111.

**[40]** W. Holstein, M. Boudart, *Fuel* 1983, *62*, 162-165.

**[41]** W. Holstein, M. Boudart, *J. Catal.* 1982, *75*, 337-353.

**[42]** X. Chu, L. Schmidt, *Carbon* 1991, *29*, 1251-1255.

**[43]** S. Oh, R. T. K. Baker, *J. Catal.* 1991, *128,* 137-147.

**[44]** R. T. K. Baker, R. Sherwood, *J. Catal.* 1981, *70*, 198-214.

**[45]** G. Hennig, *J. Inorg. Nucl. Chem*. 1962, *24*, 1129-1132.

**[46]** H. Chang, A. Bard, *J. Am. Chem. Soc.* 1991, *113*, 5588-5596.

**[47]** L. Liu, S. Ryu, M. Tomasik, E. Stolyarova, N. Jung, M. Hybertsen, M. Steigerwald, L. Brus, G. Flynn, Nano Lett.8 (7) (2008) 1965-1970.

**[48]** P. Goethel, R. Yang, J. Catal. 101 (2) (1986) 342-351.

**[49]** G. Hennig, in *Chemistry and Physics of Carbon*, Vol. 2 (Ed: P. L. Walker), Dekker, New York 1966, Ch. 1.

**[50]** C. Keep, S. Terry, M. Wells, *J. Catal.* 1980, *66*, 451-462.

**[51]** P. S. Harris, F. S. Feates, B. G. Reuben, *Carbon*. 1973, *11*, 565-566.

**[52]** R. T. K. Baker, *Catal. Rev. Sci. Eng*. 1979, *19*, 161-209.

**[53]** R.T.K. Baker, *Carbon* 1986, *24*, 715-718.

**[54]** P.S. Harris, F. S. Feates, B. G. Reuben, *Carbon* 1974, *12*, 189-197.

**[55]** P.L. Jr. Walker, M. Shelef, R. A. Anderson, in *Chemistry and Physics of Carbon*, Vol.4 (Ed: P. L. Walker) Dekker, New York 1968**,** Ch. 6.

**[56]** R.T.K. Baker, J.J. Chludzinski and R.D. Sherwood, *Carbon* . 1985, 23, 245-254

**[57]** Z. Pan, R. Yang, *J. Catal.* 1991, *130*, 161-172.

**[58]** R. T. Yang, C. Wong, *J. Catal*. 1984, 85, 154-168.

**[59]** P. Pereira, R. Csencsits, G. A. Somorjai, H. Heinemann, *J. Catal.* 1990, *123*, 463-476.

**[60]** P.J. Goethel, R. T. Yang, *J. Catal.* 1987, *108*, 356-363.

**[61]** X. Chu, L. D. Schmidt, S.G. Chen, R. T. Yang, *J. Catal.* 1993, *140*, 543-556.

**[62]** L. Bulut, A. Yan, R. H. Hurt, *Combustion and Flame* 2008, *154*, 206-216.

**[63]** S. Konishi, W. Sugimoto, Y. Murakami, Y. Takasu, *Carbon* 2006, *44*, 2338-2340.

**[64]** L. Ci, Z. Xu, L. Wang, W. Gao, F. Ding, K. Kelly, B. Yakobson, P. M. Ajayan, *Nano Res.* 2008, *1*, 116-122.

**[65]** N. Severin, S. Kirstein, I. M. Sokolov, J. P. Rabe, *Nano Lett.* 2009, *9,* 457-461.

**[66]** S. Datta, D. Strachan, S. Khamis, A. Johnson, *Nano Lett*. 2008, *8*, 1912-1915.

**[67]** A. Tomita, Y. Tamai, J. Catal. 27 (2) (1972) 293-300.

**[68]** D. McKee, Carbon 12 (4) (1974) 453-464.

**[69]** A. I. Chepurov, V.M. Sonin, J.-M. Dereppe, *Dia. and Rel. Mater*. 2000, *9*, 1435-1438.

**[70]** H. Marsh, D.W. Taylor, in *Abstracts 13th Biennial Carbon Conf.* 1977, p. 46.

**[71]** H. Shim, R. Hurt, *Energy Fuels* 2000, *14*, 340-348.

**[72]** K. Jian, H. Shim, D. Tuhus-Dubrow, S. Bernstein, C. Woodward, M. Pfeffer, D. Steingart, T. Gournay, S. Sachsmann, G. Crawford, R. Hurt, *Carbon* 2003, *41*, 2073-2083.

**[73]** S. E. Ziemniak, M. A. Goyette, K. E. S. Combs, *J. Sol. Chem.* 1999, *28*, 809-836.

**[74]** R. A. Robie, B. S. Hemingway, *U.S. Geological Survey Bulletin* 1995, 2131, Geological Survey, Reston, VA.

# Chapter 7

# *Conclusions and Recommendations*

## 7.1 Conclusions

This thesis demonstrated a novel and a practical technique which uses catalytic combustion to create patterned carbon materials. We proved that regular and predetermined micro patterns on carbon thin films can be achieved by selectively removing carbon during combustion at low temperatures with strategically placed metal catalysts. Another important contribution of the thesis is that directional etching of graphene layers was demonstrated for the first time by using magnetically steered catalyst particles. This thesis presents a powerful method to explicitly control the channeling directions, or to change direction dynamically to produce complex and preselected channel patterns in multi-layer graphene.

For the demonstartion of this new concept we first worked with carbon thin films. This thesis used carbon thin films fabricated by two methods: physical vapor deposition

(PVD) and spin coating/carbonization of an organic liquid-crystalline dye. The surface of these films is uniform, dense, and entirely anisotropic. Carbon combustion reaction, C(s) + $O_2$ → $CO/CO_2$ is catalyzed by a number of metals and under some conditions a high degree of catalytic enhancement is observed. These enhancement factors are particularly useful for the work presented in this thesis, as they become the "selectivity ratio" that is a key parameter in pattern formation.

For the oxidation catalyst we chose liquid transfer, as it allowed us to use established microprinting techniques and is applicable to a wide variety of metals in the form of water-soluble salts. Aqueous solutions of $CdCl_2$, $CoCl_2$, $CrCl_3$, $FeCl_3$, KCl, $MgCl_2$, NaCl, and $NiCl_2$ were screened as potential catalysts in this thesis. The Cd, K, Mg, Co and Ni salts were observed to give irregular drying patterns that deviated significantly from the desired circular footprint of the original microdroplet. So, the significant challenge is the accurate positioning of the catalyst and prevention of its migration during drying and combustion.

We saw that when the carbon thin films were treated with 2 wt% ozone gas in oxygen at room temperature for 10 min, significant improvement in the fidelity of the combustion pattern was observed as a result of better salt film deposition on the more hydrophilic film. By comparison, on ozonated films the same salt produced thinner catalytic films and resulted in quality combustion patterns. After ozonation, both drying patterns and combustion results improved for Na and Cr salts. In general, both the drying pattern and the subsequent combustion pattern need to be evaluated to choose the best catalyst formulation. Among the metal salts examined, sodium and chromium chlorides are most suited overall for microfeature formation by selective catalytic combustion.

We used a polydimethylsiloxane (PDMS) stamp to transfer 200-μmdiameter catalyst salt solutions as ordered droplet microarrays onto a carbon thin film. PDMS microstamping provides a route for one step generation of simultaneous parallel microfeature formation. Under the correct drying and reaction conditions, we demonstrated that it is possible to convert these microdroplet arrays into well-defined micropatterned carbon films by controlled catalytic combustion.

This technique is especially attractive for carbon due to the lack of convenient liquid-phase etchants, such as those that exist for lithographic polymers and most other materials. Carbons are quite resistant to solvents, acids, and bases and thus cannot easily be micropatterned by conventional techniques. Catalytic combustion provides a way to take advantage of $O_2$ as a dry "etchant" for selective shaping or microstructural modification of a variety of carbon materials.

Significant amount of work has been published for the behavior of catalyst particles on graphite surfaces during gas-carbon reactions when the reactants are $O_2$, $CO_2$, $H_2O$ and $H_2$. Different catalyst behavior has been observed depending on the catalysts' activity and mobility, as well as the gasification agent. The dominant mode of the catalyst action depends on the wetting condition, which depends on the gas environment and temperature. It has been reported that single-particle etch patterns in HOPG [1] or nanotrenches in few layer graphene [2] can be obtained through catalytic hydrogenation. In this thesis, we focused on controlling single particle etch patterns in graphene by using dioxygen as an alternative gasification agent, which allowed a reduction in reaction temperature below the Curie point of some magnetic materials and opened the possibility for magnetic steering to create complex patterns. Ferromagnetism is lost above the Curie

temperature, which for common magnetic phases occurs at temperatures near or below those of the graphite/hydrogen reaction. We reduced the reaction temperature to below 600 $^{o}$C using the dioxygen reaction which is below the Curie temperature of cobalt (1100 $^{o}$C) and thus the particles could be steered magnetically during etching at the reaction temperature.

Multi layer graphene was obtained by mechanical exfoliation of natural single graphite crystals and cobalt micro/nanoparticles were deposited on the freshly cleaved basal plane and oxidation carried out at temperatures between 500 $^{o}$C-600 $^{o}$C in a custom resistive heat treatment device. High temperature-resistant $Sm_2Co_{17}$ magnets were mounted to magnetically control the mobility of cobalt particles during air oxidation.

We demonstrated the ability to dynamically steer these magneto-catalytic particles by producing four uniform and distinct reaction modes (pitting, unidirectional channeling, bidirectional channeling, and tridirectional channeling) by varying only the position and motion of an external, permanent magnet while keeping reaction conditions constant. This thesis showed the possibility of etching graphite by metal particles in an oxidative environment by controlling the etching direction with a magnetic force and results are the first illustarion of multi layer graphene channeling paralel to the basal plane in response to the magnet. More work is needed to identify fundamental limitations on layer number, particle (feature) size, and feature precision, and to extend the technique if possible to nanopore fabrication or complex nanoscale channeling in few-layer or single-layer graphene.

## 7.2 Recommendations for future work

The potential of this new concept as a materials synthesis tool remains largely unexplored. We imagine a variety of other applications for this basic concept including the shaping of carbon monoliths, fibers, nanoparticles, or nanorods to make controlled pores or nanoscale features, or three-dimensional contouring of vertical carbon nanotube/fiber arrays, which is not easily accomplished by existing patterning techniques. Porous carbon structures with high dispersion of metal particles would be promising for electrocatalytic activity in fuel cell technologies, microelectrode arrays [3,4]. Also, carbon-based materials with microfluidic channels would be promising templates for the analysis of biomolecules and particles. When considering the utilization of carbon materials in catalysis, energy storage, gas or liquid separations, revolutionary advances in process technology are needed to obtain reproducible characteristics for large-scale integration of patterned carbon materials. Catalytic combustion offers a simple and effective way for selective etching of carbon in a controllable fashion and it can be used in the parallel production of uniform flow channels, pores or tunnels in the surface layers of various carbon materials to create new functions or to enhance the properties of the carbon materials. This technique shows a great potential for producing high-performance carbon materials with functional nano-architectures which would be the essential components of the next generation devices for many practical applications.

## References

**[1]** Ci L., Xu Z., Wang L., Gao W., Ding F., Kelly K., Yakobson B. I., Ajayan P. M., Controlled Nanocutting of Graphene, *Nano Res.* 2008, *1*, 116-122.

**[2]** Datta S. S., Strachan D. R., Khamis S. M., Johnson A. T., Crystallographic Etching of Few-Layer Graphene, *Nano Lett*. 2008, *8*, 1912-1915.

**[3]** Joo S.H., Choi S.J., Oh I., et al., Ordered nanoporous arrays of carbon supporting high dispersions of platinum nanoparticles, *Nature*, 412 (2001) 169-172

**[4]** Kiema G. K., Ssenyange S., McDermott M. T., Microfabrication of Glassy Carbon by Electrochemical Etching, *Journal of The Electrochemical Society*, 151 (2004) (2) C142-C148